

DESIGN, ANALYSIS AND EXPERIMENTAL VERIFICATION OF
A PIEZOELECTRIC VORTEX ENERGY HARVESTER

A THESIS SUBMITTED TO
THE GRADUATE SCHOOL OF NATURAL AND APPLIED SCIENCES
OF
MIDDLE EAST TECHNICAL UNIVERSITY

BY

AHMET LEVENT AVŞAR

IN PARTIAL FULLFILLMENT OF THE REQUIREMENTS
FOR
THE DEGREE OF DOCTOR OF PHILOSOPHY
IN
AEROSPACE ENGINEERING

FEBRUARY 2016

Approval of the thesis:

**DESIGN, ANALYSIS AND EXPERIMENTAL VERIFICATION
OF A PIEZOELECTRIC VORTEX ENERGY HARVESTER**

submitted by **AHMET LEVENT AVŞAR** in partial fulfillment of the requirements for the degree of **Doctor of Philosophy in Aerospace Engineering Department, Middle East Technical University** by,

Prof. Dr. Gülbin Dural Ünver
Dean, Graduate School of **Natural and Applied Sciences**

Prof. Dr. Ozan Tekinalp
Head of Department, **Aerospace Engineering**

Assoc. Prof. Dr. Melin Şahin
Supervisor, **Aerospace Engineering Dept., METU**

Examining Committee Members:

Prof. Dr. Yavuz Yaman
Aerospace Engineering Dept., METU

Assoc. Prof. Dr. Melin Şahin
Aerospace Engineering Dept., METU

Assoc. Prof. Dr. Ender Ciğeroğlu
Mechanical Engineering Dept., METU

Prof. Dr. Cihangir Duran
Materials Engineering Dept., Yıldırım Beyazıt Uni.

Asst. Prof. Dr. Levent Ünlüsoy
Aeronautical Engineering Dept., UTAA

Date: 26/02/2016

I hereby declare that all information in this document has been obtained and presented in accordance with academic rules and ethical conduct. I also declare that, as required by these rules and conduct, I have fully cited and referenced all material and results that are not original to this work.

Name, Last Name : Ahmet Levent Avşar

Signature :

ABSTRACT

DESIGN, ANALYSIS AND EXPERIMENTAL VERIFICATION OF A PIEZOELECTRIC VORTEX ENERGY HARVESTER

Avşar, Ahmet Levent

PhD, Department of Aerospace Engineering

Supervisor: Assoc. Prof. Dr. Melin Şahin

February 2016, 141 Pages

In recent days, alternative energy resources are discussed as an important topic for different applications, therefore an extensive study is conducted for the sustainable and renewable energy resources. The importance of the sustainable and renewable energy resources is also increased due to the fossil fuels usage and environmental pollution. For this reason, techniques for obtaining alternative energy resources, such as from sun and wind, are developed rapidly. Moreover, the energy loss during the operational conditions of engineering structures can be regained and the efficiency can also be increased via various novel energy harvesting methods.

During the operation of structures, vibration can be seen in different frequency range and amplitude. By using piezoelectric material coupled with passive host structure, energy can be harvested from vibrating structures. Due to the nature of piezoelectric material, voltage is obtained by deformation of the piezoelectric material and harvested voltage can be converted to the practicable energy through a special circuit. This energy can be optimized by using a suitable piezoelectric material via selection of the geometry and application of piezoelectric material to proper positions over the host structure.

The objective of this study is to harvest energy from vortex air loading by using piezoelectric material. Therefore, different piezoelectric materials and structures coupled with suitable host structural components are investigated in the framework of this study. It is also aimed to use both analytical/numerical and experimental methods effectively during the design of the vortex energy harvester. Finally, it is aimed to design piezoelectric vortex energy harvester, which consists of a special mechanism to change the diameter of the bluff body and works at different flow velocities. This design can be expected to be made as smart by arranging the diameter of the bluff body with respect to different flow velocities with a dedicated control system.

Keywords: Vibration, energy harvesting, piezoelectric material, vortex flow

ÖZ

BİR PİEZOELEKTRİK VORTEKS ENERJİ HASATÇISININ TASARIMI, ANALİZİ VE DENEYSEL DOĞRULANMASI

Avşar, Ahmet Levent

Doktora, Havacılık ve Uzay Mühendisliği Bölümü

Tez Yöneticisi: Doç. Dr. Melin Şahin

Şubat 2016, 141 Sayfa

Günümüzde alternatif enerji kaynağı ihtiyacının sağlanması önemli bir konu olarak tartışılmaktadır. Özellikle sürdürülebilir ve yenilenebilir enerji kaynakları üzerine yoğun çalışmalar bulunmaktadır. Fosil yakıt kullanımının arttığı ve çevre kirliliği problemlerinin yaşandığı bu dönemde alternatif enerji kaynaklarının önemi de hızla artmaktadır. Bu amaçla güneş ve rüzgar gibi alternatif enerji kaynakları için farklı yöntemler geliştirilmektedir. Ayrıca hali hazırda çalışan yapılar üzerinden de bir miktar enerji elde edilmesine yönelik yöntemlerin uygulanabilirliği de araştırılmaktadır. Böylelikle yapıların çalışma koşullarında (yani operasyonel durumlarında) kaybolan enerjilerinin bir kısmı özgün enerji hasat yöntemleri ile geri kazanılabilmeye ve enerji verimliliği açısından ilerleme kaydedilmesine de çalışılmaktadır.

Yapılar üzerinde, bu yapıların çalışma ortam ve şekline bağlı olarak farklı frekans aralığında ve genliğinde titreşimler oluşmaktadır. Bu titreşimlerden piezoelektrik malzemeler kullanılarak enerji elde edilmesi mümkündür. Piezoelektrik malzemeler doğası gereği üzerlerinde oluşan yer değiştirmeler sonrası voltaj üretmektedirler. Elde edilen voltaj uygun bir devreden geçirildiğinde de enerji elde edilebilmektedir. Uygun piezoelektrik malzeme/yapı kullanımı, geometri seçimi ve piezoelektrik

malzemenin yapı üzerinde uygulanacakları yerinin optimum belirlenmesi ile enerji elde edimini maksimize edilebilmektedir.

Bu tez kapsamında, bahsi geçen amaca yönelik olarak; farklı tipte piezoelektrik malzemeler ve yapılar uygun misafir yapılar üzerine yerleştirilerek vorteks içeren hava akışından enerji hasat etmektir. Yine hasatçı tasarımına yönelik yapılan arařtırmalar kapsamında, ihtiyaç duyulan analitik/sayısal ve deneysel yöntemlerin verimli şekilde kullanılması da hedeflenmektedir. Tez kapsamında amaçlanan, farklı akış hızlarında çalışan ve özel bir mekanizma ile çapı deęirilebilen yapı içeren vorteks enerji hasatçısı tasarlamaktır. Tasarlanan piezoelektrik vorteks enerji hasatçısı uygun kontrol sistemi ile akıllı hale getirilerek yapının çapı farklı akış hızlarına göre ayarlanabilmelidir.

Anahtar Kelimeler: Titreşim, enerji hasatı, piezoelektrik malzeme, vorteksli akış

To My Family...

ACKNOWLEDGEMENTS

The author wishes to express his deepest and thanksgiving to his supervisor, Assoc. Prof. Dr. Melin Şahin for his boundless help, excellent supervision and leading guidance from beginning to end of thesis work.

The author gratefully acknowledges the support provided by the Middle East Technical University under grant number BAP-03-13-2012-001 for the project titled "Vibration-based Energy Harvesting from Aerial Vehicle via Piezoelectric Material".

The author would also like to thank his family for their vulnerable support and endless patience since the beginning of primary school till the end of PhD study.

The author acknowledges the important contribution provided by Prof. Dr. Yavuz Yaman and Assoc. Prof. Dr. Ender Ciğeroğlu during thesis progress committee meetings.

The author would also like to thank Erol Başaran, Ali Aydoğmus, Yusuf Yazar and Nuri Beştepe during the all manufacturing and integration of piezoelectric materials in this thesis. They are so helpful and talented.

Also thanks to METEKSAN SAVUNMA, for using its facility and precious knowledge.

TABLE OF CONTENTS

ABSTRACT	v
ÖZ	vii
ACKNOWLEDGEMENTS	x
TABLE OF CONTENTS	xi
LIST OF TABLES	xv
LIST OF FIGURES	xvii
LIST OF SYMBOLS	xxiii
LIST OF SYMBOLS	xxiii
LIST OF ABBREVIATIONS	xxiv
CHAPTERS	
1. INTRODUCTION	1
1.1 Literature Review	2
2. ENERGY HARVESTING FROM THE VERTICAL FIN-LIKE STRUCTURE BY DIRECT ATTACHMENT OF THE PIEZOELECTRIC PATCHES	17
2. 1. Introduction	17
2. 2. Dynamic Model of the Vertical Fin-Like Structure	18
2.2.1 Finite Element Model of the Vertical Fin-Like Structure	18
2.2.2 Experimental Validation of the Finite Element Model of the Vertical Fin- Like Structure	19
2.3. Construction of Smart Fin by Direct Attachment of BM500 to Vertical Fin- like Structure	21
2.3.1. Finite Element Model of the Smart Fin comprising BM500 Patches	21

2.4. Construction of the Smart Fin by Direct Attachment of MFC to Vertical Fin-Like Structure	25
2.4.1. Finite Element Model of the Smart Fin comprising MFC Patches	25
2.5. Energy Harvesting Performance of the Smart Fin	30
2.5.1. Ground Vibration Test of the Smart Fin	30
2.5.2. Wind Tunnel Test of the Smart Fin.....	33
2.6. Conclusion.....	40
3. ENERGY HARVESTING FROM VERTICAL FIN-LIKE STRUCTURE BY ATTACHMENT OF THE BIMORPH PIEZOELECTRIC BEAM	41
3. 1. Introduction	41
3.2. Attachment of the Bimorph Piezoelectric Beam to the Vertical Fin-Like Structure	42
3.2.1. Finite Element Model of the Vertical Fin-Like Structure with the Bimorph Piezoelectric Beam	44
3.2.2. Experimental Validation of the Finite Element Model of the Vertical Fin-Like Structure with the Bimorph Piezoelectric Beam	48
3.3.1. Ground Vibration Test of the Bimorph Piezoelectric Beam with the Vertical Fin-Like Structure	50
3.3.2. Wind Tunnel Test of the Bimorph Piezoelectric Beam with the Vertical Fin-Like Structure	53
3.4. Conclusion	57
4. DESIGN OF A PIEZOELECTRIC VORTEX HARVESTER BY USING CYLINDER AS A BLUFF BODY	61
4.1. Introduction	61
4.2 Design of the Bimorph Piezoelectric Beam used as a Piezoelectric Vortex Energy Harvester.....	61

4.2.1. Selection of the Bimorph Piezoelectric Beam for the Piezoelectric Vortex Energy Harvester.....	62
4.2.2. Experimental Analysis of the Bimorph Piezoelectric Beam.....	63
4.3. Wind Tunnel Test of the Piezoelectric Vortex Energy Harvester.....	66
4.4. Conclusion	79
5. CHAPTER 5	81
DESIGN OF A PIEZOELECTRIC VORTEX HARVESTER BY USING PLATE AS A BLUFF BODY	81
5.1. Introduction	81
5.2 Design of the Bimorph Piezoelectric Beam used as a Piezoelectric Vortex Energy Harvester.....	81
5.3. Wind Tunnel Test of the Piezoelectric Vortex Energy Harvester.....	86
5.4. Conclusion	102
6. DEVELOPMENT OF AN ADAPTIVE PIEZOELECTRIC VORTEX ENERGY HARVESTER	105
6.1. Introduction	105
6.2. Design of the Diameter Change Mechanism	108
6.2.1. Kinematic Analysis of the Diameter Change Mechanism	110
6.2.2. Finite Element Analysis of the Diameter Change Mechanism	111
6.2.2.1. Strength Analysis of the Neoprene	112
6.2.2.2. Strength Analysis of the Diameter Change Mechanism	113
6.3. Automation of the Adaptive Piezoelectric Vortex Energy Harvester.....	120
6.4. Conclusion	123
7. CONCLUSION	125

7.1 General Conclusions	125
7.2 Recommendations for Future Work.....	126
REFERENCES.....	129
CURRICULUM VITAE	139

LIST OF TABLES

TABLES

Table 1. 1 Piezoelectric Energy Harvesting.....	5
Table 2. 1 Material Properties of AL-6061-T6 [58]	18
Table 2. 2 Natural Frequency of the Fin-like Structure	19
Table 2. 3 Natural Frequencies of the Fin-like Structure.....	21
Table 2. 4 The First Two Resonance Frequencies of the Smart Fin	22
Table 2. 5 Natural/Resonance Frequencies of the Fin-like Structure with PZT	25
Table 2. 6 Voltage Response of BM500-1, MFC-1, BM500-2 and MFC-2.....	29
Table 3. 1 The First Two Natural Frequencies of the Vertical Fin-like Structure	42
Table 3. 2 Natural Frequencies of the Vertical Fin-like Structure with Bimorph Piezoelectric Beam.....	46
Table 3. 3 Natural and Resonance Frequencies of the Vertical Fin-like Structure with Bimorph Piezoelectric Beam	53
Table 4. 1 Diameter of Cylinder vs. Different Flow Speed	65
Table 4. 2 Wind Tunnel Test for the Maximum Voltage output for Diameter 20 and 30 mm	74
Table 4. 3 Wind Tunnel Test for the Maximum Voltage output for Diameter 40 and 50 mm	74
Table 5. 1 Rotation Angle and Effective Length of Plate vs. Different Flow Speed for A=40 mm Plate	85
Table 5. 2 Rotation Angle and Effective Length of Plate vs. Different Flow Speed for A=50 mm Plate	85

Table 5. 3 Rotation Angle and Effective Length of Plate vs. Different Flow Speed for A=60 mm Plate.....	85
Table 5. 4 Maximum PSD Values ($V^2/\sqrt{\text{Hz}}$) for 40 mm Plate and Slot 1.....	88
Table 5. 5 Maximum PSD Values ($V^2/\sqrt{\text{Hz}}$) for 40 mm Plate and Slot 2.....	88
Table 5. 6 Maximum PSD Values ($V^2/\sqrt{\text{Hz}}$) for 40 mm Plate and Slot 3.....	88
Table 5. 7 Maximum PSD Values ($V^2/\sqrt{\text{Hz}}$) for 40 mm Plate and Slot 4.....	89
Table 5. 8 Maximum PSD Values ($V^2/\sqrt{\text{Hz}}$) for 40 mm Plate and Slot 5.....	89
Table 5. 9 Maximum PSD Values ($V^2/\sqrt{\text{Hz}}$) for 50 mm Plate and Slot 1.....	91
Table 5. 10 Maximum PSD Values ($V^2/\sqrt{\text{Hz}}$) for 50 mm Plate and Slot 2.....	91
Table 5. 11 Maximum PSD Values ($V^2/\sqrt{\text{Hz}}$) for 50 mm Plate and Slot 3.....	92
Table 5. 12 Maximum PSD Values ($V^2/\sqrt{\text{Hz}}$) for 50 mm Plate and Slot 4.....	92
Table 5. 13 Maximum PSD Values ($V^2/\sqrt{\text{Hz}}$) for 50 mm Plate and Slot 5.....	92
Table 5. 14 Maximum PSD Values ($V^2/\sqrt{\text{Hz}}$) for 60 mm Plate and Slot 1.....	94
Table 5. 15 Maximum PSD Values ($V^2/\sqrt{\text{Hz}}$) for 60 mm Plate and Slot 2.....	94
Table 5. 16 Maximum PSD Values ($V^2/\sqrt{\text{Hz}}$) for 60 mm Plate and Slot 3.....	95
Table 5. 17 Maximum PSD Values ($V^2/\sqrt{\text{Hz}}$) for 60 mm Plate and Slot 4.....	95
Table 5. 18 Maximum PSD Values ($V^2/\sqrt{\text{Hz}}$) for 60 mm Plate and Slot 5.....	95
Table 6. 1 Specifications of the Linear Actuator [95].....	122

LIST OF FIGURES

FIGURES

Figure 1. 1 Estimates of Energy Harvesting from Different Sources [6].....	3
Figure 1. 2 Piezoelectric Action.....	4
Figure 1. 3 The Electromagnetic Energy Harvester [59]	9
Figure 1. 4 Bluff Body Attached to the Piezoelectric Flow Harvester [60].....	9
Figure 1. 5 Bluff Body in Front of the Piezoelectric Flow Harvester [54]	10
Figure 1. 6 MEMS Piezoelectric Flow Harvester [62]	10
Figure 2. 1 Geometry (a), Dimension (b) and Mesh (c) of Fin-like Structure.....	18
Figure 2. 2 Strain Mode Shapes of the Fin-like Structure.....	19
Figure 2. 3 Experimental Modal Analysis Setup for Vertical Fin-like Structure	20
Figure 2. 4 FRF for Each Measuring Location	20
Figure 2. 5 Smart Fin (a) Geometry (b) Mesh (c) BM500 Geometry.....	22
Figure 2. 6 Mode Shape of Smart Fin (a) 1 st Out-of-Plane Bending (b) 2 nd Out-of-Plane Bending	22
Figure 2. 7 Experimental Modal Analysis Setup for Smart Fin.....	23
Figure 2. 8 FRF for the Smart Fin.....	24
Figure 2. 9 Effect of the Stiffener of Shaker.....	24
Figure 2. 10 Structure of MFC [74] and Geometry of M2814-P3.....	25
Figure 2. 11 Locations of the MFC Patches on Fin-like Structure	26
Figure 2. 12 Finite Element Model of the Vertical Fin-like Structure.....	26
Figure 2. 13 Displacement Response of the Smart Fin at the Tip.....	27
Figure 2. 14 Voltage Response of BM500-1 and MFC-1	28

Figure 2. 15 Voltage Response of BM500-2 and MFC-2	28
Figure 2. 16 FRF of the Smart Fin	30
Figure 2. 17 Experimental Setup for Smart Fin	31
Figure 2. 18 Voltage Output of MFC-1 and BM500-1 (at 27.5 Hz)	31
Figure 2. 19 Voltage Output of MFC-2 and BM500-2 (at 27.5 Hz)	32
Figure 2. 20 Voltage Output of MFC-3 and BM500-3 (at 92.5 Hz)	32
Figure 2. 21 (a) Energy Harvesting Module (b) DC Voltage Output of the BM500-1 and MFC-1	33
Figure 2. 22 Schematic View of the Wind Tunnel.....	34
Figure 2. 23 Wind Tunnel Test Setup	34
Figure 2. 24 Vortex Generator Test Setup [82].....	35
Figure 2. 25 Voltage Output of BM500-1 and MFC-1	36
Figure 2. 26 Voltage Output of BM500-2 and MFC-2	36
Figure 2. 27 Voltage Output of BM500-3 and MFC-3	37
Figure 2. 28 FFT of the signal obtained from BM500-1 and MFC-1	38
Figure 2. 29 FFT of the signal obtained from BM500-2 and MFC-2	38
Figure 2. 30 DC Voltage Generation of BM500-1 and MFC-1	39
Figure 3. 1 Displacement Mode Shape - 1 st Out-of-plane Bending	43
Figure 3. 2 Displacement Mode Shape - 1 st Torsion.....	43
Figure 3. 3 Bimorph Piezoelectric Beam and the Host Fin-like Structure.....	45
Figure 3. 4 Mount Detail of the Bimorph Piezoelectric Beam.....	45
Figure 3. 5 Displacement Mode Shapes - 1 st Out-of-plane bending mode of the fin.	47
Figure 3. 6 Displacement Mode Shapes - 1 st Out-of-plane bending mode of the bimorph piezoelectric beam	47

Figure 3. 7 Displacement Mode Shapes – 2 nd Out-of-plane Bending mode of the fin	48
Figure 3. 8 Modal Test Setup.....	49
Figure 3. 9 Frequency Response of Vertical Fin-like Structure with Bimorph Piezoelectric	49
Figure 3. 10 Shaker Test Setup (a) Excitation Point (b) Response Point	51
Figure 3. 11 Frequency Response of Bimorph Piezoelectric Beam.....	51
Figure 3. 12 Voltage Response of Bimorph Piezoelectric Beam.....	52
Figure 3. 13 Wind Tunnel Test Setup	54
Figure 3. 14 AC Voltage Response of Bimorph Piezoelectric Beam in Time.....	55
Figure 3. 15 DC Voltage Response of Bimorph Piezoelectric Beam in Time.....	56
Figure 3. 16 PSD of Voltage Response of Bimorph Piezoelectric Beam in Time.....	57
Figure 4. 1 Schematic Representation of the Working Principles of the Piezoelectric Vortex Energy Harvester.....	62
Figure 4. 2 3D Solid Model of Piezoelectric Vortex Energy Harvester	63
Figure 4. 3 Test Setup for Determination of the Fundamental Resonance Frequency of the Vortex Energy Harvester	64
Figure 4. 4 Frequency Response of the Vortex Energy Harvester (Mide V25W).....	64
Figure 4. 5 Manufactured Piezoelectric Vortex Energy Harvester and Bluff Bodies	65
Figure 4. 6 Wind Tunnel Test Setup for the Vortex Energy Harvester	66
Figure 4. 7 X and Y Coordinates and the Slot Numbers.....	67
Figure 4. 8 Power Spectral Density for 20 mm Diameter and Position 1	68
Figure 4. 9 Power Spectral Density for 20 mm Diameter and Position 2.....	68
Figure 4. 10 Power Spectral Density for 20 mm Diameter and Position 3.....	69

Figure 4. 11 Power Spectral Density for 30 mm Diameter and Position 1	69
Figure 4. 12 Power Spectral Density for 30 mm Diameter and Position 2	70
Figure 4. 13 Power Spectral Density for 30 mm Diameter and Position 3	70
Figure 4. 14 Power Spectral Density for 40 mm Diameter and Position 1	71
Figure 4. 15 Power Spectral Density for 40 mm Diameter and Position 2	71
Figure 4. 16 Power Spectral Density for 40 mm Diameter and Position 3	72
Figure 4. 17 Power Spectral Density for 50 mm Diameter and Position 1	72
Figure 4. 18 Power Spectral Density for 50 mm Diameter and Position 2	73
Figure 4. 19 Power Spectral Density for 50 mm Diameter and Position 3	73
Figure 4. 20 Maximum PSD of the Voltage Generation for Different Flow Speed and Diameter of the Cylinder at the Resonance Frequency,	75
Figure 4. 21 General Locations for the Cylinder for Maximum PSD Output.....	75
Figure 4. 22 Maximum Voltage Generation for Different Diameter of the Cylinder	76
Figure 4. 23 Frequency Response of the Voltage Data for 50 mm Diameter Cylinder in the Determination of the Fundamental Resonance Frequency of the Vortex Energy Harvester	77
Figure 4. 24 DC Voltage Generation of the Vortex Energy Harvester	78
Figure 4. 25 Power Generation of the Vortex Energy Harvester	79
Figure 5. 1 Schematic Representation of the Working Principles of the Piezoelectric Vortex Energy Harvester.....	82
Figure 5. 2 Schematic Representation of the Working Principles of the Piezoelectric Vortex Energy Harvester.....	82
Figure 5. 3 3D Solid Model of Piezoelectric Vortex Energy Harvester	83
Figure 5. 4 Manufactured Piezoelectric Vortex Energy Harvester and Bluff Body ..	84
Figure 5. 5 Plate Geometries	84

Figure 5. 6 Wind Tunnel Test Setup for the Vortex Energy Harvester	86
Figure 5. 7 X and Y Coordinates and the Slot Numbers.....	87
Figure 5. 8 PSD for 40 mm Plate, Maximum Wind Tunnel Speed and Slot 2	90
Figure 5. 9 Surface Plots for 40 mm Plate, (a) Wind Tunnel Speed=1.97 m/s, (b) Wind Tunnel Speed=5.66 m/s, (c) Wind Tunnel Speed=9.81 m/s and Wind Tunnel Speed=11.33 m/s	90
Figure 5. 10 PSD for 50 mm Plate, Maximum Wind Tunnel Speed and Slot 2	93
Figure 5. 11 Surface Plots for 50 mm Plate, (a) Wind Tunnel Speed=2.46 m/s, (b) Wind Tunnel Speed=7.08 m/s, (c) Wind Tunnel Speed=12.26 m/s and Wind Tunnel Speed=14.16 m/s	93
Figure 5. 12 PSD for 60 mm Plate, Maximum Wind Tunnel Speed and Slot 3	96
Figure 5. 13 Surface Plots for 60 mm Plate, (a) Wind Tunnel Speed=2.95 m/s, (b) Wind Tunnel Speed=8.50 m/s, (c) Wind Tunnel Speed=14.72 m/s and Wind Tunnel Speed=16.99 m/s	96
Figure 5. 14 General Locations for the Plate for Maximum PSD Output.....	97
Figure 5. 15 Maximum Voltage Generation for Plates (a) 40 mm Plate (b) 50 mm Plate (c) 60 mm Plate	99
Figure 5. 16 Frequency Response of the Voltage Data for 60 mm Plate in the Determination of the Fundamental Resonance Frequency of the Vortex Energy Harvester	100
Figure 5. 17 DC Voltage Generation of the Vortex Energy Harvester.....	101
Figure 5. 18 Power Generation of the Vortex Energy Harvester.....	101
Figure 5. 19 Flow Patterns of Flat Plate [88].....	103
Figure 5. 20 Flow Around a Plate, Re=10000 and 20° Incidence [89].....	103
Figure 6. 1 Lens Type Mechanism [91].....	106
Figure 6. 2 Flower Type Mechanism [91]	106

Figure 6. 3 Cam Type Mechanism [91]	106
Figure 6. 4 A Sample Flight Profile of an Air Vehicle [92].....	107
Figure 6. 5 Scissor Mechanism [93].....	108
Figure 6. 6 Morphing Cylinder Mechanism (Top View).....	109
Figure 6. 7 Morphing Cylinder Mechanism: Isometric View (a) with skin (b) without skin	109
Figure 6. 8 Diameter Change of the Morphing Cylinder Mechanism	110
Figure 6. 9 Extended View of the Morphing Cylinder Mechanism.....	111
Figure 6. 10 Neoprene Geometry	112
Figure 6. 11 (a) Mesh and (b) Boundary Conditions on Neoprene Geometry.....	112
Figure 6. 12 (a) Deformation and (b) Stress in Neoprene Geometry.....	113
Figure 6. 13 Mesh of Mechanism.....	114
Figure 6. 14 Revolute (a) and Slider (b) Joint Mechanism	114
Figure 6. 15 (a) Fixed Support and (b) Joint Velocity of Mechanism	115
Figure 6. 16 Pressure Application Location.....	117
Figure 6. 17 Total Displacement of Mechanism under the Loading.....	117
Figure 6. 18 Total Displacement of Mechanism after 1s	118
Figure 6. 19 Stress vs Time during the Extension of the Scissor Mechanism	118
Figure 6. 20 Stress After the Extension of Scissor Mechanism.....	119
Figure 6. 21 Reaction Force at the Slotted Joint (Possible Actuator Mount Location)	120
Figure 6. 22 Adaptive Piezoelectric Vortex Energy Harvester	121
Figure 6. 23 Linear Actuator, Frigelli [98].....	121

LIST OF SYMBOLS

C	Capacitance
D	Displacement, Diameter
d	Strain Constant
E	Field Strength, Modulus of Elasticity
f	Frequency
f _s	Vortex Shedding Frequency
g	Electrical Generation
H	Height
Hz	Hertz
L	Length
Re	Reynolds Number
S	Strain
s	Compliance
St	Strouhal Number
T	Applied Stress
U	Flow Velocity
W	Weight
X	X Direction Position
Y	Y Direction Position
ε	Permittivity
ρ	Density
ν	Poisson Ratio

LIST OF ABBREVIATIONS

AC	Alternating Current
AFC	Active Fiber Composite
DC	Direct Current
FFT	Fast Fourier Transform
FRF	Frequency Response Function
LVDT	Linear Variable Differential Transformer
MEMS	Micro Electromechanical System
MFC	Multi Fiber Composite
PFC	Piezo Fiber Composite
PS	Piezosystem
PSD	Power Spectral Density
PZT	Lead Zirconate Titanate
UAV	Unmanned Aerial Vehicle

CHAPTER 1

INTRODUCTION

In order to reduce an environmental pollution, carbon emission of ground vehicles is aimed to decrease. There are different studies for air vehicles in order to decrease the carbon emission in recent days and one of the important studies for reducing the carbon emission is “Clean Sky” [1]. Clean Sky is an important European research programme for improving the environmental performance of air vehicles and this leads to lighter, less noisy and less fuel consumer aircrafts. In this programme, different companies, such as Airbus, Rolls-Royce, EADS, Thales etc., give support to the research studies. One of the studies for decreasing the fuel consumption of an aircraft is to use piezoelectric material on aerodynamic surfaces. For example, one of the activities of the Clean Sky is actually a “SMART Fixed Wing Aircraft”.

The usage of clean energy becomes more and more important topic in recent days due to increase in air traffic and number of different size of aircrafts. Another good example for clean aircraft is “Solar Impulse”, which completely works with solar energy [2]. Moreover, aircraft engines are also tried to be improved so as to decrease the carbon emission [3]. Both solar cell and piezoelectric material are used together in mini unmanned aerial vehicles (UAVs) to supply its energy need.

Nowadays, it is impossible to supply all the energy require for a middle size aircraft by piezoelectric energy harvesting but energy need of various components of

the aircraft can be supplied. For example, sensors which are used for structural health monitoring purposes should continue its operation without energy loss as piezoelectric material can be used for energy need of these sensors. As changing of batteries is generally not an issue, the maintenance of the system is not required. Furthermore, using fewer batteries for any application helps to decrease the environmental pollution due to low consumption of lead.

1.1 Literature Review

Energy harvesting through different techniques, such as solar, wind or vibration, is a very hot topic in recent days. Environmental pollution and global warming are increasing rapidly due to increase in carbon pollution. In order to eliminate or to decrease carbon emission, alternative energy sources should be found. As the energy need of middle and small size structures can also be supplied by batteries and using batteries is not effective regarding the maintenance cost and the reliability of the system. Therefore, batteries might be replaced by energy harvesting systems.

Energy harvesting is defined as [4]:

“ ... Energy harvesting: Energy recovery from freely available environmental resources. Primarily, the selection of the energy harvester as compared to other alternatives such as battery depends on two main factors: cost effectiveness and reliability. Another goal for energy harvesters has been to recharge the batteries in existing applications. ... ”

By using thermal, solar, or vibration sources; energy can be obtained and this energy can used to operate different kinds of devices. For example, a human can produce around 200 Watts of power during the climbing of a mountain. A smart phone can also be charged by around 2.5 Watts [5]. As seen from this example, if the energy is harvested from human vibration, it can easily be used to charge different types of batteries. Typical energy sources and harvested power from them are summarized in Figure 1.1 [6].

Energy Source	Harvested Power
Vibration/Motion	
Human	4 $\mu\text{W}/\text{cm}^2$
Industry	100 $\mu\text{W}/\text{cm}^2$
Temperature Difference	
Human	25 $\mu\text{W}/\text{cm}^2$
Industry	1–10 mW/cm^2
Light	
Indoor	10 $\mu\text{W}/\text{cm}^2$
Outdoor	10 mW/cm^2
RF	
GSM	0.1 $\mu\text{W}/\text{cm}^2$
WiFi	0.001 $\mu\text{W}/\text{cm}^2$

Figure 1. 1 Estimates of Energy Harvesting from Different Sources [6]

As seen from Figure 1. 1, it is not easy to operate large scale devices with energy harvesting techniques but energy harvesting can be used for micro scale applications, such as battery recharging. Energy harvesting from vibration becomes more and more important due to decreased energy needs of small structures or small sensors, which may be used for a structural health monitoring purposes and play a critical role in the overall system [7]. By using vibration-based energy harvesting system, replacement cost and chemical contamination of the batteries due to excessive lead, can also be eliminated [7].

Piezoelectric Theory Background

Piezoelectric materials are used in vibration-based energy harvesting systems. The reason is from the fact that when piezoelectric material is deformed, it can produce voltage difference due to the occurrence of electric dipole moments, which is a measure of the separation of positive and negative electrical charges in a system of electric charges in solids. This phenomenon can happen conversely and so, piezoelectric material can be used as a sensor in order to monitor the motion of structures [8]. These two behaviours can be called as generator action and motor

action as seen in Figure 1. 2 [9]. In the generator action, piezoelectric material can generate voltage and it stretches or compresses during the motor action due to applied voltage.

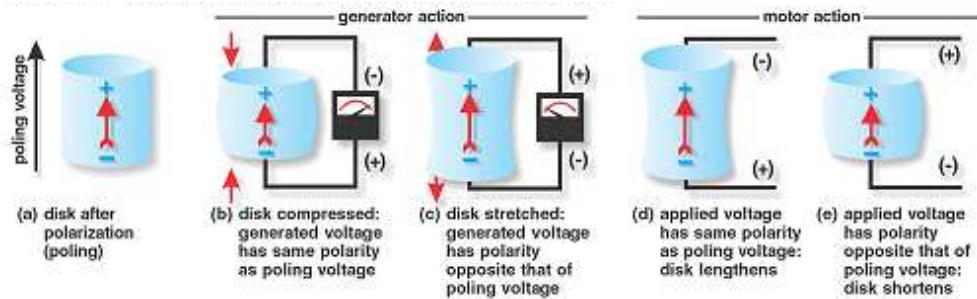


Figure 1. 2 Piezoelectric Action

These two actions, i.e. piezoelectricity, can be explained in a mathematical model by using piezoelectric material properties. Electrical condition of the unstressed piezoelectric material under the applied electric field can be expressed by two quantities, one is field strength (E) and the other is dielectric displacement (D). The relation between E and D is given in equation (1).

$$D = \epsilon E \quad (1.1)$$

where, ϵ is the permittivity of the piezoelectric material.

Moreover, the mechanical condition of the piezoelectric material can be explained by applied stress (T) and strain (S). The relation between these two is given in equation (2).

$$S = sT \quad (1.2)$$

where, s is the compliance of the piezoelectric material.

It is known that piezoelectricity is the interaction of both electrical and mechanical behaviour. Therefore, this interaction can be defined by the relation below and it is in stress-charged form [10] as;

$$S = sT + dE \quad (1.3)$$

$$D = dT + \varepsilon^T E \quad (1.4)$$

where, d is the strain constant of the piezoelectric material. The strain constant, d , can be defined as charge per electrode area due to applied stress. Also another important parameter is g , which is the piezoelectric stress constant. This parameter can be express in equation (5). The definition of g is an electrical generation performance of piezoelectric material due to applied stress.

$$g = \varepsilon^{-1} d \quad (1.5)$$

By using these parameters, piezoelectric material can be modelled in order to find the performance of it under applied stress or voltage. In energy harvesting application, electric generation characteristic of piezoelectric material can found under applied load, therefore material properties of the piezoelectric material should be known in advance.

Piezoelectric Energy Harvesting

Different examples and study about piezoelectric energy harvesting are summarized in Table 1.1. Modeling, experimental study and different application of piezoelectric energy harvesting are given by references.

Table 1. 1 Piezoelectric Energy Harvesting

Piezoelectric Energy Harvesting		
	Study	Reference
Modeling and Simulation	Single Degree of Freedom Modeling, Williams and Yates Model	[11]
	Analytical Modeling of Unimorph and Bimorph Piezoelectric Beam	[12], [13]
	Finite Element Analysis of Cantilever Piezoelectric Beam	[14], [15]

Table 1. 1 Piezoelectric Energy Harvesting (Continued)

Experimental Study	Validation of Analytical Model of Piezoelectric Bimorph Cantilever Beam	[16]
Battery Charging Application	AC Voltage to DC Voltage Conversion, Rectifier Circuit	[17]
	Battery Charging by Piezoelectric Material	[18], [19]
	Battery Free Structural Health Monitoring System	[20], [21], [22], [23]
	Self Charging Structure by combination of PZT and Thin Film Batteries	[24], [25], [26], [27]
Applications of Piezoelectric Energy Harvesting on Aircrafts	Piezoaeroelastic System	[28]
	Integration of PZTs to the UAVs	[29], [30], [31], [32]
	Wireless Structural Health Monitoring System for Air Vehicle	[33]
	Micro Energy Harvesting System for Micro UAV	[34]

Table 1. 1 Piezoelectric Energy Harvesting (Continued)

Various Other Piezoelectric Energy Harvesting Applications	Attachment of the PZTs to Backpack of Military Person	[35]
	Hydrophone Harvesting Device	[36]
	Integration of PZT Beam to the Bike	[37]
	Energy Harvesting by Impulsive Loading via Tonpilz Transducer	[38]
	Piezoelectric Bender Transducer for Energy Harvesting	[39]
	Micro Energy Harvesting Systems	[40], [41]
	Bistable Plate with PZTs	[42]
	Piezomagnetoelastic Structure	[43]
	Mechanically Tuneable Piezoelectric Energy Harvesting	[44]
	Mechanically Tuneable Piezoelectric Energy Harvesting By Spring and Screw	[45]
	Six Piezoelectric Cantilever Beam Design	[46]
	Three Degree of Freedom Energy Harvester	[47]
Using Different Types of Piezoelectric Materials in Energy Harvesting	Special Piezoelectric Materials: MFC, Quickpack, Thunder	[48], [49], [50]
	Mide Piezoelectric Harvesting Kit	[49]
	Performance Investigation of Different Piezoelectric Materials	[51]

Flow Harvester Applications

Flow energy harvesters are also receiving an attention in the literature. Flutter and vortex induced vibration can be given as examples for flow induced vibration and the energy can also be harvested from the flow induced vibration via piezoelectric energy harvester [52]. Aeroelastic energy harvesting is widely studied in literature as well. In one of the studies, Abdelkefi presented [53] different types of flow induced vibration energy harvester. Moreover, M. Bryant [54] developed novel piezoelectric energy harvester which consists of simple pin connected flap and beam and this works under aeroelastic flutter vibration. In another study, [55] it is studied nonlinear aeroelastic behavior of a piezoelectric energy harvester and it was modelled by a two dimensional typical section airfoil. C. D. Marqui Jr. [56] also worked on dimensionless electroaeroelastic equations for predicting the power output at the flutter boundary. Electrical power output and flutter speed are investigated for both piezoelectric and electromagnetic energy harvester. Furthermore, a cantilevered plate like wing with embedded piezoceramics performance evolution was investigated by considering aeroelastic vibrations [57]. In another study, performance of the piezoelectric energy harvester is analyzed by considering free play nonlinearity and performance enhancement of it is investigated [58].

In the literature, there are different examples for vortex energy harvester working under the vortex excitation. In one of the research studies, an electromagnetic energy harvester is designed to work under flow loading [59]. In the electromagnetic energy harvester example, a bluff body is positioned in front of the harvester. Operational principle of the device is also given in Figure 1. 3. Due to the bluff body, vortices can be generated and the fundamental resonance frequency of cantilever beam is excited.

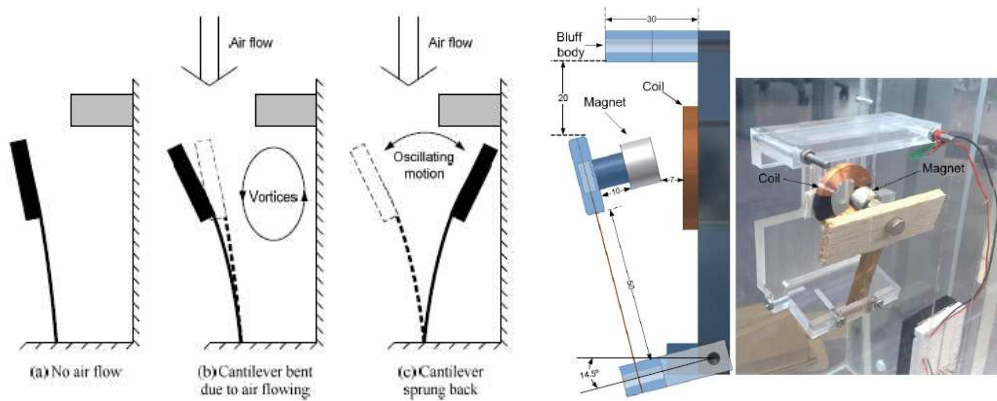


Figure 1. 3 The Electromagnetic Energy Harvester [59]

However, it is showed that bluff body can also be directly attached to the energy harvester [60]. In this design, total system can resonate around its resonance frequency when the flow is passing around a bluff body. This piezoelectric flow harvester is also designed to obtain energy under the flow loading with an attached cylindrical bluff body to the cantilever piezoelectric beam.

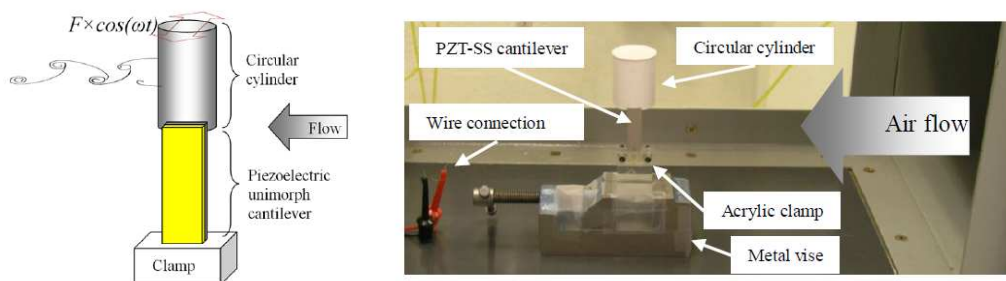


Figure 1. 4 Bluff Body Attached to the Piezoelectric Flow Harvester [60]

Another study for piezoelectric flow harvester is given in Figure 1. 5 [61]. In this study, cylindrical bluff body is located in front of the piezoelectric cantilever beam. Due to the cylindrical bluff body, vortices are generated and if the resonance frequency of the piezoelectric cantilever beam is known, the vortex frequency can be

equalized to the resonance frequency of the beam by arranging the flow speed and the diameter of the cylinder.

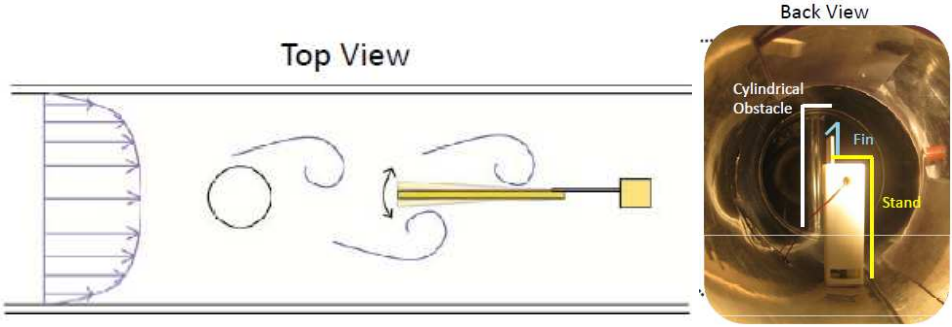


Figure 1. 5 Bluff Body in Front of the Piezoelectric Flow Harvester [54]

The micro electromechanical system (MEMS) piezoelectric flow harvester, Figure 1. 6, is designed to harvest energy for a structural health monitoring system [62]. In this study, it is stated that [62]:

“..... A microstructure in the air-flow undergoes “turbulence induced vibration”. A structure exposed to turbulence will typically have a modulated response. The modulation is produced by the interaction of the components of turbulence that produce the resonant response. That is, vibration frequency of the turbulence-induced vibration is natural frequency modulated form while that of the vortex-induced vibration depends upon the vortex shedding frequency. ...”

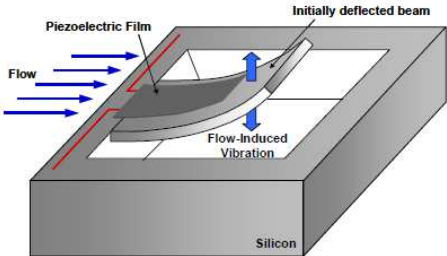


Figure 1. 6 MEMS Piezoelectric Flow Harvester [62]

Numerical solution for energy harvesting from piezoelectric transducer attached to a cylinder is studied due to vortex-induced vibration [63]. In another study, piezoelectric micro cantilever sensor is used to harvest energy from wind [64]. J. D. Hobeck developed a bio-inspired design for harvesting energy from low-velocity, highly turbulent fluid flow environments such as streams or ventilation systems [65]. In this particular design, piezoelectric grass is used to as array of piezoelectric cantilevers for harvesting energy. A flexible piezo-film is also developed as a transducer for harvesting energy from water flow [66]. In this design, a bluff body is used in front of the transducer in order to generate vortices in water flow as an excitation. Theoretical model is also constructed for piezoelectric energy harvester attached to a cylinder [67]. In this model, a nonlinear distributed-parameter model for harvesting energy from vortex-induced vibrations is developed and it is validated by experimental techniques. Moreover, Dai et al. studied that energy is harvested by piezoelectric material from both base and vortex induced vibration excitations [68]. In this study, The Euler–Lagrange principle and the Galerkin procedure are used to develop nonlinear model for this problem. Three different types of bluff bodies are attached to electromagnetic generator to observe the effect of it in energy harvesting performance under the galloping oscillations of wind [69]. A numerical model is constructed for aeroelectromechanical performance of the piezoelectric energy harvester in the wake of the bluff body [70]. Fluid, structure and electrical model for the two different harvesters are coupled to obtain the performance and the comparative study is also presented. In literature, macro fiber composite (MFC) types of piezoelectric materials are used as energy harvester. Piezoelectric energy harvester is designed by using MFC piezoelectric patch and energy is harvested by vortex generation in water flow due to cylinder [71]. R. Song et al. designed special piezoelectric energy harvester by using two cylinders and two MFC patches [72]. In this design, both vortex induced vibration and wake induced vibration are used as source of harvested energy.

1. 2. Objective of the Study

The primary aim of this thesis is to develop an energy harvester, which can be integrated to an aerial vehicle and generate energy under the vortex flow. For this harvester, piezoelectric patches are used to harvest energy from ambient vibration and the primary excitation for this vibration is the frequency content of the vortex flow. To generate a vortex flow, a bluff body is used and it can change its size automatically (in an adaptive way) to make energy harvesting possible at different flow velocities.

The objectives of this thesis are summarized as follow:

- To investigate the effect of various ways of piezoelectric energy harvesting from aircraft structure via vortex flow excitation;
 - Direct attachment of a piezoelectric patch.
 - Design of a bimorph piezoelectric energy harvester.
- To develop a piezoelectric energy harvester, which may work under vortex flow excitation.
- To construct a finite element model for both an aircraft structure and a piezoelectric energy harvester.
- To validate the finite element model by ground vibration test.
- To investigate the performance of the proposed piezoelectric energy harvesters in wind tunnel applications.
- To develop a mechanism for an adaptive flow harvester to harvest energy at different flow velocities.

1. 3. Scope of the Thesis

The purpose of the thesis is to obtain energy from an aircraft with a special design of piezoelectric energy harvester. For this reason, different alternatives for

piezoelectric energy harvesting devices, the materials used and various applications are studied in Chapter 1 as a literature review.

In Chapter 2, energy is harvested from a vertical fin-like structure by direct attachment of two different types of piezoelectric patches. Before attachment of these patches, a finite element model is constructed for the vertical fin-like structure in order to find the locations corresponding to maximum strains in the vibration modes of interest. Having decided these spatial locations, a finite element model is constructed to investigate the dynamic characteristics of the vertical fin-like structure after the attachment of these two different types of piezoelectric patches. Then, modal tests are performed to validate the finite element model and to investigate the energy harvesting performance of each piezoelectric patch. Finally, various performance checks are also done through wind tunnel tests.

Following these studies, a bimorph piezoelectric beam is designed in order to harvest energy from an aircraft structure and all related studies are presented in Chapter 3. The main aim of this chapter is to integrate a bimorph piezoelectric beam to an aircraft structure with the minimum effect on the passive dynamic characteristics of the host structure. The same plate structure is used again as a vertical fin-like structure and by considering the results of the finite element analysis of it (i.e. the minimum displacement locations of the vibration modes of interest), the location of the bimorph piezoelectric beam on the host structure is found. First of all, a finite element model is constructed to find the dynamic characteristics of the aircraft structure with bimorph piezoelectric beam. Then, an experimental modal analysis is conducted to validate the finite element analyses results. Finally, wind tunnel tests are performed to investigate the energy harvesting performance of the bimorph piezoelectric beam in real life scenarios.

Chapter 4 and Chapter 5 present the development of a flow harvester which works under vortex excitation. In this particular study, a commercial bimorph piezoelectric beam is used as a flow harvester. First of all, the fundamental resonance frequency of the harvester is tuned and validated by experimental techniques. In

Chapter 4, a cylinder is used as a bluff body to generate vortex. Then, in order to investigate the effect of the position and the diameter of the cylinder, an experimental setup is constructed. Moreover, the plate is used as a bluff body to generate vortex in Chapter 5. To find the best position, the size and angle of the plate, an experimental setup is constructed. The performance of the flow harvester is tested for both cylinder and plate in the wind tunnel. During the tests, the harvested energy is monitored for various diameters and the spatial locations of the cylinder and also various angles, sizes and locations of the plate. Finally, the results corresponding to each case are compared to find the best combination for maximum possible energy to be harvested.

Chapter 6 is devoted to design of an adaptive flow harvester. By using the knowledge gained through the results obtained in Chapter 4, an adaptive flow harvester having a bimorph piezoelectric beam is developed. It is known that the frequency content of a vortex flow depends on both flow velocity and size of a bluff body. Therefore, the diameter of the bluff body used in the adaptive flow harvester should automatically be changed regarding different flow velocities. For these purposes, a mechanism is developed and various kinematic and structural analyses are performed in order to validate the mechanism. Moreover, an efficiency analysis is performed to compare the required energy to drive the mechanism and the harvested energy via adaptive flow harvester.

Finally, Chapter 7 comprises concluding remarks focusing on the achievements and the recommendation for future work.

1. 4. Limitation of the Thesis

Finite element method is used to obtain the dynamic characteristics of the structures, however, analytical analysis cannot be performed because of the complexity of the structures.

MFC, which is a type of piezoelectric material and used as a piezoelectric energy harvester, is modelled as point mass in some finite element analysis due to very thin thickness of this structure.

The accelerometers used in experimental analysis are modelled as point mass in finite element analysis in order to simulate the mass loading effect of them.

Wind tunnel test is performed up to 17 m/s air speed due to the capacity of it.

Reynolds and Strouhal Number for wind tunnel test are calculated by omitting the wall effect of the wind tunnel.

Computational fluid dynamic analysis is not conducted prior to wind tunnel tests; therefore flow characteristics for all cases are not known very well. Results obtained during the wind tunnel tests are generally interpreted through literature.

CHAPTER 2

ENERGY HARVESTING FROM THE VERTICAL FIN-LIKE STRUCTURE BY DIRECT ATTACHMENT OF THE PIEZOELECTRIC PATCHES

2. 1. Introduction

In this chapter, a plate structure is selected as a vertical fin-like structure of an aircraft in order to attach the piezoelectric material directly. First of all, a finite element model is constructed to investigate the dynamic behavior of the vertical fin-like structure. Then, this model is validated by experimental vibration tests. By investigating the strain mode shapes of the vertical fin-like structure, position of the two different types of piezoelectric materials are decided as those materials can generate maximum voltage at the locations where maximum strain occur. BM500 [73] and MFC [74] types of piezoelectric materials are used and before the application of them, a finite element model is also constructed for the smart fin, which is so-called a vertical fin-like structure with piezoelectric materials. The analysis results of the finite element model is then compared by that of the ground vibration and the wind tunnel tests to investigate the voltage generation performance of the smart fin in real life conditions. Furthermore, the performance of the BM500 and MFC types of piezoelectric materials are also compared in order to understand the effect of two different materials on the passive host structure.

2. 2. Dynamic Model of the Vertical Fin-Like Structure

2.2.1 Finite Element Model of the Vertical Fin-Like Structure

In order to see the dynamic characteristics of the vertical fin-like structure, a finite element analysis is performed in ANSYS Workbench [14]. The geometry and dimension of the vertical fin-like structure can be seen in Figure 2. 1. Aluminum 6061-T6 [75], material properties of which are given in Table 2. 1, is used for this fin-like structure. First of all, modal analysis is done for vertical fin-like structure without PZT to find the first two natural frequencies and the corresponding strain mode shapes. In this analysis, cantilevered boundary condition is applied to the long edge of the structure and Solid 186 [14] is used for modeling purposes as seen in Figure 2. 1. The first two natural frequencies and associated strain mode shapes of the structure are given in Table 2. 2 and Figure 2. 2, respectively.

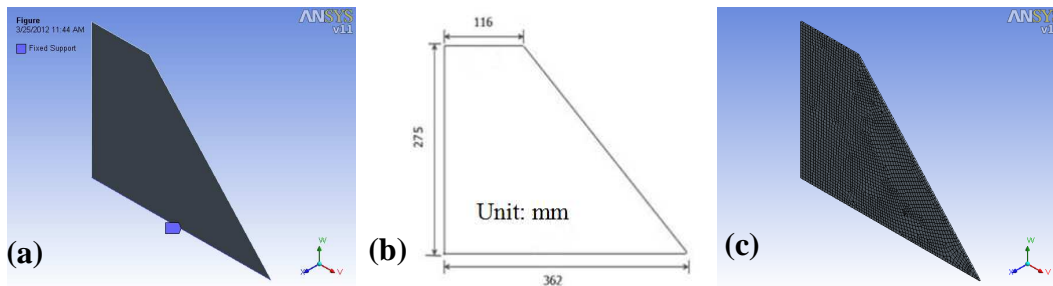


Figure 2. 1 Geometry (a), Dimension (b) and Mesh (c) of Fin-like Structure

Table 2. 1 Material Properties of AL-6061-T6 [58]

Material Properties of AL-6061-T6	
Modulus of Elasticity, E (GPa)	68.90
Density, ρ (kg/m ³)	2700
Poisson Ratio, ν	0.33

Table 2. 2 Natural Frequency of the Fin-like Structure

Natural Frequency (Hz)	
1 st Out-of-Plane Bending	27.13
2 nd Out-of-Plane Bending	89.03

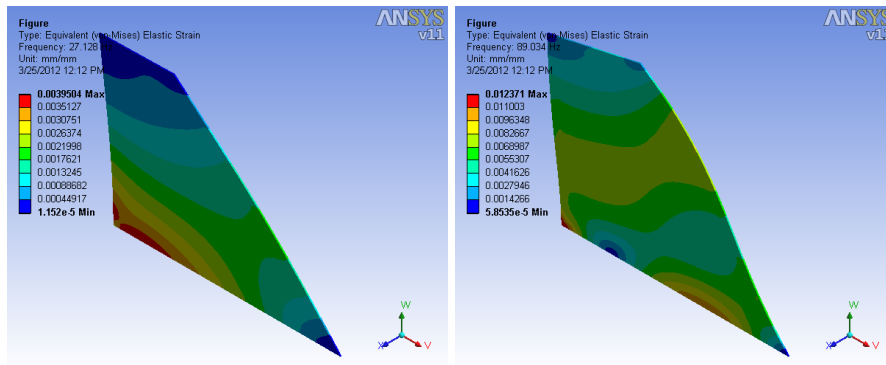


Figure 2. 2 Strain Mode Shapes of the Fin-like Structure

2.2.2 Experimental Validation of the Finite Element Model of the Vertical Fin-Like Structure

The experimental modal analysis is done for the vertical fin-like structure in order to validate the finite element analysis results. Experimental modal analysis (Figure 2. 3) is conducted by using a modal shaker and Bruel&Kjaer 4517-002 [76] accelerometer and frequency response function of the vertical fin-like structure are calculated through Pulse Software [77]. During the modal analysis, random vibration signal is sent to the vertical fin-like structure and the acceleration from three different locations is measured (Figure 2. 3). The frequency response of each location is also calculated and shown in Figure 2. 4. The experimental results are then compared with the finite element results in Table 2. 3 in order to show the accuracy of the finite element analysis.

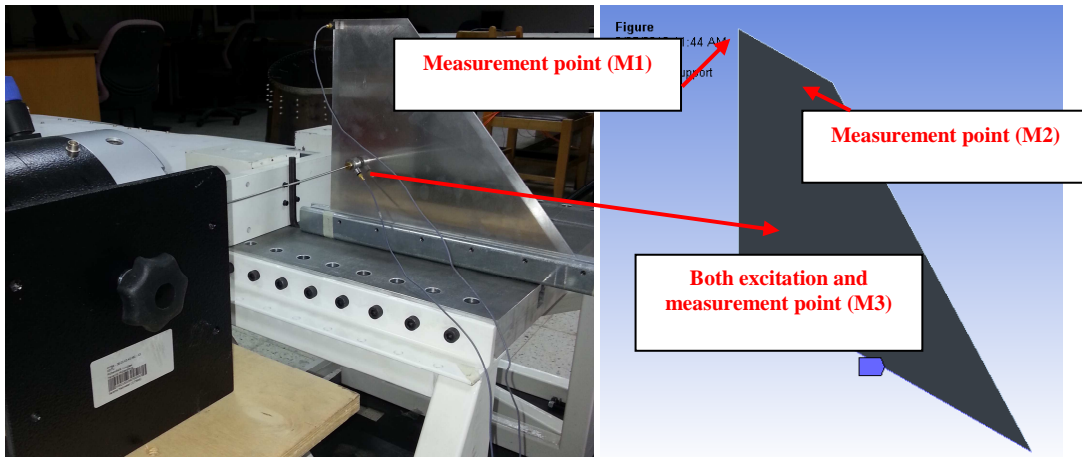


Figure 2. 3 Experimental Modal Analysis Setup for Vertical Fin-like Structure

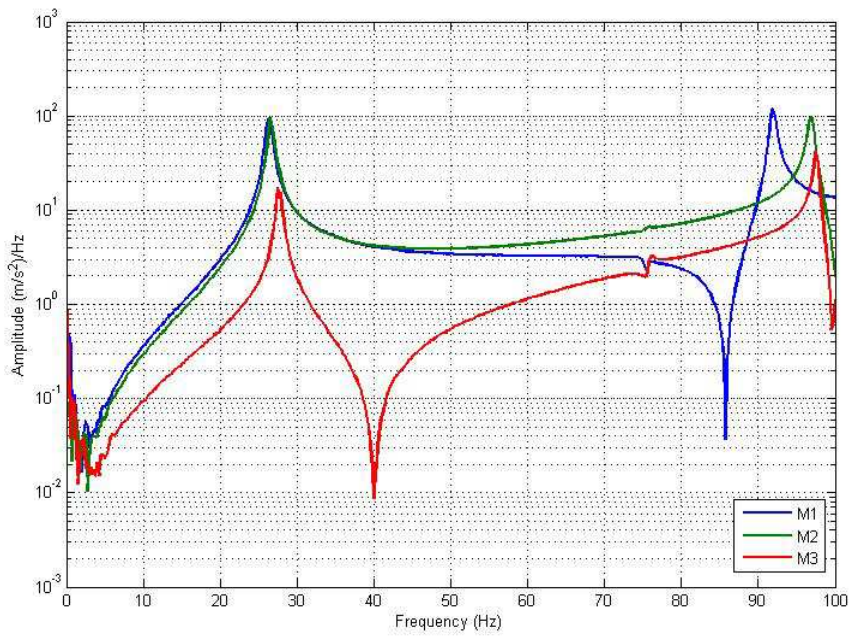


Figure 2. 4 FRF for Each Measuring Location

Table 2. 3 Natural Frequencies of the Fin-like Structure

	Finite Element (Hz)	Experimental (Hz)	Deviation (%)
1 st Out-of-Plane Bending	27.13	26.50	2.38
2 nd Out-of-Plane Bending	89.03	91.80	3.02

2.3. Construction of Smart Fin by Direct Attachment of BM500 to Vertical Fin-like Structure

2.3.1. Finite Element Model of the Smart Fin comprising BM500 Patches

It is known that piezoelectric material (PZT) can create more voltage when it is located at a high strain spatial location. In order to increase the voltage response of PZT, it should be placed on the maximum strain location of vertical fin-like structure. Therefore, BM500 PZTs are located by considering this condition and the places of these PZTs are selected by investigating the strain mode shape of the vertical fin-like structure given in Figure 2.2. The location and geometry of the BM500 PZTs can also be seen in Figure 2. 5. Modal analysis is then performed by ANSYS Workbench for this smart structure and the natural frequencies for the smart fin and the vertical fin-like structure are compared in Table 2. 4. Moreover, strain mode shapes of the smart fin are also given in Figure 2. 6.

As it is seen from the analyses results, the passive dynamic characteristic of the vertical fin-like structure is not affected from the placement of the BM500 type piezoelectric patches.

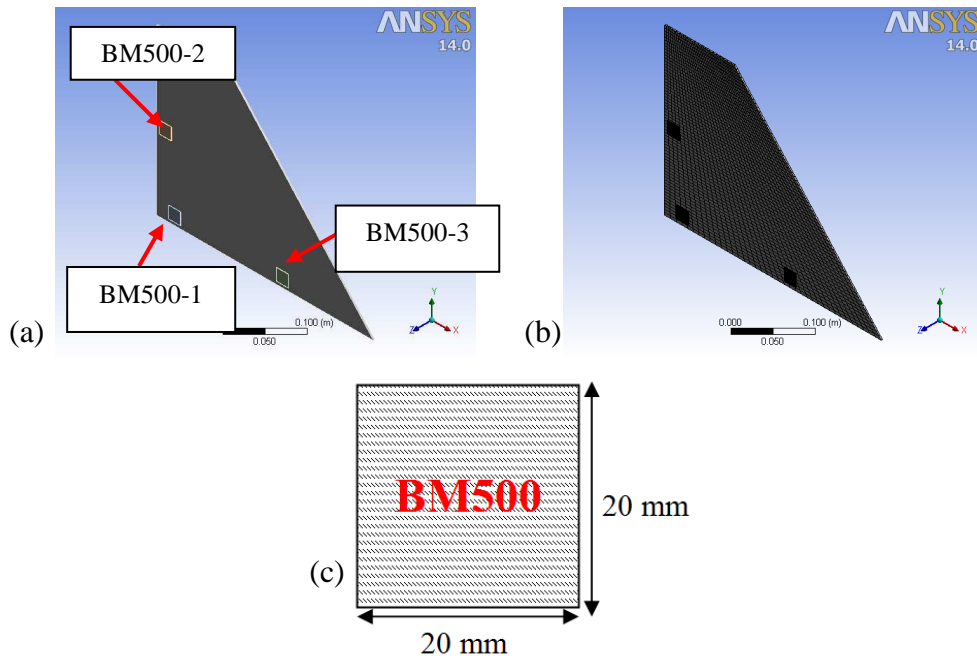


Figure 2. 5 Smart Fin (a) Geometry (b) Mesh (c) BM500 Geometry

Table 2. 4 The First Two Resonance Frequencies of the Smart Fin

Natural Frequency (Hz)		Difference from Table 2.2 (%)
1 st Out-of-Plane Bending	27.39	0.95
2 nd Out-of-Plane Bending	88.67	0.41

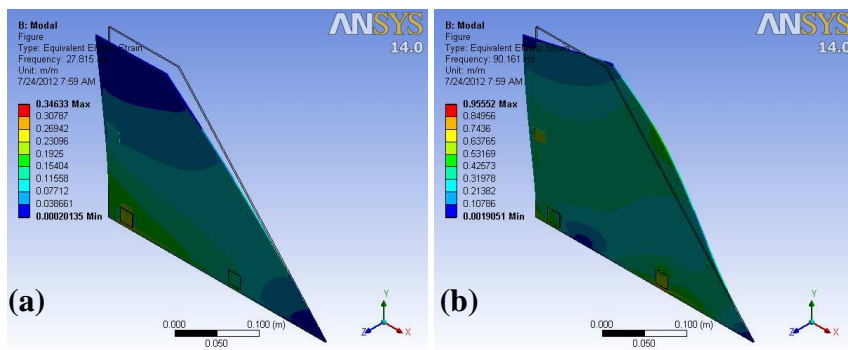


Figure 2. 6 Mode Shape of Smart Fin (a) 1st Out-of-Plane Bending (b) 2nd Out-of-Plane Bending

2.3.2. Experimental Validation of Finite Element Model of the Smart Fin comprising BM500 Patches

In order to validate the finite element analysis for the smart fin, three BM500 piezoelectric patches are attached to the fin-like structure. Then, experimental modal analysis is conducted to obtain the natural frequencies. Moreover, under random vibration loading, the voltage generation of each PZTs is also analyzed experimentally.

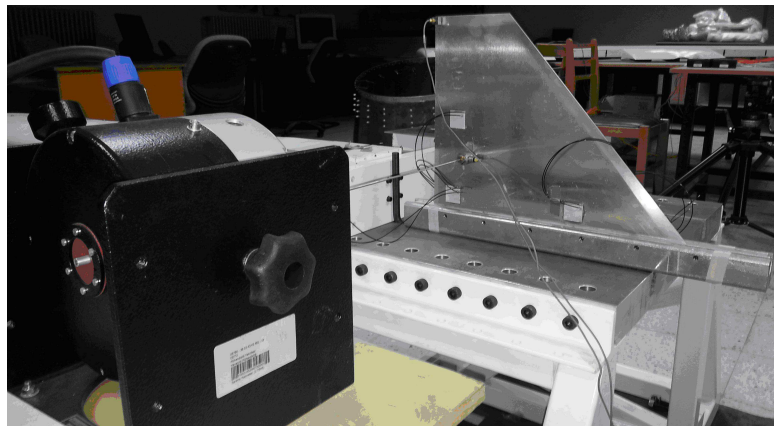


Figure 2. 7 Experimental Modal Analysis Setup for Smart Fin

Frequency response functions (FRFs) taken for the each location on the smart fin, which are same as the ones obtained from the vertical fin-like structure, are obtained by PULSE software and they are presented in Figure 2. 8. As seen from this figure, there is a new resonance frequency around 85 Hz and it is caused by the interaction between the stiffener of the shaker and the smart fin. Therefore, another modal test is performed by impact hammer with the existence of the attached shaker and without shaker to further investigate this case and the obtained results are given in Figure 2. 9.

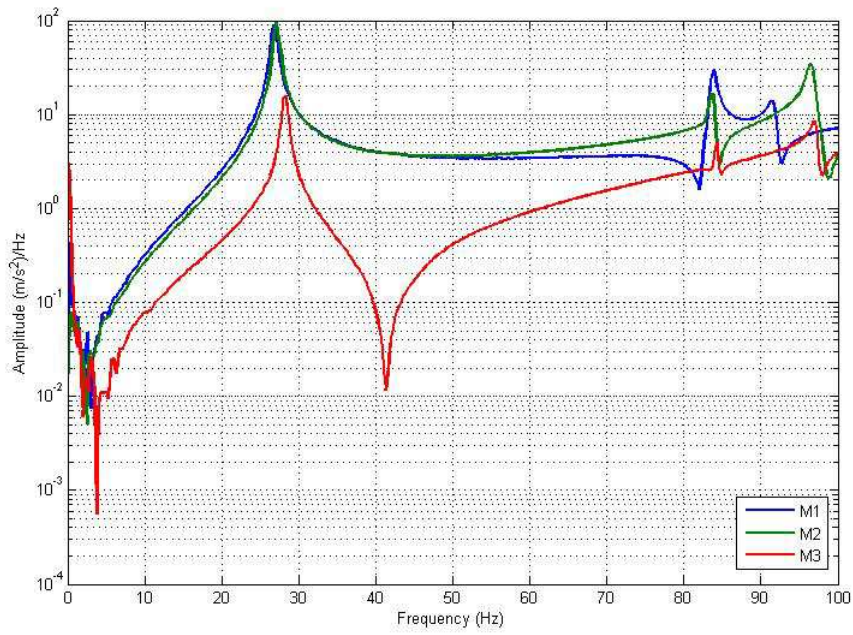


Figure 2. 8 FRF for the Smart Fin

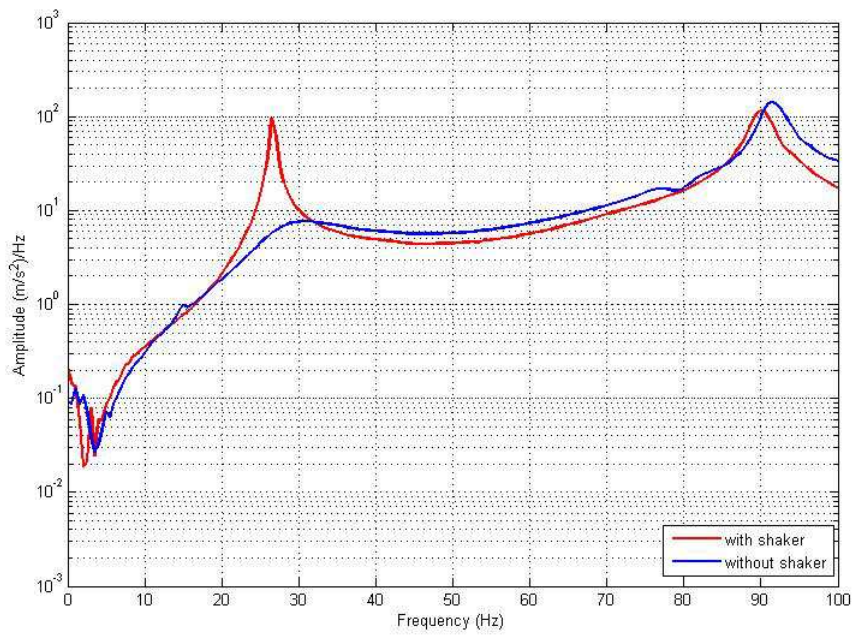


Figure 2. 9 Effect of the Stiffener of Shaker

Table 2. 5 Natural/Resonance Frequencies of the Fin-like Structure with PZT

	Finite Element (Hz)	Experimental (Hz)	Deviation (%)
1 st Out-of-Plane Bending	27.40	26.50	3.40
2 nd Out-of-Plane Bending	88.70	90.00	1.40

2.4. Construction of the Smart Fin by Direct Attachment of MFC to Vertical Fin-Like Structure

2.4.1. Finite Element Model of the Smart Fin comprising MFC Patches

In the previous section, the vertical fin-like structure is used as a host structure in the energy harvesting studies. BM500 is attached to the maximum strain locations to maximize the harvested energy. In this particular study, both finite element and experimental work are used to validate the proposed procedure. In order to compare different types of piezoelectric materials, micro fiber composite (MFC) [74] type piezoelectric patches (Figure 2. 10) are also attached to the other side of vertical fin-like structure. In this study, M2814-P3 is used and material properties of this piezoelectric patch can be found in [74]. Three M2814-P3s are placed to the fin-like structure (Figure 2. 11) at the same location of BM500s but on the opposite side of the host structure.

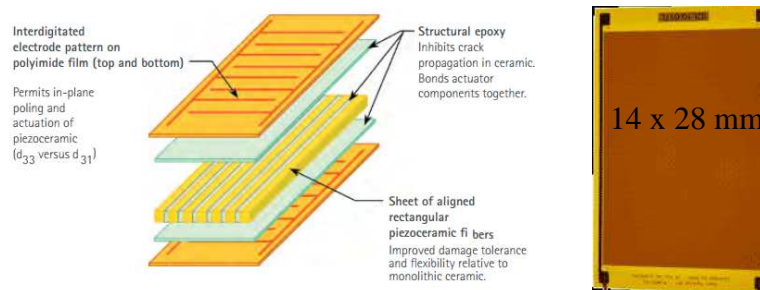


Figure 2. 10 Structure of MFC [74] and Geometry of M2814-P3

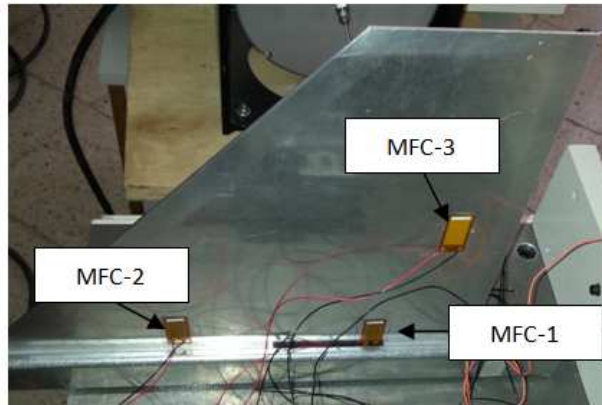


Figure 2. 11 Locations of the MFC Patches on Fin-like Structure

It is known that the geometric properties of both MFC and BM500 are different and therefore in order to compare the voltage outputs of them, a finite element model is constructed in ANSYS Workbench [14]. SOLID 186 [14] type of element is used for vertical fin and SOLID 225 [14] is used for piezoelectric patches (Figure 2. 12). The finite element mesh consists of 28500 elements and 4500 nodes in total. Full harmonic response analysis [14] is then performed to compare the voltage generation performance of the different type of piezoelectric patches. In this analysis, a point mass is added to the model so as to simulate the mass loading effect of the accelerometer located at the tip of the fin-like structure which is also used in the experimental study.

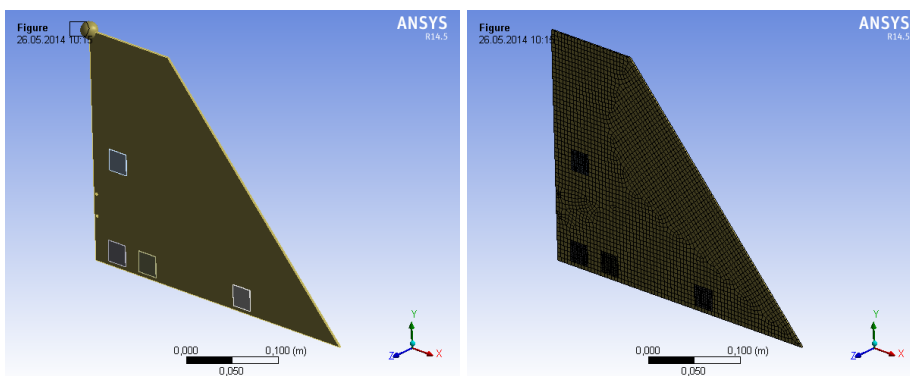


Figure 2. 12 Finite Element Model of the Vertical Fin-like Structure

In the harmonic analysis, structure is excited in the range of 14-40 Hz by keeping the tip deflection at the values of 1 mm and the displacement response of the structure at the same location is obtained and presented in Figure 2. 13. The resonance frequency of the smart fin is found as 28.00 Hz from the same figure.

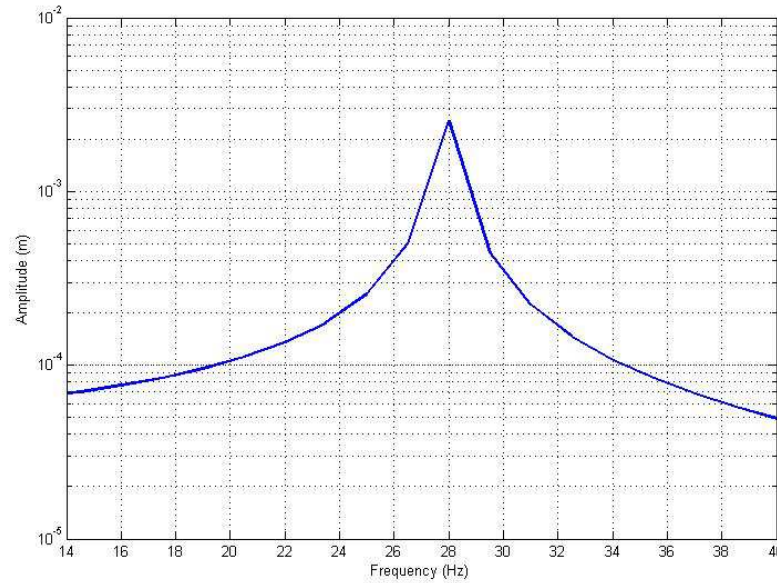


Figure 2. 13 Displacement Response of the Smart Fin at the Tip

The voltage response of the each piezoelectric patch is also calculated by harmonic analysis at the resonance frequency and the results are given in Figure 2. 14 and Figure 2. 15. Results obtained from the MFC piezoelectric materials are normalized to 1 and that of obtained from the BM500 piezoelectric materials are normalized with respect to the MFCs. Comparison of these results is also presented in Table 2. 6.

As it is seen from Table 2. 6, BM500 type piezoelectric patch can create voltage output approximately three times higher than that of MFC type piezoelectric patch. It is known that g_{31} of BM500 (-11.5×10^{-3} Vm/N) is almost same as M2814-P2 (-11.2×10^{-3} Vm/N); however, BM500 is three times thicker than MFC patch. This

explains why BM500 piezoceramic patch generates three times higher voltage output than that of MFC patch in the finite element analysis.

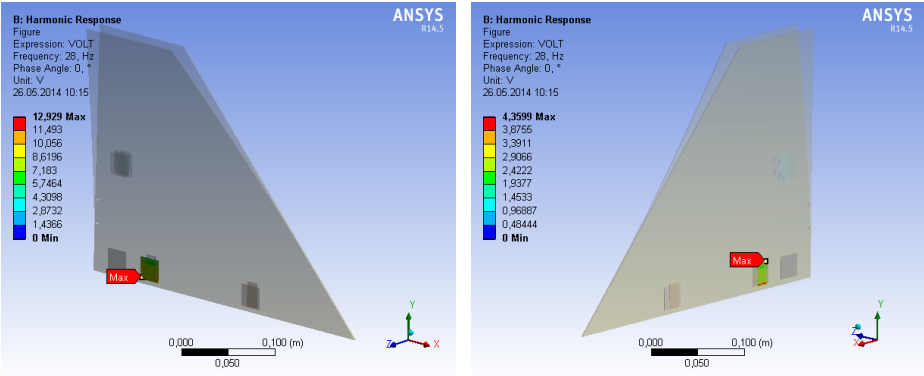


Figure 2. 14 Voltage Response of BM500-1 and MFC-1

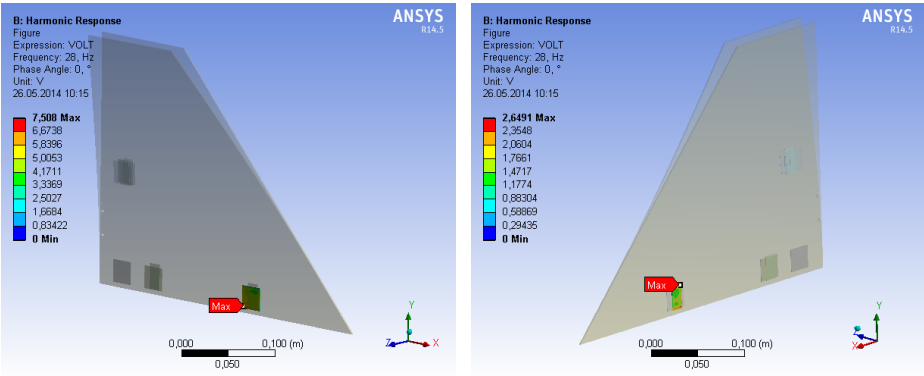


Figure 2. 15 Voltage Response of BM500-2 and MFC-2

Table 2. 6 Voltage Response of BM500-1, MFC-1, BM500-2 and MFC-2

	Normalized Voltage Response at Resonance, 28.00 Hz (V/V)
BM500-1	2.97
MFC-1	1
BM500-2	2.83
MFC-2	1

2.4.2. Experimental Validation of Finite Element Model of the Smart Fin comprising MFC Patches

Experimental modal analysis is done by hammer test to validate the finite element analysis. In this test, modal hammer (Bruel&Kjaer 8206 [78]) and miniature accelerometer (Bruel&Kjaer 4517-002 [76]) are used. Frequency response function of the smart structure is obtained by PULSE Software [77] and it is given in Figure 2. 16. As it can be seen from this particular FRF, the first two resonance frequencies of the smart structure are found as 27.50 and 92.50 Hz. They are very close to the resonance frequencies of the smart fin with BM500 (i.e. $f_1=26.50$ Hz and $f_2=91.65$ Hz). Therefore it can be concluded that the passive dynamic characteristics of the fin-like structure is not altered much with the inclusion of the bonded MFC patches.

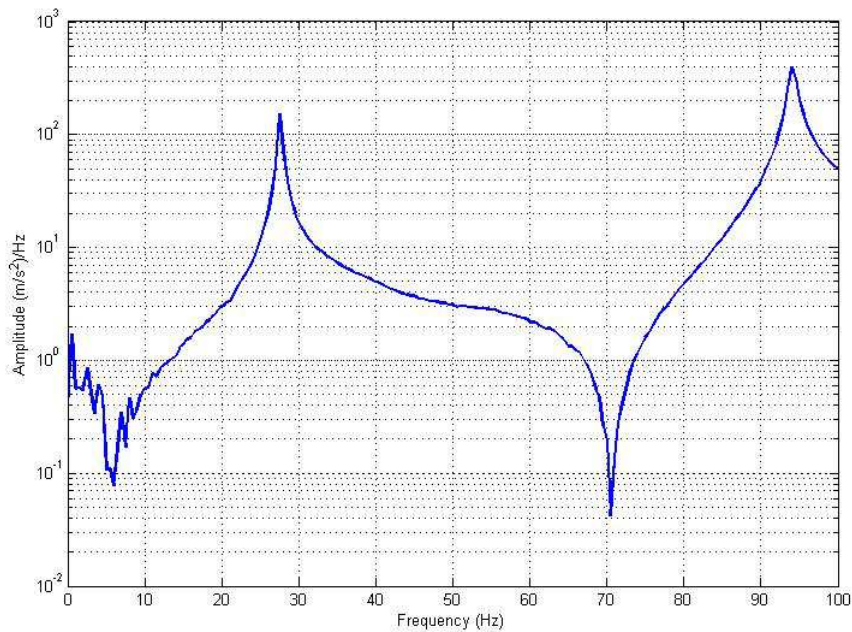


Figure 2. 16 FRF of the Smart Fin

2.5. Energy Harvesting Performance of the Smart Fin

2.5.1. Ground Vibration Test of the Smart Fin

In order to investigate the performance of both MFC and BM500 patches, a ground vibration test is performed by modal shaker. In this test, an excitation signal (i.e. sinus input at 27.5 and 92.5 Hz) is given to the smart fin as 1g tip acceleration and its is controlled by a miniature accelerometer (Bruel&Kjaer 4517-002 [76]). During the test, NI Data Acquisition System [7961] is used to obtain the voltage output of each piezoelectric patch. The test setup can be seen in Figure 2. 17. The voltage output of the BM500s and MFCs (locations can be seen in Figure 2. 11) are also given in Figure 2. 18 to Figure 2. 20.

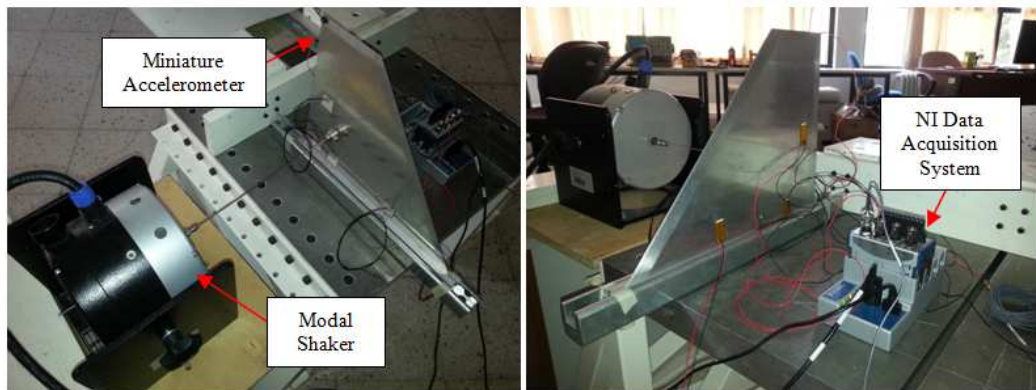


Figure 2. 17 Experimental Setup for Smart Fin

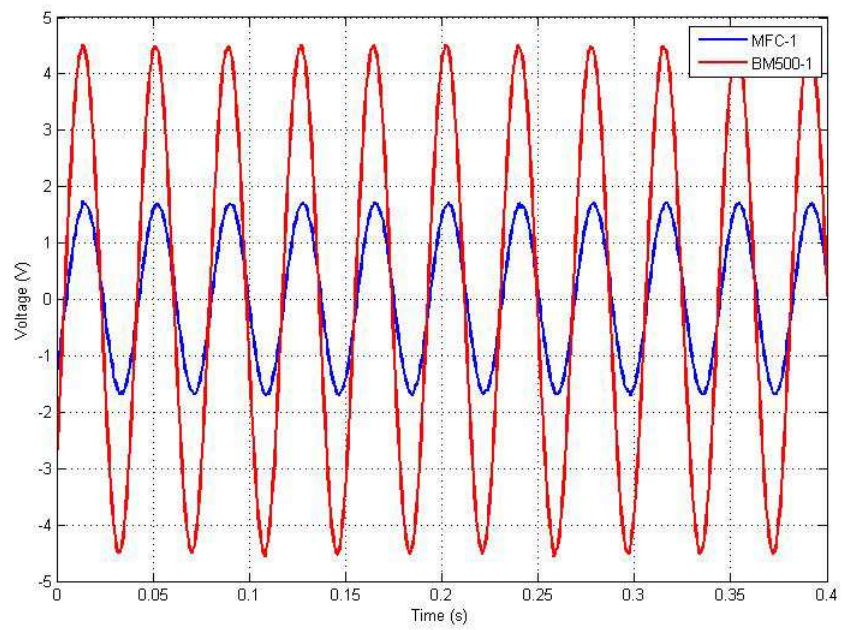


Figure 2. 18 Voltage Output of MFC-1 and BM500-1 (at 27.5 Hz)

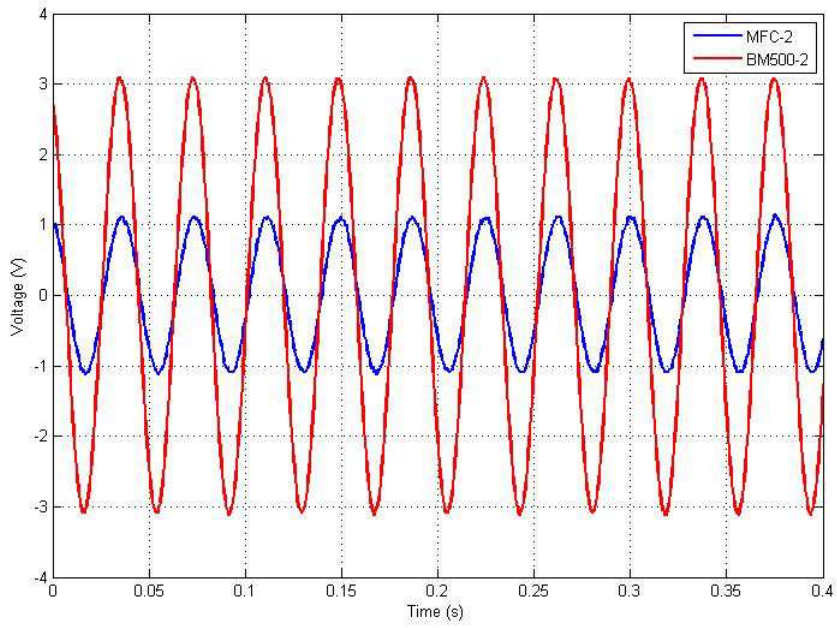


Figure 2. 19 Voltage Output of MFC-2 and BM500-2 (at 27.5 Hz)

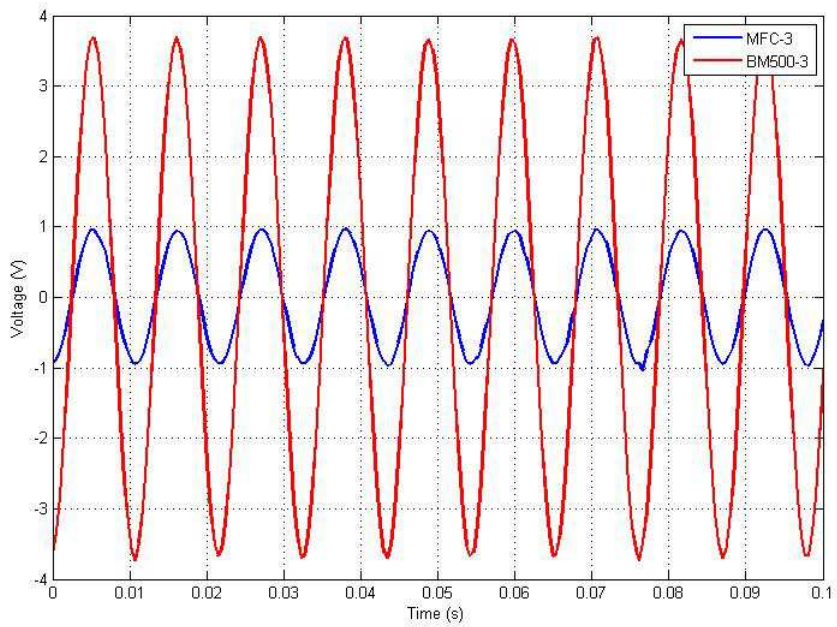


Figure 2. 20 Voltage Output of MFC-3 and BM500-3 (at 92.5 Hz)

In this test, energy harvesting electronic (i.e. a rectifier circuit) [80], which is acquired from Smart Material GmbH, is also used to convert AC type voltage to DC type one through BM500-1 and MFC-1. The rectifier circuit and the obtained results can be seen in Figure 2. 21.

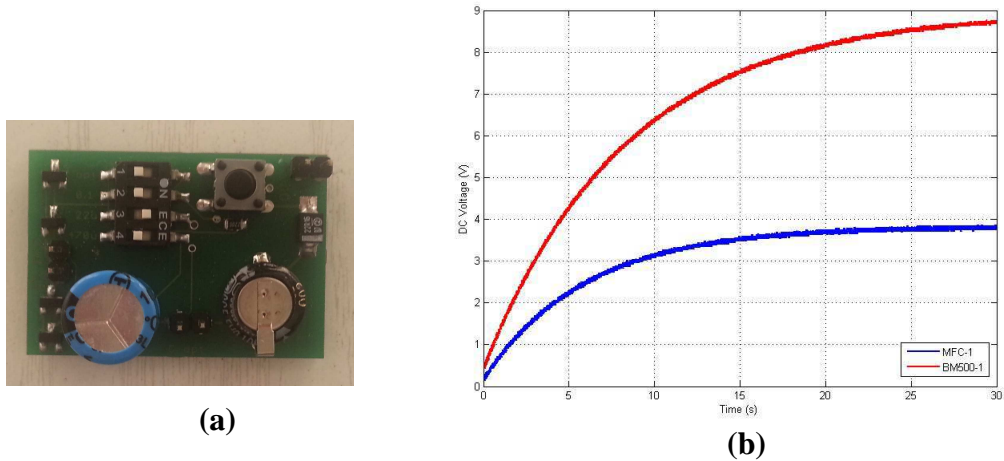


Figure 2. 21 (a) Energy Harvesting Module (b) DC Voltage Output of the BM500-1 and MFC-1

2.5.2. Wind Tunnel Test of the Smart Fin

In order to investigate the energy harvesting performance of the piezoelectric patches, MFC and BM500, in real life conditions, a wind tunnel test is conducted. Schematic view of wind tunnel is given in Figure 2. 22 and the setup for this test is shown in Figure 2. 23. During the test, the voltage generated from every individual patch is obtained by NI CompactDAQ [79]. The position and the name of each piezoelectric patch are already given in Figure 2. 5 and Figure 2. 11.

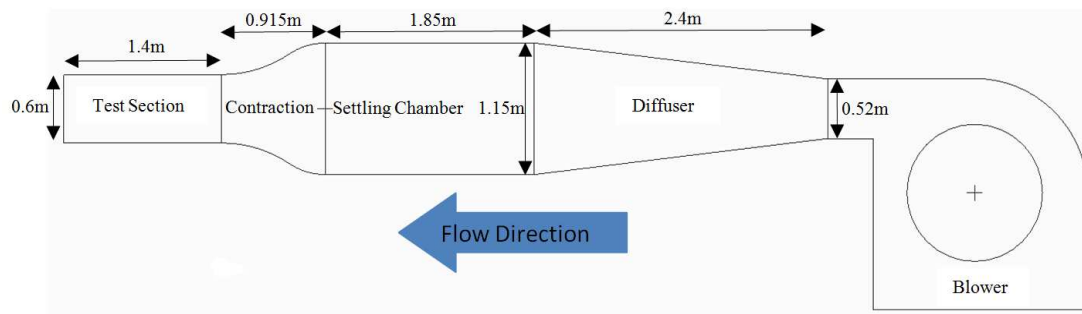


Figure 2. 22 Schematic View of the Wind Tunnel

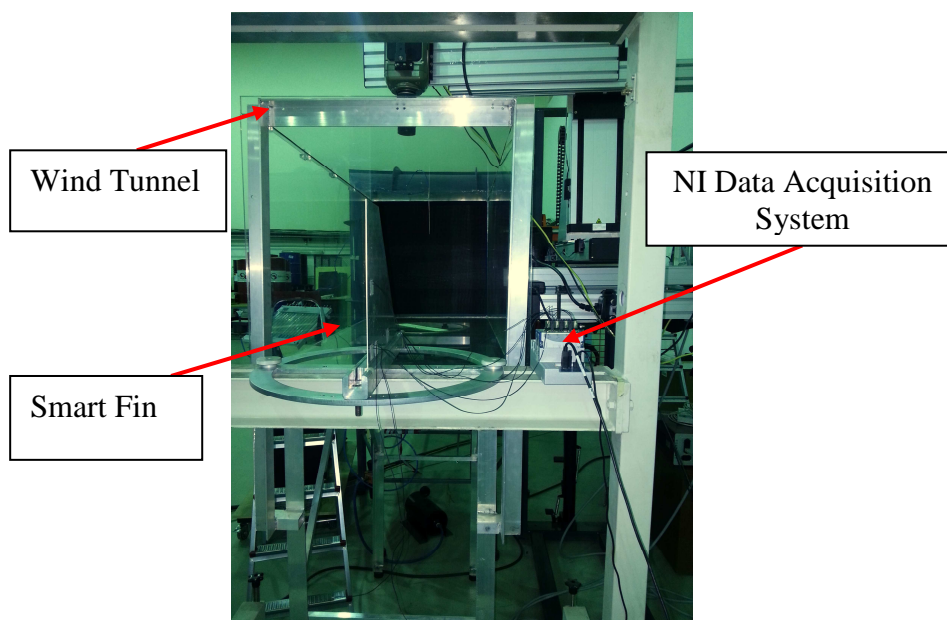


Figure 2. 23 Wind Tunnel Test Setup

Vortex generator is used to excite the smart fin around its first natural frequency. If the vortex shedding frequency is close to the first resonance frequency of the smart fin, it is possible to excite the smart fin and the voltage generation of the piezo patch will be high. For this reason, 0.05 m diameter cylinder is used in the wind tunnel. Strouhal Number (St) can be taken as 0.2 for Reynolds Number (Re) $< 10^5$ for subcritical flow [81]. For the test condition, the flow is assumed to be

subcritical and the St is also taken as 0.2. The vortex shedding frequency should be at around 27.68 Hz which is the frequency corresponding to the first out-of-plane bending mode of the smart fin. By using these parameters and the equation 2.1, the flow speed can be calculated as 6.92 m/s.

$$St = \frac{f_s D}{U} \quad (2.1)$$

where; St is Strouhal Number, D is the diameter of cylinder, f_s is the vortex shedding frequency and U is the flow speed. Finally, the test setup for the vortex generator (Figure 2. 24) can be constructed [82] by taking X as 0.2 m and Y as 0.025 m.

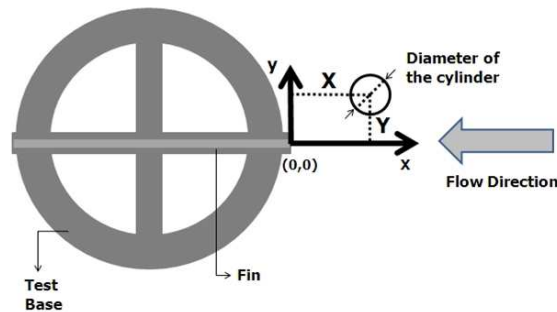


Figure 2. 24 Vortex Generator Test Setup [82]

During the tests, time series of each piezo voltage output is collected by NI Data Acquisition System. The results obtained with the existence of the vortex generator are presented in Figure 2. 25 to Figure 2. 27.

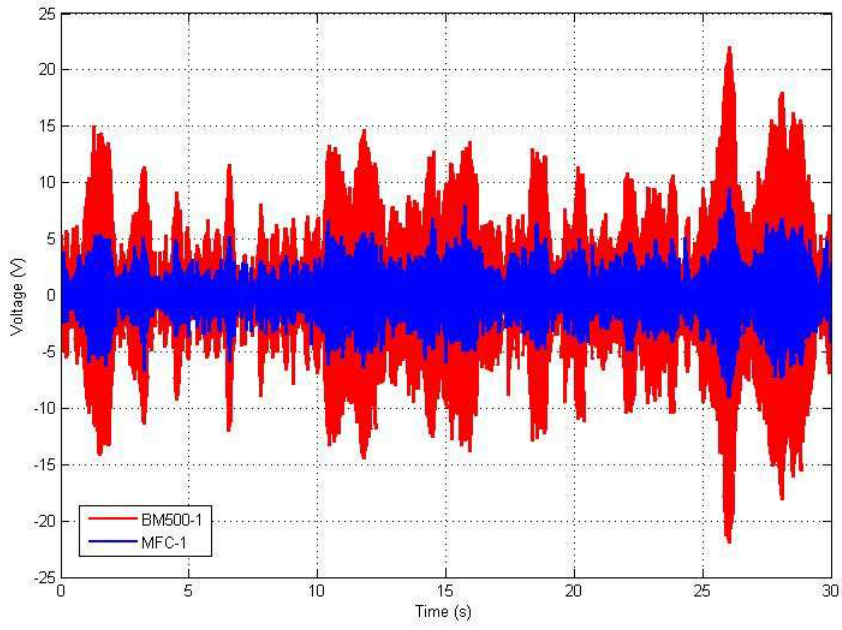


Figure 2. 25 Voltage Output of BM500-1 and MFC-1

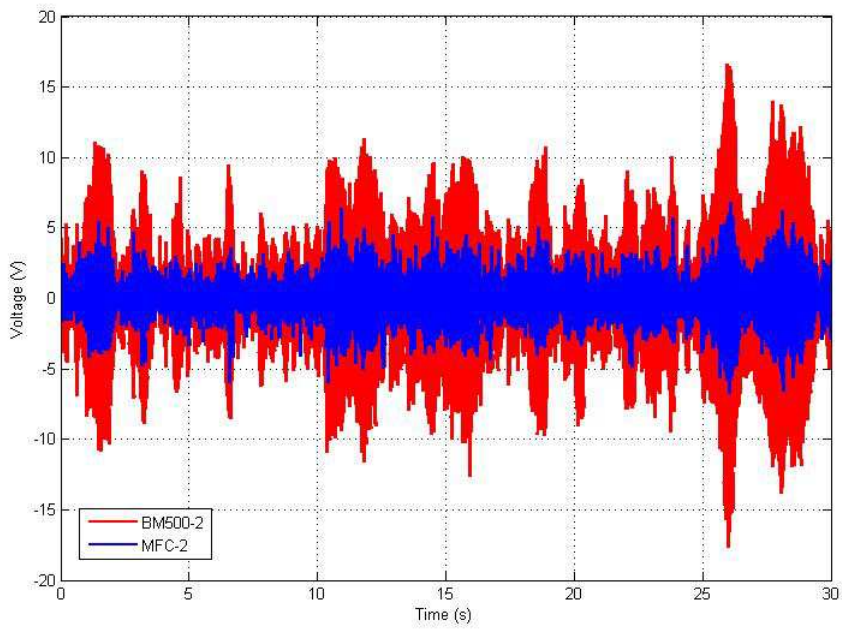


Figure 2. 26 Voltage Output of BM500-2 and MFC-2

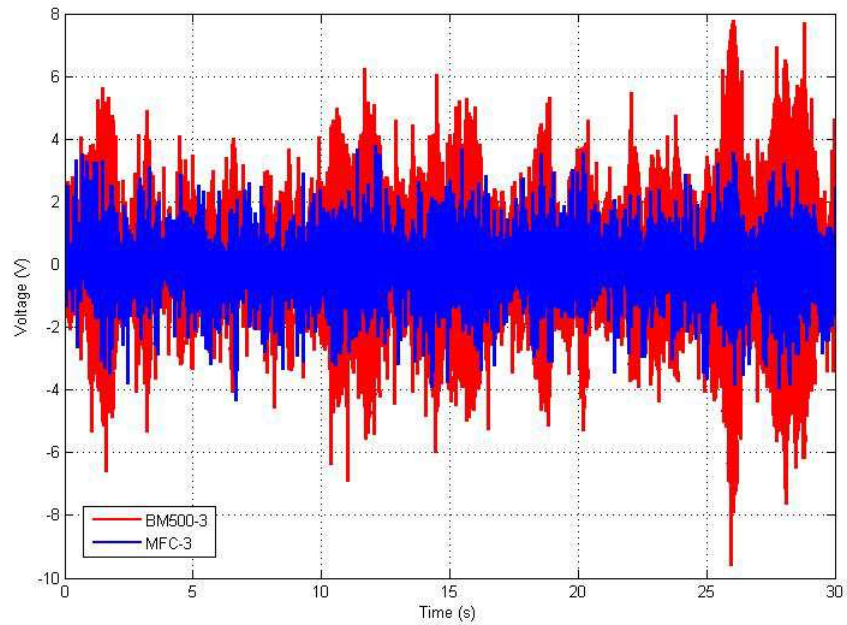


Figure 2. 27 Voltage Output of BM500-3 and MFC-3

By taking the FFT of the recorded time series of piezoelectric patches in MATLAB [83], the response of the smart fin is found in the frequency domain and given in Figure 2. 28 and Figure 2. 29. The first two resonance frequencies of the smart fin can also be obtained from these two figures and they appear to be very close to the results of both finite element and experimental modal analysis.

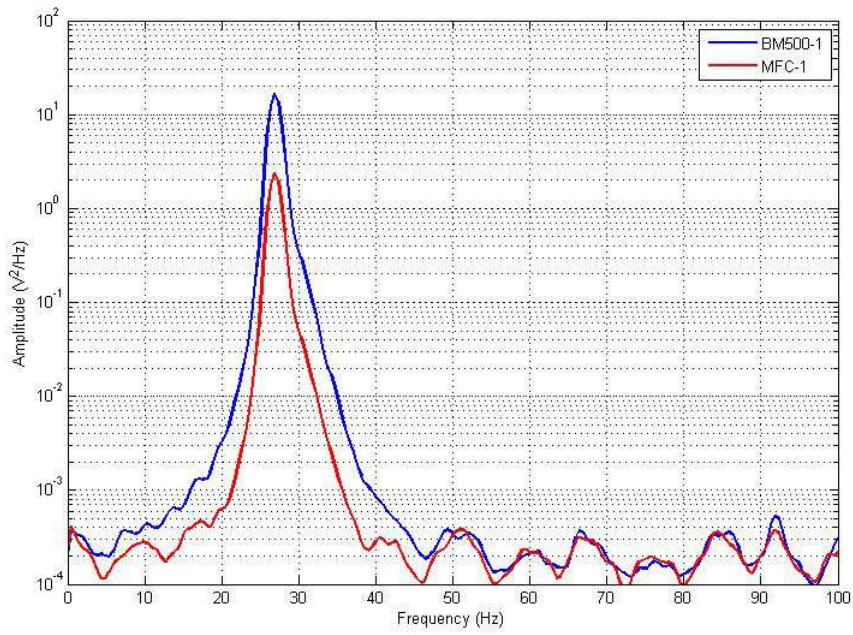


Figure 2. 28 FFT of the signal obtained from BM500-1 and MFC-1

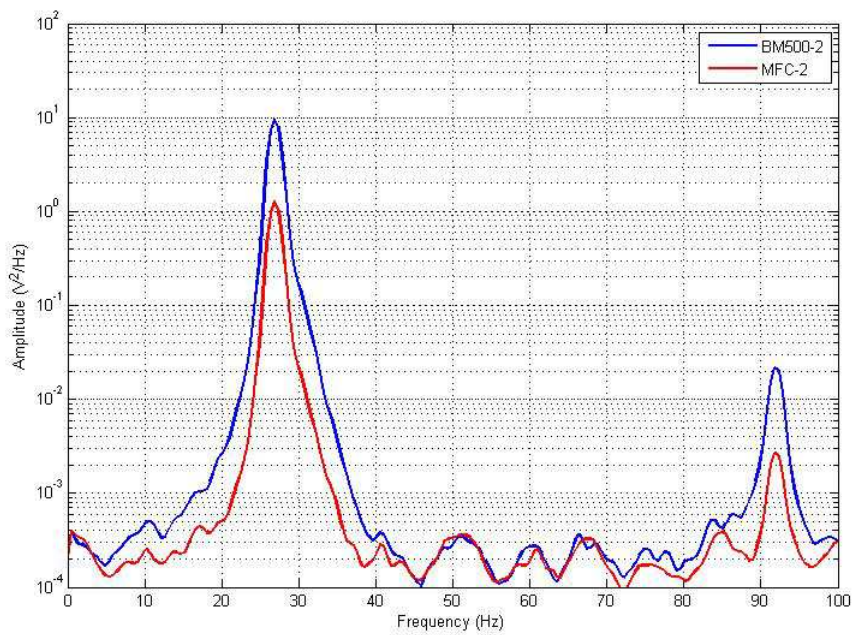


Figure 2. 29 FFT of the signal obtained from BM500-2 and MFC-2

As it is previously observed from the wind tunnel test results, piezoelectric patches generate AC voltage during the excitation of the smart fin. It is practically not possible to use this type of voltage to operate a system or charge a battery. In order to make this voltage useable, rectifier circuit should be used. Therefore, a rectifier circuit [80] converting AC voltage to DC one is used during the wind tunnel tests. BM500-1 and MFC-1 are connected to this circuit and AC voltage generation of this piezoelectric patch is rectified to the DC one and the result for this test is shown in Figure 2. 30. As it can be seen from DC voltage outputs, they are lower than AC voltage outputs of the piezoelectric materials due to efficiency of the rectifier circuit. Additionally, BM500 and MFC do not generally provide constant AC voltage and this may also affect the DC voltage output.

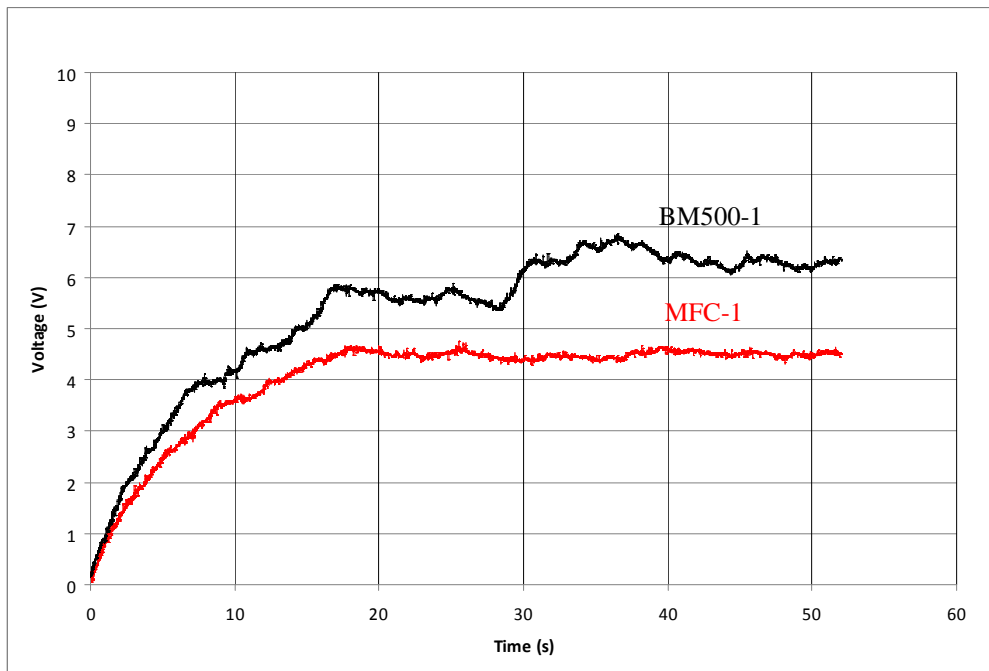


Figure 2. 30 DC Voltage Generation of BM500-1 and MFC-1

2.6. Conclusion

In this study, two different types of piezoelectric patches are directly attached to the vertical fin-like structure to harvest energy under air loading. Before attachment of these materials, a finite element model is constructed in order to find the suitable positions of the piezoelectric patches. The objectives are to increase the voltage output of the piezoelectric patch and at the same time not to change the passive dynamic characteristic of the vertical fin. After the attachment of these patches, a finite element analysis is also performed to investigate the dynamic behavior of the smart fin which is also validated through an experimental modal analysis.

The energy generation of the piezoelectric patches on the vertical fin-like structure is also examined by both ground vibration and wind tunnel tests. The results indicated that, in order to reach higher voltage levels, the smart fin should be excited at around its resonances as the maximum strain levels can be achieved.

Moreover, the dynamic characteristics of the smart fin are also obtained under the operational conditions (i.e. wind tunnel tests with vortex generator) by simply taking the FFT of the time series of piezo patches.

Additionally, a rectifier type of circuit is used to convert AC voltage of piezoelectric patches to DC one by making the voltage generation of piezoelectric patches useable for the energy harvesting systems.

Finally, the study is showed that energy can be harvested from an aircraft structure by attaching various piezoelectric patches without changing the passive dynamic characteristic of the host structure.

CHAPTER 3

ENERGY HARVESTING FROM VERTICAL FIN-LIKE STRUCTURE BY ATTACHMENT OF THE BIMORPH PIEZOELECTRIC BEAM

3. 1. Introduction

In general, before integrating any external structure to an aircraft, dynamic characteristic of the aircraft should be investigated before and after the integration to investigate the effect of this structure. Sometimes, it is impossible to avoid the change in dynamic characteristic of the aircraft and therefore special precautions should be taken not to degrade the dynamic performance of the aircraft. However, the best solution is to integrate the structures without any impact on the passive dynamic characteristic of the aircraft. Therefore, dynamic characteristic of the aircraft should be very well known in advance and for this reason, analytical and/or finite element methods can be used. If the structure is complex, it is very hard to use analytical methods and thus finite element methods turn out to be the only way to find the dynamic characteristic of the aircraft. In this research study, finite element method is used to obtain the passive dynamic characteristic of the vertical fin-like structure. By performing a modal analysis through a finite element method, the natural frequencies and the corresponding displacement mode shapes are determined. After these analyses, the location for the beam harvester can be determined by

observing the displacement mode shapes of the structure. This particular finite element analysis is then validated via experimental techniques.

3.2. Attachment of the Bimorph Piezoelectric Beam to the Vertical Fin-Like Structure

The dynamic behavior of the aluminum 6061-T6 [58] vertical fin-like structure is already found by a finite element modeling and analysis in Chapter 2. In order to recall the results of modal analysis, the first two natural frequency of the vertical fin-like structure are given in Table 3.1.

Table 3. 1 The First Two Natural Frequencies of the Vertical Fin-like Structure

Mode Type	Finite Element Analysis Results (Hz)
1st Out-of-plane Bending	27.76
1st Torsion	90.14

In Chapter 2, the strain mode shapes of the vertical fin-like structure are provided as the location of the piezoelectric patches are decided by considering the maximum strain locations on the vertical fin-like structure at each natural frequency of interest. In Chapter 3, on the other hand, the main aim is not to change the dynamic characteristics of the vertical fin-like structure by attaching a bimorph piezoelectric beam and therefore the displacement mode shapes for the first two natural frequencies are obtained and given in Figure 3. 1 and Figure 3. 2.

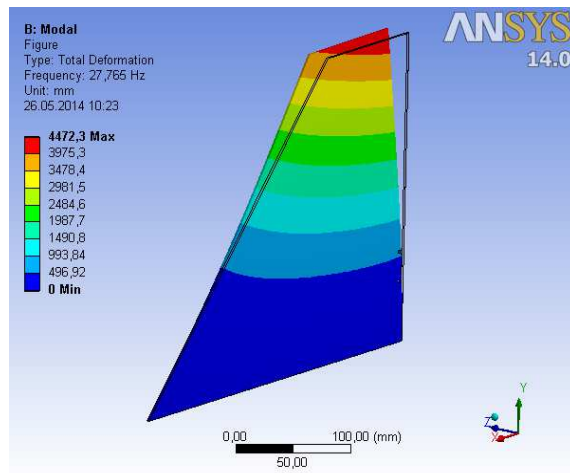


Figure 3. 1 Displacement Mode Shape - 1st Out-of-plane Bending

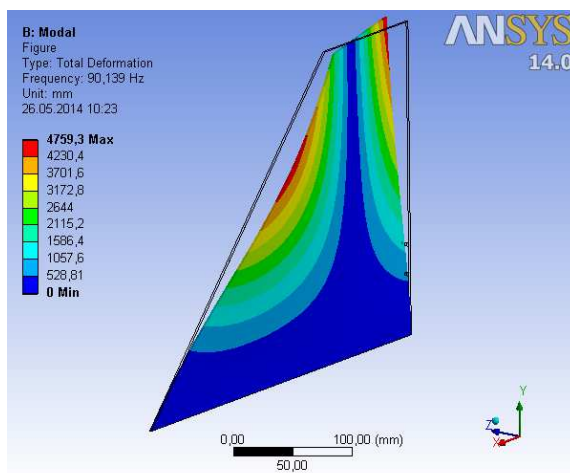


Figure 3. 2 Displacement Mode Shape - 1st Torsion

In order to harvest energy from the vertical fin-like structure, a bimorph piezoelectric beam is attached on its surface. Bimorph piezoelectric beam is formed by Macro Fiber Composite (MFC) type of piezoelectric material [57]. This is a special material due to its flexibility and energy harvesting capacity. Two identical MFCs are placed and glued to either side of the aluminum beam (Figure 3.3). After this process, bimorph piezoelectric beam is ready for integration onto the vertical fin-like structure. During the integration process, the main objective is not to change the

passive dynamic properties of the vertical fin-like structure drastically, in other words, the natural frequencies of the fin should not be affected much from the existence of the bimorph piezoelectric beam harvester. For this reason, optimization process is performed in order to find the suitable position for the bimorph piezoelectric beam. In the optimization process, position of the bimorph piezoelectric beam is found by considering the displacement mode shapes of the fin-like structure comprising the first out-of-plane plane bending and the torsional one (Figure 3. 1). Minimum displacement location in the aforementioned two mode shapes is chosen to position the bimorph piezoelectric beam. After finding the proper position of the bimorph piezoelectric beam, experimental analysis is performed to validate the finite element analysis results.

3.2.1. Finite Element Model of the Vertical Fin-Like Structure with the Bimorph Piezoelectric Beam

MFC type piezoelectric material is used to construct bimorph piezoelectric beam. Schematic representation of the beam and its position is given in Figure 3.3. The dimension of the aluminum beam is 103x31x2 mm (LengthxWidthxThickness). The details and the geometric properties of MFC can also be seen in Figure 3.3. The bimorph piezoelectric beam is integrated to the vertical fin-like structure by so-called a separator and is fixed by two M3 screw and nuts. Mechanical details of the integration can be seen in Figure 3. 4.

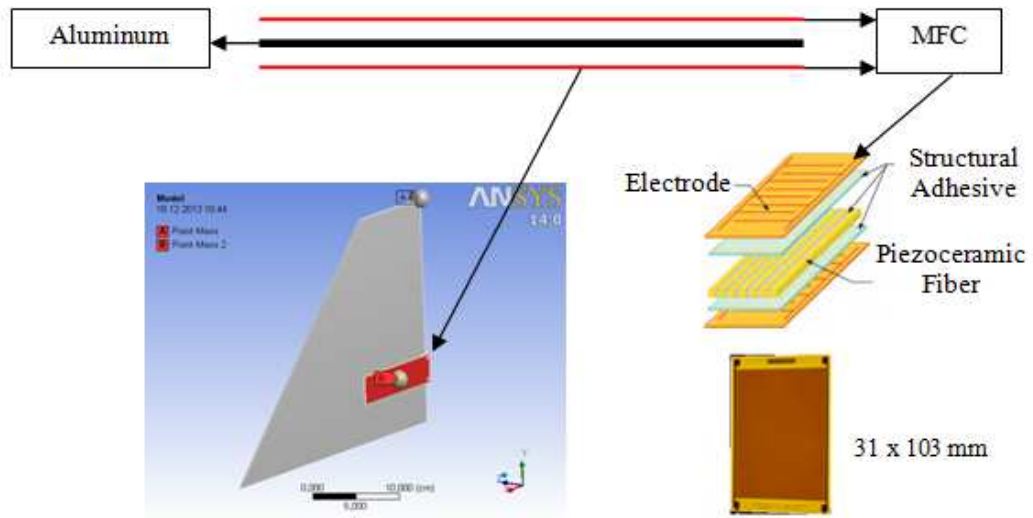


Figure 3. 3 Bimorph Piezoelectric Beam and the Host Fin-like Structure

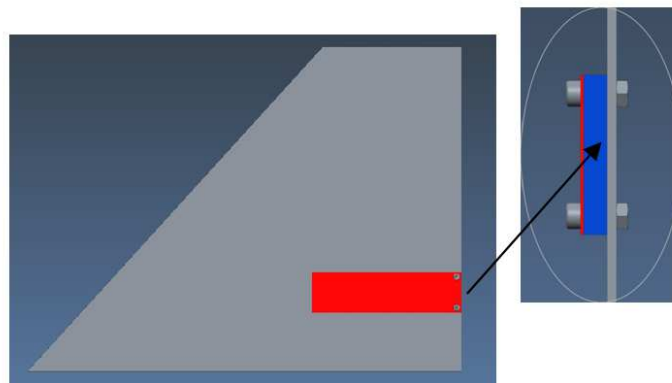


Figure 3. 4 Mount Detail of the Bimorph Piezoelectric Beam

Finite element model for the vertical fin-like structure with bimorph piezoelectric beam is also constructed in ANSYS Workbench [14] to find the first two natural frequencies of the vertical fin and the bimorph piezoelectric beam. Finite element mesh of this model has 32000 elements and 4500 nodes in total. In this particular model, MFC is modeled as point mass due to its flexibility and thickness. The fixed boundary condition is given to the long horizontal edge of fin. After

performing modal analysis in finite element software, the first three natural frequencies of the structure are found and compared with finite element results of vertical fin-like structure without bimorph piezoelectric beam in Table 3. 2 in order to investigate the effect of the bimorph piezoelectric beam on the dynamic characteristics of the passive vertical fin-like structure. The corresponding mode shapes are also shown in Figure 3. 5 to Figure 3. 7.

As it can be seen from the analysis results, after the integration of the bimorph piezoelectric beam harvester, the natural frequencies of the fin are slightly changed and the fundamental natural frequency of the piezoelectric beam is observed to be well separated from the rest of the frequencies. By looking the newly obtained mode shapes of the vertical fin-like structure with harvester, it is seen that they are similar to results of vertical fin-like structure without the bimorph piezoelectric beam. Finally, it can be said that dynamic behavior of the fin-like structure is not affected much from existence of the bimorph piezoelectric beam harvester.

Table 3. 2 Natural Frequencies of the Vertical Fin-like Structure with Bimorph Piezoelectric Beam

Mode Number and Type	Finite Element Analysis for Vertical Fin-like Structure with Bimorph Piezoelectric Beam (Hz)	Difference from Table 3.1 [%]
1st Out-of-plane Bending	29.24	5.33
1st Out-of-plane Bending of Bimorph Piezoelectric Beam	48.46	-
2nd Out-of-plane Bending	92.26	2.35

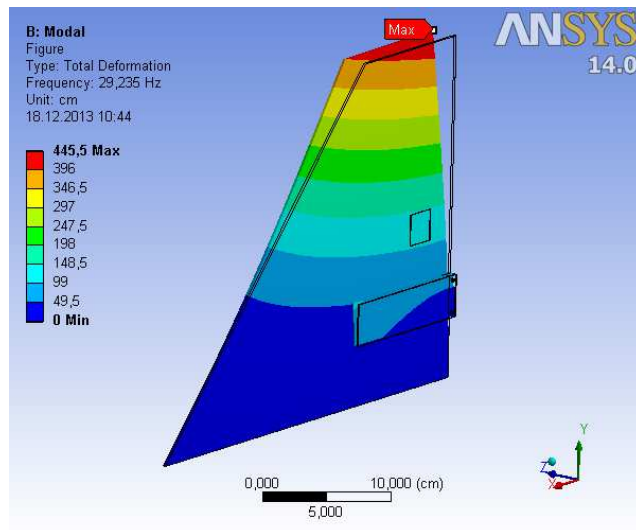


Figure 3. 5 Displacement Mode Shapes - 1st Out-of-plane bending mode of the fin

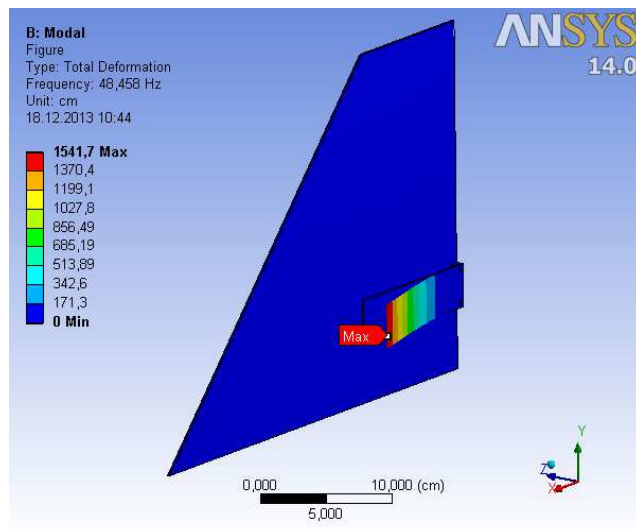


Figure 3. 6 Displacement Mode Shapes - 1st Out-of-plane bending mode of the bimorph piezoelectric beam

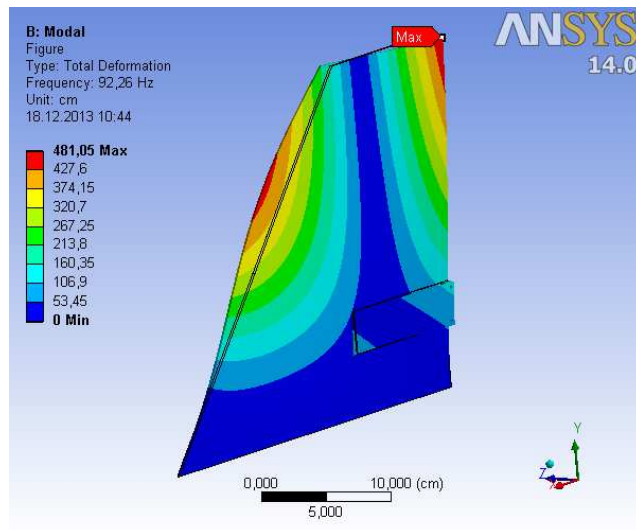


Figure 3. 7 Displacement Mode Shapes – 2nd Out-of-plane Bending mode of the fin

3.2.2. Experimental Validation of the Finite Element Model of the Vertical Fin-Like Structure with the Bimorph Piezoelectric Beam

So as to investigate the dynamic behavior of the vertical fin-like structure with bimorph piezoelectric beam, an experimental study is performed via impact hammer. During the modal test, impact hammer (Brüel&Kjaer 8206 [78]) and miniature accelerometer (Brüel&Kjaer 4517-002 [76]) are used (Figure 3. 8), and the location of accelerometer and excitation point by impact hammer is given in Figure 3. 8. Frequency response of the whole structure is obtained by PULSE Software [77] (Figure 3. 9) in the frequency range of 10-100 Hz and the first two resonance frequencies are found as 27.50 and 93.00 Hz, respectively.

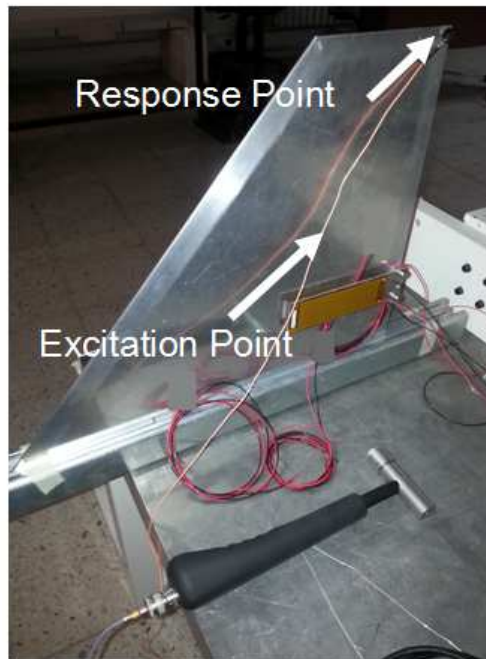


Figure 3. 8 Modal Test Setup

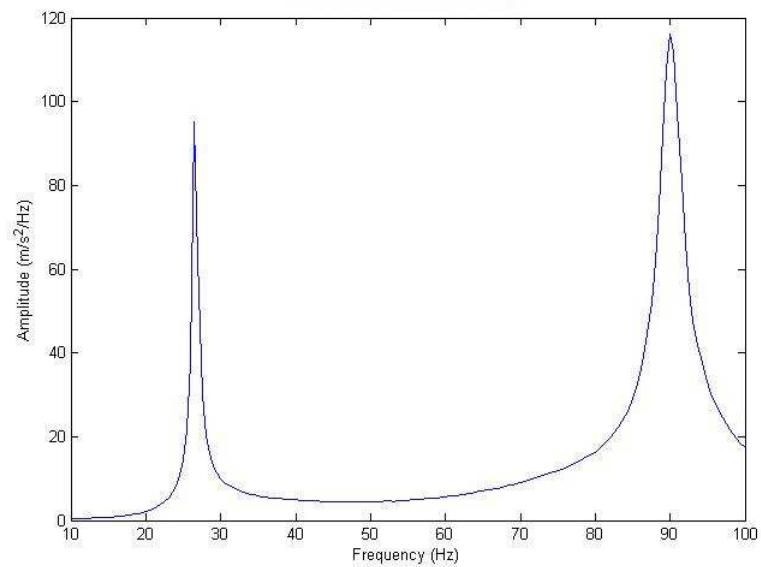


Figure 3. 9 Frequency Response of Vertical Fin-like Structure with Bimorph Piezoelectric

In this test, the first out-of-plane bending mode of the bimorph piezoelectric beam is investigated and as it is observed from the finite element results that the first natural frequency of the piezoelectric bimorph beam is well separated from that of the fin-like structure.

3.3. Energy Harvesting Performance of the Bimorph Piezoelectric Beam with the Vertical Fin-Like Structure

3.3.1. Ground Vibration Test of the Bimorph Piezoelectric Beam with the Vertical Fin-Like Structure

Another test setup with modal shaker is constructed (Figure 3. 10) and used to give the system a sine sweep excitation between 40-60 Hz. During the modal test, the whole structure is excited through modal shaker (Figure 3. 10a) and voltage output of one MFC, which is already used in bimorph piezoelectric beam, is collected by NI CompactDAQ [79] (Figure 3. 10b). For the each sweep frequency, voltage output of the MFC is read by NI Signal Express Software [84], and then voltage versus frequency graph is drawn in Figure 3. 11. As it can be seen from the voltage response of the bimorph piezoelectric beam, the fundamental natural frequency of the beam is found as 49.00 Hz. Moreover, in order to see the voltage output of the bimorph piezoelectric beam, ground vibration test is conducted. In this test, excitation at resonance frequency of the bimorph piezoelectric beam is given to the structure and tip acceleration, which is tuned to 1g, is controlled by a miniature accelerometer (Brüel&Kjaer 4517-002). During the test, NI CompactDAQ is used to obtain the voltage output (i.e. response) of the bimorph piezoelectric beam (Figure 3. 12) at its resonance frequency. As it can be seen from Figure 3. 12, the bimorph piezoelectric beam is generated considerable voltage at its fundamental resonance frequency for the controlled 1g vibration at its tip.

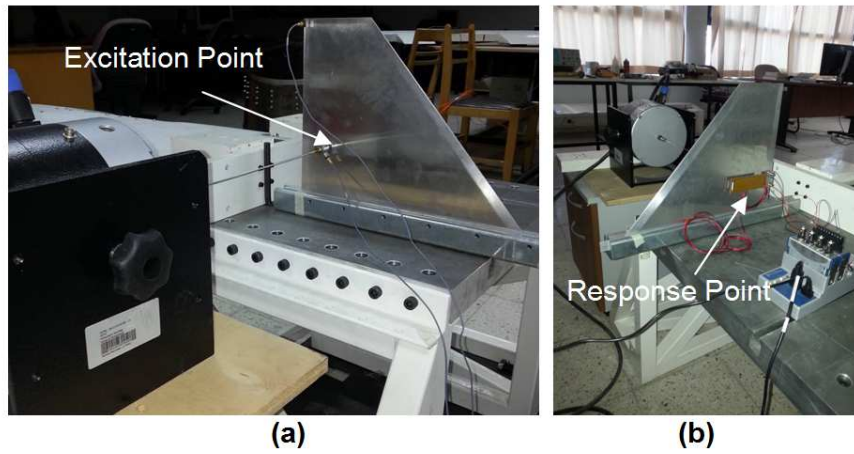


Figure 3.10 Shaker Test Setup (a) Excitation Point (b) Response Point

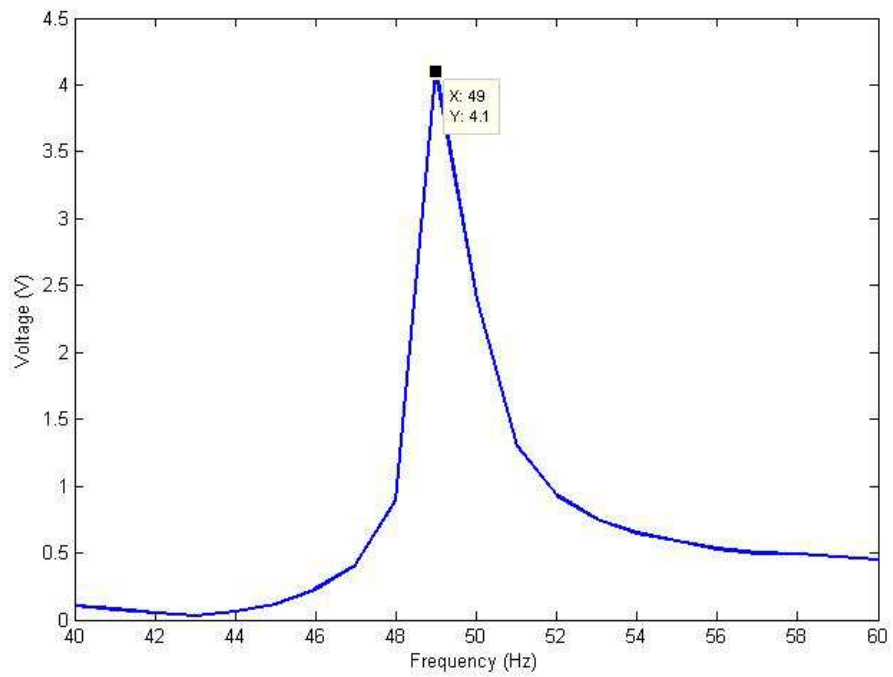


Figure 3.11 Frequency Response of Bimorph Piezoelectric Beam

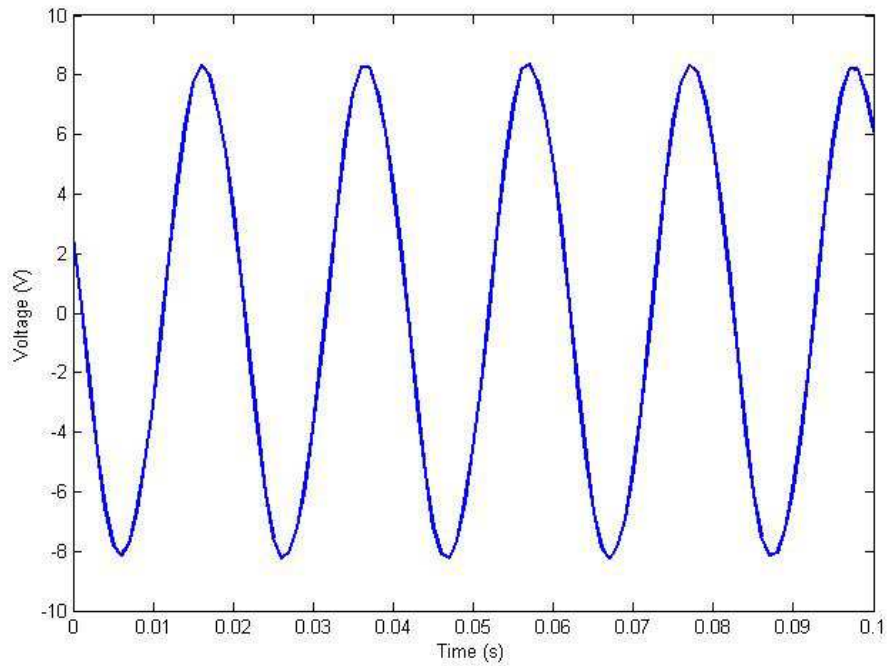


Figure 3. 12 Voltage Response of Bimorph Piezoelectric Beam

Finally, Table 3.3 is constructed in order to summarize and compare the results of the vertical fin-like structure without bimorph piezoelectric beam. Considering the results tabulated in Table 3. 3, it can be said that the finite element model is validated via experimental techniques. Moreover, it is also proven experimentally that dynamic characteristic of the vertical fin-like structure is not affected much by the integration of the bimorph piezoelectric beam.

Table 3. 3 Natural and Resonance Frequencies of the Vertical Fin-like Structure with Bimorph Piezoelectric Beam

Mode Number and Type	Finite Element Analysis (Hz)	Experimental Modal Analysis (Hz)	Deviation (%)
1st Out-of-plane Bending	29.24	27.50	6.33
1st Out-of-plane Bending of Bimorph Piezoelectric Beam	48.46	49.00	1.10
1st Torsion	92.26	93.00	0.79

3.3.2. Wind Tunnel Test of the Bimorph Piezoelectric Beam with the Vertical Fin-Like Structure

In order to investigate the energy harvesting performance of the bimorph piezoelectric beam in real life conditions, wind tunnel tests are conducted. During the wind tunnel tests (a schematic view of which is already given in Figure 2. 22), a vertical fin-like structure with the bimorph piezoelectric beam is positioned in front of the test section of the wind tunnel as shown previously in Figure 2. 24. Test setup for the smart fin can be seen in Figure 3.13.

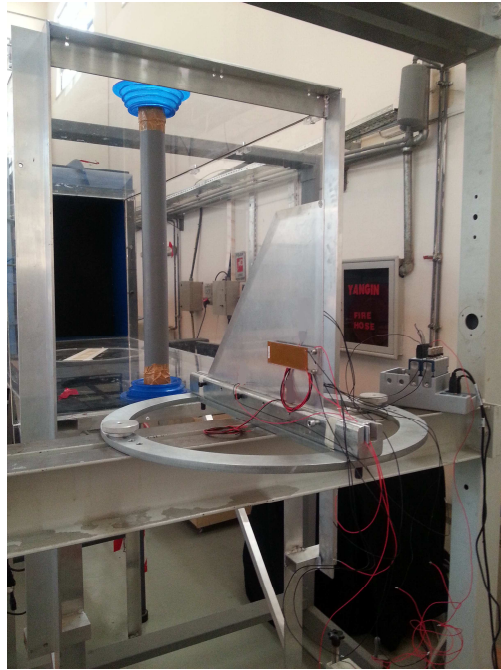


Figure 3. 13 Wind Tunnel Test Setup

If flow only goes around the vertical fin-like structure hosting the bimorph piezoelectric beam as a harvester, the beam may not be excited by the flow and the expected voltage generation of the bimorph piezoelectric beam might be comparably low. Therefore, a vortex generator is used to excite the bimorph piezoelectric beam around its first natural frequency so as to increase the voltage generation of MFC by making the vortex shedding frequency close to the first resonance frequencies of the beam harvester.

In order to generate a vortex shed by the flow, a bluff body should be used in front of the excited structure. In this study, a cylinder is used as a bluff body. Equation 2.1 can also be used in the calculation of both the cylinder diameter and the frequency content of the flow. A 0.05 m diameter cylinder is used in the wind tunnel and St can be taken as 0.2 for Reynolds Number (Re) $< 10^5$ for subcritical flow [81]. For the test condition, the flow is assumed to be subcritical and the St is also taken as 0.2. The vortex shedding frequency should be at 49 Hz which is the first out-of-plane bending frequency of the beam. By using these parameters and Equation 2.1, the

flow speed of wind tunnel is calculated as 12.25 m/s. By using this velocity, Re is found as approximately 42000 and therefore Strouhal Number assumption is validated for the subcritical flow. Moreover, the position of the cylinder is also important from the excitation point of view of the bimorph piezoelectric beam as explained in Chapter 2. For this reason, various positions of the cylinder are previously investigated [85]. Finally, test setup for the vortex generator, given in Figure 2.24, can be constructed by using this information. X is taken as 0.2 m and Y is chosen as 0.025 m in the test to increase the vortex excitation density.

During the test, flow speed of the wind tunnel is set to 12.25 m/s. After flow goes around the cylinder, the bimorph piezoelectric beam vibrates around its first resonance frequency. Then, the voltage output of MFC is obtained by NI CompactDAQ and read by NI Signal Express Software. In the first test, AC voltage generation performance of the bimorph piezoelectric beam is investigated by using rectifier circuit [80] and the obtained result is given in Figure 3. 14. The peak to peak voltage generated by the beam harvester is around 4 Volts with some variations.

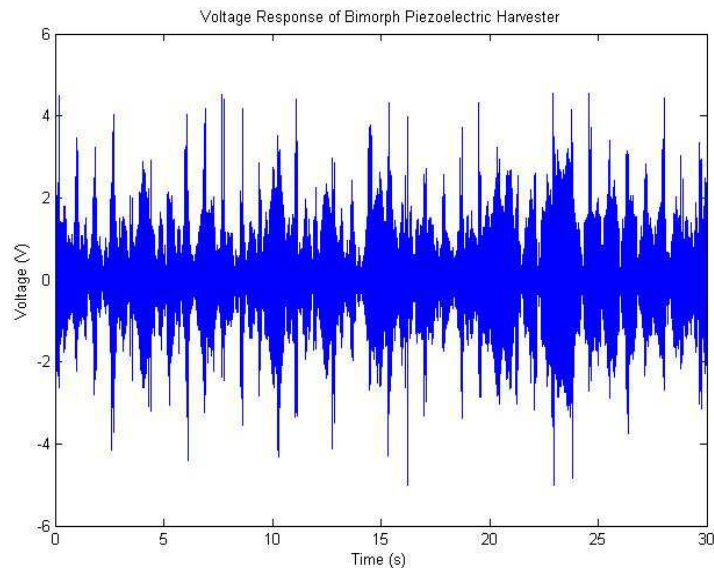


Figure 3. 14 AC Voltage Response of Bimorph Piezoelectric Beam in Time

In order to operate an electrical system or to charge some batteries, DC voltage should be supplied. Therefore, a rectifier circuit or specially designed circuit for energy harvesting should be used to convert AC voltage into DC one in order to operate a particular system. In this study, a rectifier circuit is used to investigate the DC voltage generation performance of the bimorph piezoelectric beam harvester. During the wind tunnel test, a rectifier circuit is connected to the bimorph piezoelectric beam and the DC voltage output of the beam is obtained by NI CompactDAQ which is shown in Figure 3.15. As it can be seen from the voltage response results, the harvester is capable of generating approximately 7 Volt-DC under the air flow load and by using proper power electronic circuits, a small battery can be charged by the beam harvester.

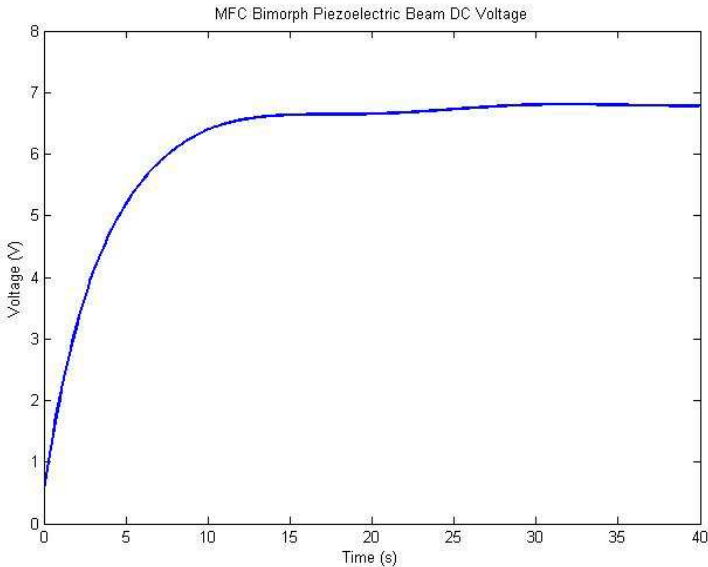


Figure 3. 15 DC Voltage Response of Bimorph Piezoelectric Beam in Time

The power spectral density (PSD) of the obtained time history of MFC is then obtained and presented in Figure 3. 16. The peak frequency of PSD is found as 49.32 Hz and it is very close to that of the ones obtained both from the finite element analysis and the modal test results. This also concludes that the bimorph piezoelectric

beam harvester is excited near its resonance frequency via vortex shed in the flow field generated.

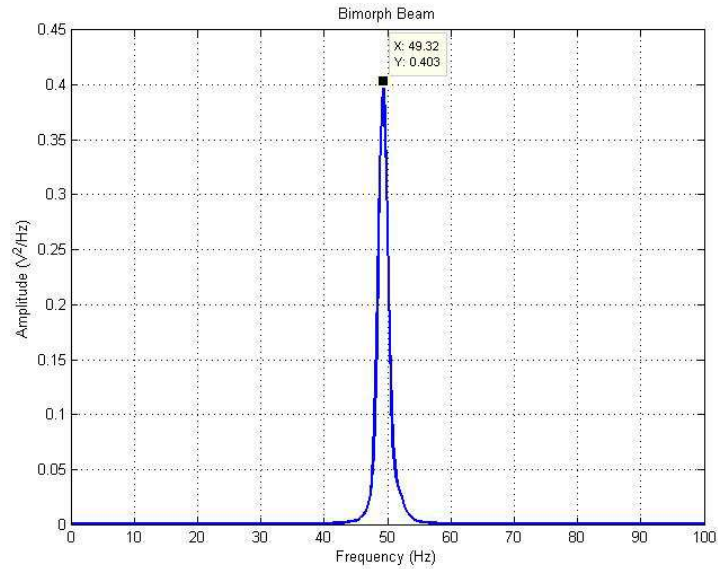


Figure 3. 16 PSD of Voltage Response of Bimorph Piezoelectric Beam in Time

3.4. Conclusion

In this chapter, energy harvesting from a vertical fin-like structure via bimorph piezoelectric beam is investigated by also providing a design approach for the integration of a bimorph piezoelectric beam to an aircraft structure. Knowing the fact that the integration of any external device onto a host structure might easily alter the passive dynamic characteristics of the host structure, various analyses are performed in order to avoid this undesirable situation and to keep the dynamic characteristics same after the integration. First, the finite element analyses are performed for the vertical fin-like structure to obtain its dynamic characteristics before the integration of the bimorph piezoelectric beam harvester. Then, these analyses results are also validated through experimental modal analyses. The suitable location for the integration of the bimorph piezoelectric beam is decided by investigating the first and the second out-of-plane bending displacement mode

shapes of the fin-like structure. The harvester is finally located by choosing the minimum displacement locations of the vertical fin-like structure in order to maintain the same passive dynamic characteristics of the structure. Following this, finite element analysis is conducted again for the vertical fin-like structure hosting the bimorph piezoelectric beam. It is observed from the finite element analysis and the experimental verification studies results that the resonance frequencies of the vertical fin-like structure are slightly altered although the fundamental resonance frequency of the bimorph piezoelectric energy harvester is decoupled from these. After verifying the proposed design approach, ground vibration and wind tunnel tests are performed to investigate the energy harvesting capability of the bimorph piezoelectric beam. In ground vibration tests, voltage output of the bimorph piezoelectric beam harvester around its first resonance frequency is investigated through a shaker excitation. Furthermore, the energy generated by the bimorph piezoelectric beam harvester is also examined via the wind tunnel tests. It can be concluded from the analyses results that in order to get higher voltage levels, the flow harvester should be excited around its fundamental natural frequency as the maximum strain levels are achieved at around this resonance.

During the wind tunnel test, both AC and DC voltage generation of the flow harvester are investigated. As it is known, piezoelectric materials generate AC voltage under the vibration excitation. In order to make AC voltage generation of the bimorph piezoelectric beam usable, a rectifier type of circuit should be used to transform this voltage to DC voltage. By using DC voltage, batteries can be charged or any low energy level system of an aircraft can also be operated. Therefore, in this study, a rectifier circuit is used to convert AC voltage of piezoelectric patches to DC one. As it can be seen from the obtained analyses result, considerable amount of DC voltage is generated by the bimorph piezoelectric beam harvester and it can be concluded that a low energy level system could be operated or batteries could be charged through this rectified voltage.

In this study, a design methodology of a piezoelectric energy harvester for an aircraft structure is provided. From the preliminary design to real life test scenarios

are explained in details. A finite element model is constructed both for the host structure and the harvester and this model is then validated through experimental studies. Moreover, wind tunnel tests are also performed in order to investigate the real life performance of the harvester. Finally, it is observed that the proposed design is a realizable one as a piezoelectric beam energy harvester which could be used on aircraft structures.

CHAPTER 4

DESIGN OF A PIEZOELECTRIC VORTEX HARVESTER BY USING CYLINDER AS A BLUFF BODY

4.1. Introduction

Having motivated by the research progressing in the field and the recent developments in the piezoelectric materials, in this particular chapter, a piezoelectric vortex energy harvester is designed in order to obtain energy from flow induced vibration. For this reason, a piezoelectric bimorph harvester, which is a commercial off the shelf product, is used and the resonance frequency of it is also tuned to reach higher energy levels. During the design stage of the harvester, the effect of the diameter and the position of the bluff body are also investigated via wind tunnel tests.

4.2 Design of the Bimorph Piezoelectric Beam used as a Piezoelectric Vortex Energy Harvester

The vortex energy harvester comprising piezoelectric material is designed to work under the flow induced vibration. In order to increase the voltage output, a solid cylinder is used as a bluff body in front of the harvester in order to generate vortices around the piezoelectric vortex energy harvester which can be seen in Figure 4. 1. The fundamental resonance frequency of the piezoelectric vortex energy

harvester can be excited via vortex induced flow and Equation 2.1 can be used to calculate the frequency content of the vortex induced flow by using the diameter of the cylinder and the flow speed.

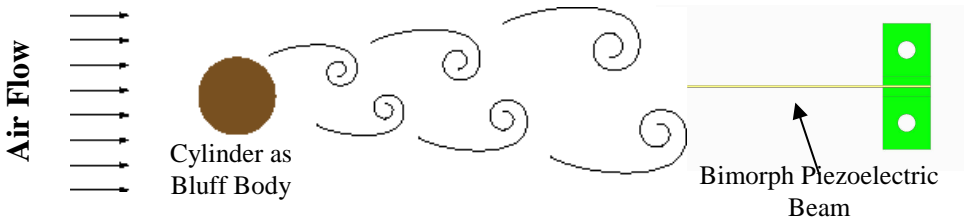


Figure 4. 1 Schematic Representation of the Working Principles of the Piezoelectric Vortex Energy Harvester

4.2.1. Selection of the Bimorph Piezoelectric Beam for the Piezoelectric Vortex Energy Harvester

In this study, commercially available bimorph piezoelectric energy harvester, Mide Vulture V25W [86], is used to construct the vortex energy harvester. A cylinder is also used as a bluff body in order to generate vortices. The 3-D model of the piezoelectric flow harvester can be seen in Figure 4. 2. The vortices do not generally develop downstream of the cylinder; therefore, in order to generate a maximum excitation in the piezoelectric vortex energy harvester, the position of the cylinder with respect to the vortex energy harvester should be determined correctly. Therefore, there are slots opened in the base plate to adjust the position of the cylinder in X and Y coordinates in order to find the correct position for the maximum excitation of the vortex energy harvester around its fundamental resonance frequency.

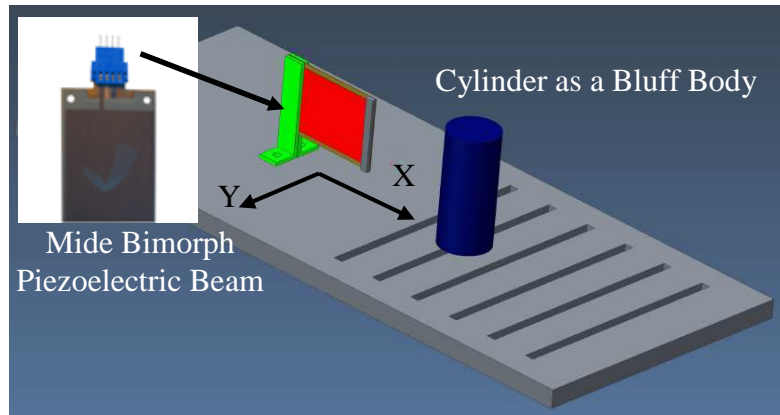


Figure 4. 2 3D Solid Model of Piezoelectric Vortex Energy Harvester

4.2.2. Experimental Analysis of the Bimorph Piezoelectric Beam

The fundamental resonance frequency of the Vulture V25W vortex energy harvester is tuned by adding an 8.2 gram tip mass which is a necessity regarding the working range of the wind tunnel. Then, so as to find the exact fundamental resonance frequency of the piezoelectric flow harvester, a modal test via shaker is performed through the base excitation. In this test, white noise input is generated and given to the modal shaker by Pulse Data Acquisition System [77] and is controlled by a single axis accelerometer (Bruel&Kjaer 4517-002 [76]). Voltage output of the piezoelectric energy harvester is collected via NI Data Acquisition System [79] (Figure 4. 3). This collected voltage output is then processed in MATLAB [65] to obtain the power spectrum of it and as is shown in the Figure 4. 4 that the fundamental resonance frequency of the flow harvester is obtained as 56.64 Hz.

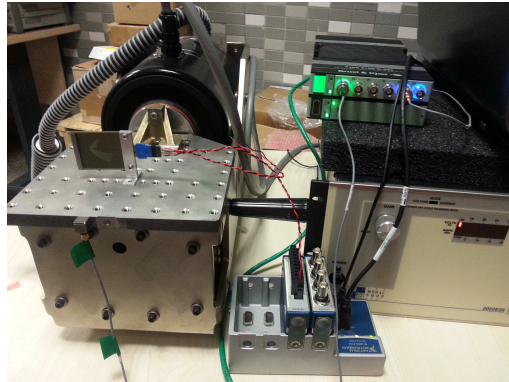


Figure 4. 3 Test Setup for Determination of the Fundamental Resonance Frequency of the Vortex Energy Harvester

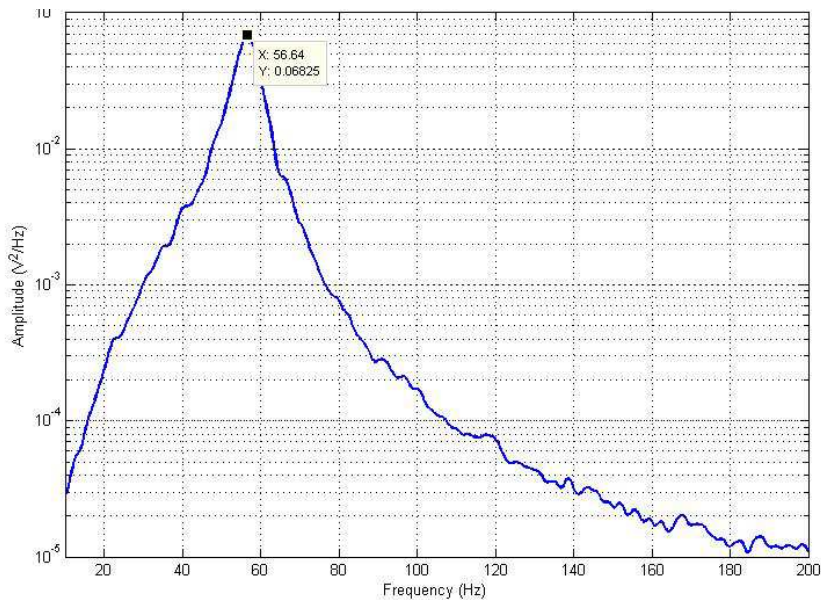


Figure 4. 4 Frequency Response of the Vortex Energy Harvester (Mide V25W)

In order to understand the effect of the diameter and the position of the cylinder in the performance of the vortex energy harvester, the model given in Figure 4. 2 is manufactured and shown in Figure 4. 5. In this model, four different diameters of cylinders (i.e. 20, 30, 40 and 50 mm) are used during the wind tunnel test to investigate the effect of the size of the bluff body. Flow speeds can be re-

calculated by using these cylinder diameters and the fundamental resonance frequency of the vortex energy harvester through Equation 2.1 for the generation of vortices. The corresponding obtained flow speeds are presented in Table 4.1.



Figure 4. 5 Manufactured Piezoelectric Vortex Energy Harvester and Bluff Bodies

Table 4. 1 Diameter of Cylinder vs. Different Flow Speed

Frequency of Vortex Harvester (Hz)	Diameter of Cylinder (m)	Flow Speed (m/s)
56.64	0.02	5.70
56.64	0.03	8.55
56.64	0.04	11.40
56.64	0.05	14.25

In the calculations, the Strouhal Number (St) can be taken as 0.2 as an assumption for Reynolds Number (Re) $< 10^5$ for subcritical flow [81]. After finding the flow speeds, maximum Re is re-calculated as around 42000 and the Strouhal Number assumption is validated for the subcritical flow before the planned wind tunnel tests.

4.3. Wind Tunnel Test of the Piezoelectric Vortex Energy Harvester

In order to investigate the energy harvesting performance of the vortex energy harvester in real life conditions, wind tunnel test is conducted. Schematic view of the wind tunnel used in the test is given in Figure 2. 22. During the wind tunnel test, the piezoelectric vortex energy harvester is positioned in the test section of the wind tunnel (Figure 4. 6).

The main aim of the study is to analyze the effect of the diameter and the position of the cylinder on the energy harvesting performance. In order to find the best position for each cylinder, 6 slots (seen in Figure 4. 7) are used in order to arrange the position in X direction. Moreover, each cylinder is also positioned in Y direction with respect $Y/D=0$ (i.e. cylinder position in Y direction for $Y/D=0$ is called as P1 which stands for the Position 1), $Y/D=0.5$ (cylinder position in Y direction for $Y/D=0.5$ is called as P2 which stands for the Position 2) and $Y/D=1$ (cylinder position in Y direction for $Y/D=1$ is called as P3 which stands for the Position 3), as it is mentioned in the study [85] that the effect of vortices is diminished after $Y/D=1.5$.

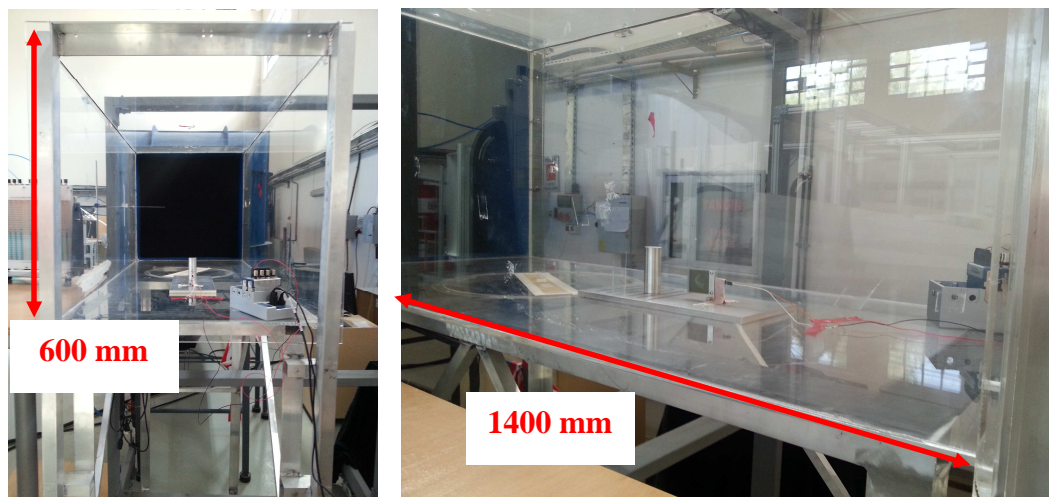


Figure 4. 6 Wind Tunnel Test Setup for the Vortex Energy Harvester

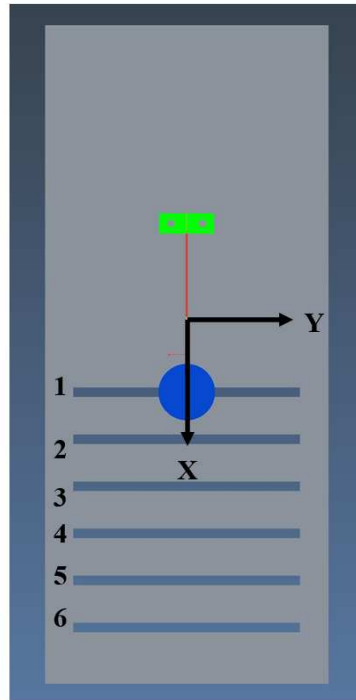


Figure 4. 7 X and Y Coordinates and the Slot Numbers

During the wind tunnel test, the voltage generation of the vortex energy harvester is collected by NI Compact DAQ and read by NI Signal Express Software [84]. In various test cases, Y/D ratio is fixed and X direction position is changed by using the slots. There are, in total, 4 different diameters are used and 18 different positions are selected for the wind tunnel test. Therefore, in order to compare the results of the each test case, the power spectral density (PSD) of the time record of the voltage output is obtained through MATLAB [83] and the results are presented from Figure 4. 8 to Figure 4. 19. Moreover, the maximum value of the PSD for 20 mm and 30 mm diameters, and for 40 mm and 50 mm diameters are given in Table 4. 2 and Table 4.3, respectively. In these tables, the maximum voltage output is given with respect to diameter and the position of cylinder and the results presented in these tables are also summarized in Figure 4. 20. Furthermore, the general location for the cylinder for each test case is given in Figure 4. 21. Finally, the maximum

voltage generation obtained for four different diameters are presented in Figure 4. 22 in order for better visualization of the test results.

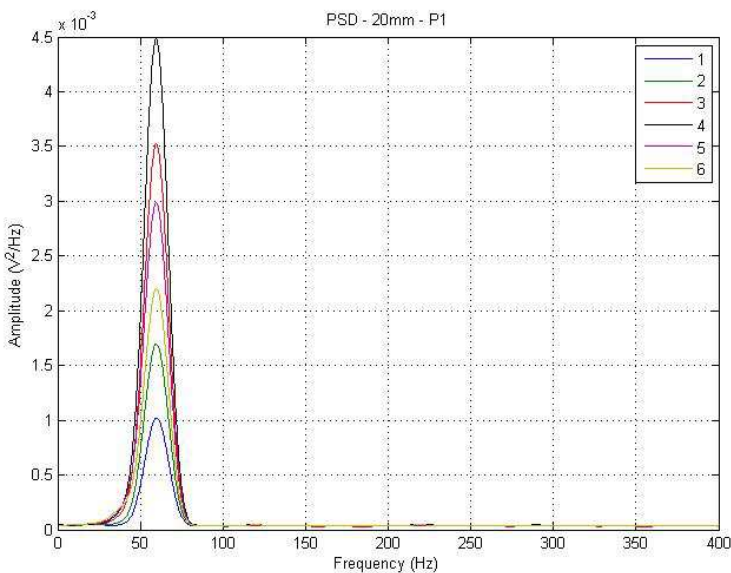


Figure 4. 8 Power Spectral Density for 20 mm Diameter and Position 1

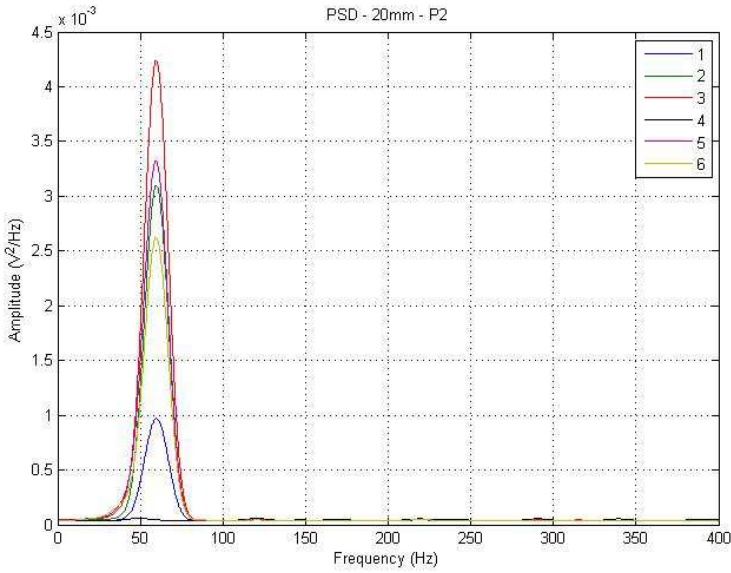


Figure 4. 9 Power Spectral Density for 20 mm Diameter and Position 2

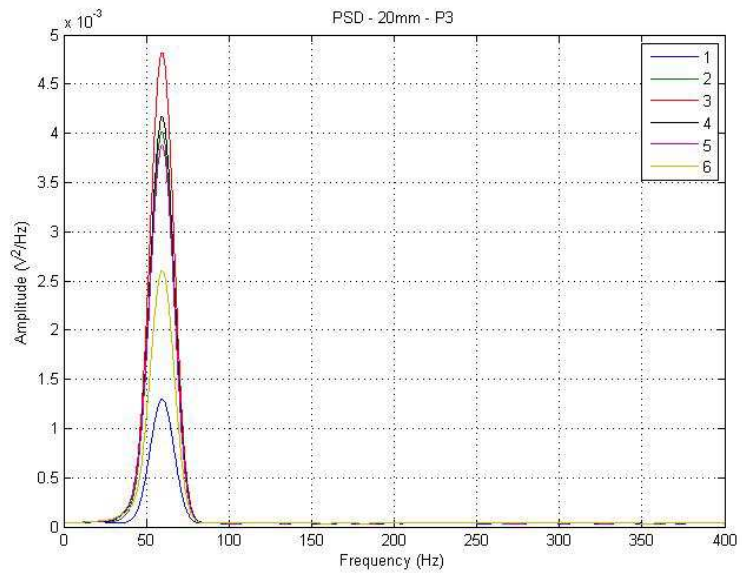


Figure 4. 10 Power Spectral Density for 20 mm Diameter and Position 3

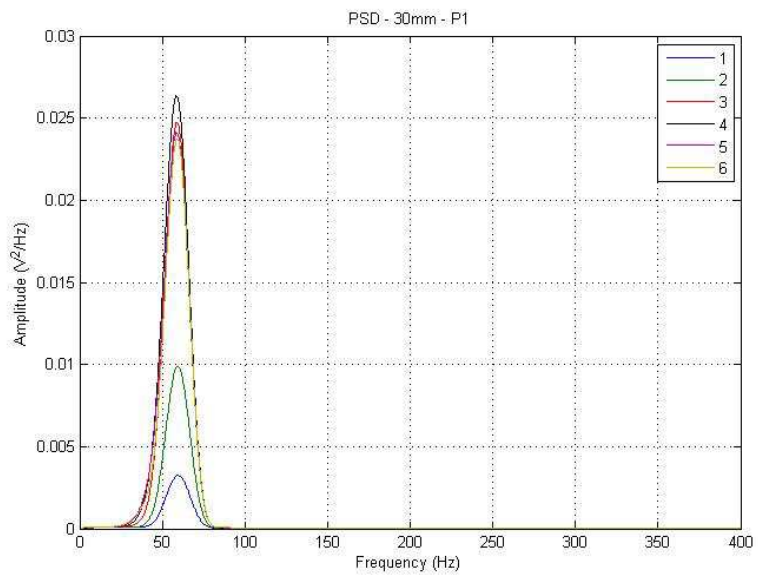


Figure 4. 11 Power Spectral Density for 30 mm Diameter and Position 1

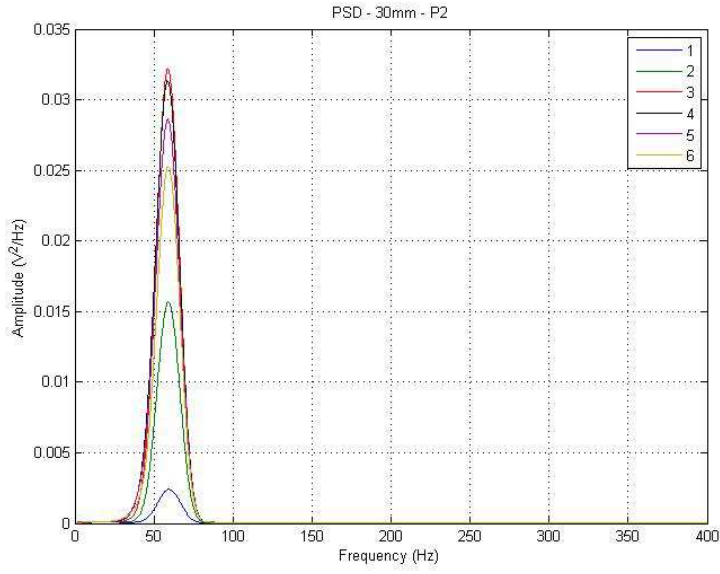


Figure 4. 12 Power Spectral Density for 30 mm Diameter and Position 2

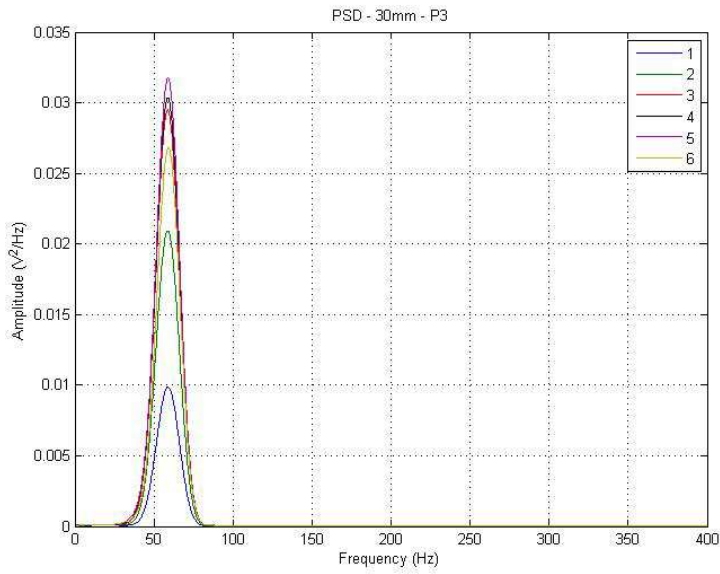


Figure 4. 13 Power Spectral Density for 30 mm Diameter and Position 3

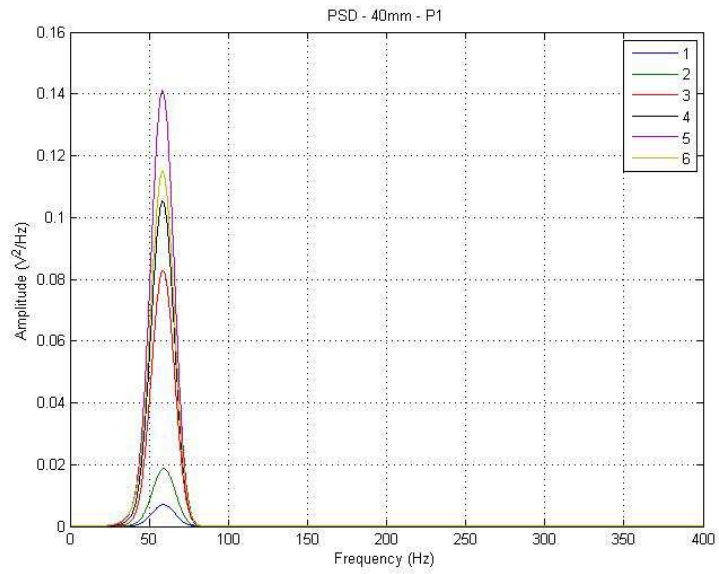


Figure 4. 14 Power Spectral Density for 40 mm Diameter and Position 1

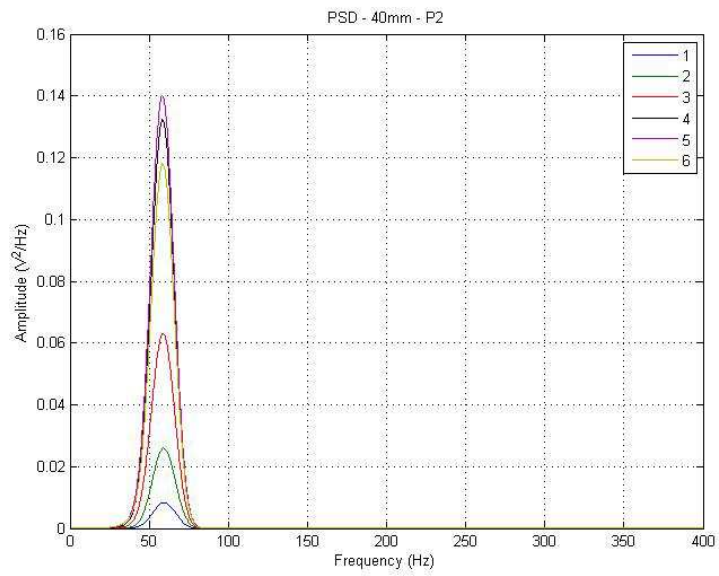


Figure 4. 15 Power Spectral Density for 40 mm Diameter and Position 2

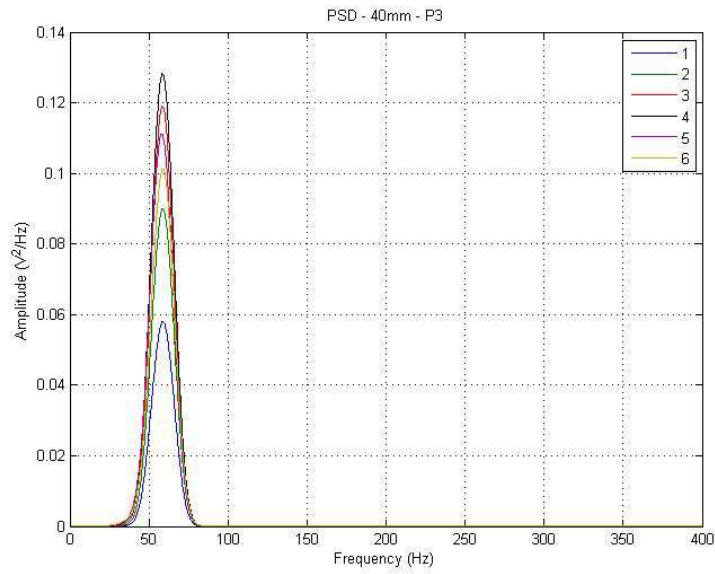


Figure 4. 16 Power Spectral Density for 40 mm Diameter and Position 3

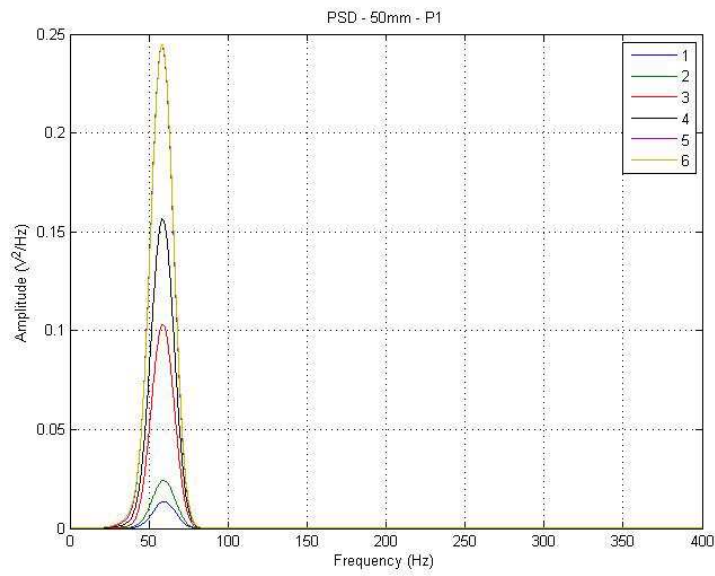


Figure 4. 17 Power Spectral Density for 50 mm Diameter and Position 1

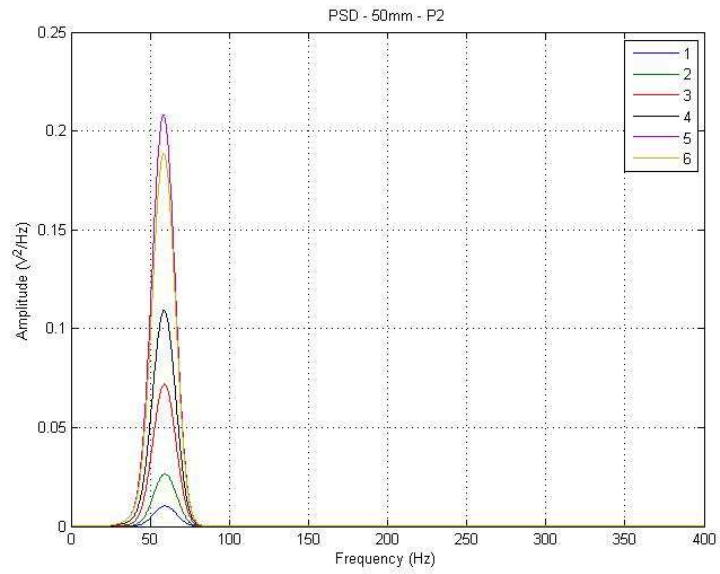


Figure 4. 18 Power Spectral Density for 50 mm Diameter and Position 2

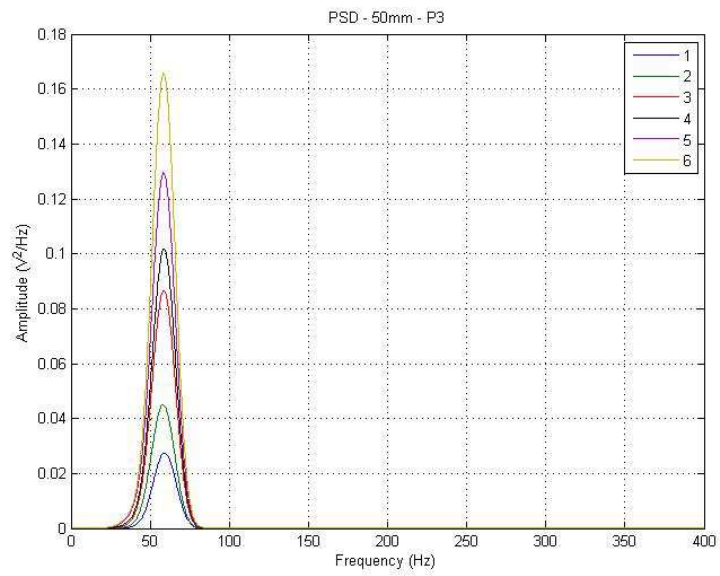


Figure 4. 19 Power Spectral Density for 50 mm Diameter and Position 3

Table 4. 2 Wind Tunnel Test for the Maximum Voltage output for Diameter 20 and 30 mm

	Diameter					
	20mm			30mm		
Position	P1 Slot 4	P2 Slot 3	P3 Slot 3	P1 Slot 4	P2 Slot 3	P3 Slot 3
Voltage Output (V²/Hz)	0.0045	0.0043	0.0048	0.0260	0.0320	0.0310

Table 4. 3 Wind Tunnel Test for the Maximum Voltage output for Diameter 40 and 50 mm

	Diameter					
	40mm			50mm		
Position	P1 Slot 5	P2 Slot 5	P3 Slot 4	P1 Slot 6	P2 Slot 5	P3 Slot 6
Voltage Output (V²/Hz)	0.1410	0.1400	0.1280	0.2450	0.2080	0.1650

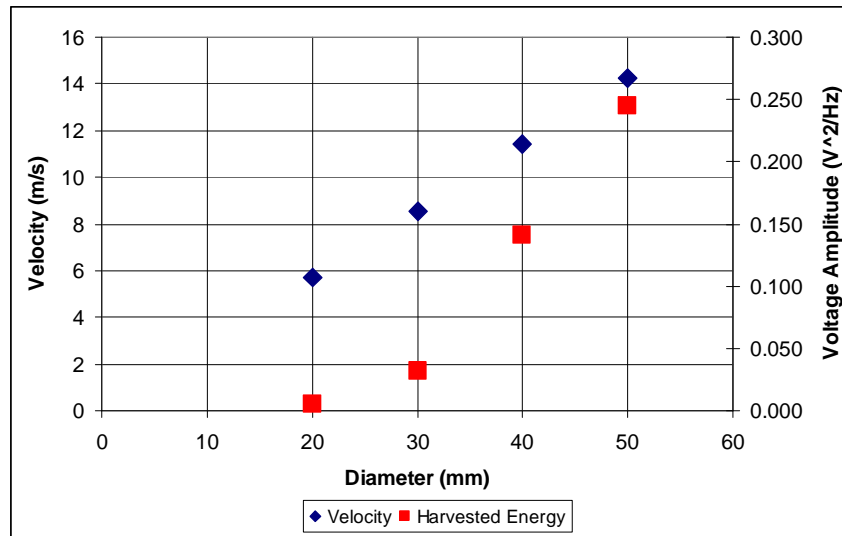


Figure 4. 20 Maximum PSD of the Voltage Generation for Different Flow Speed and Diameter of the Cylinder at the Resonance Frequency,

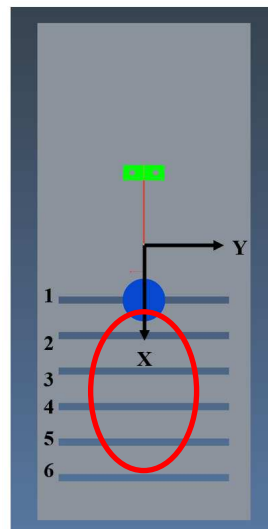


Figure 4. 21 General Locations for the Cylinder for Maximum PSD Output

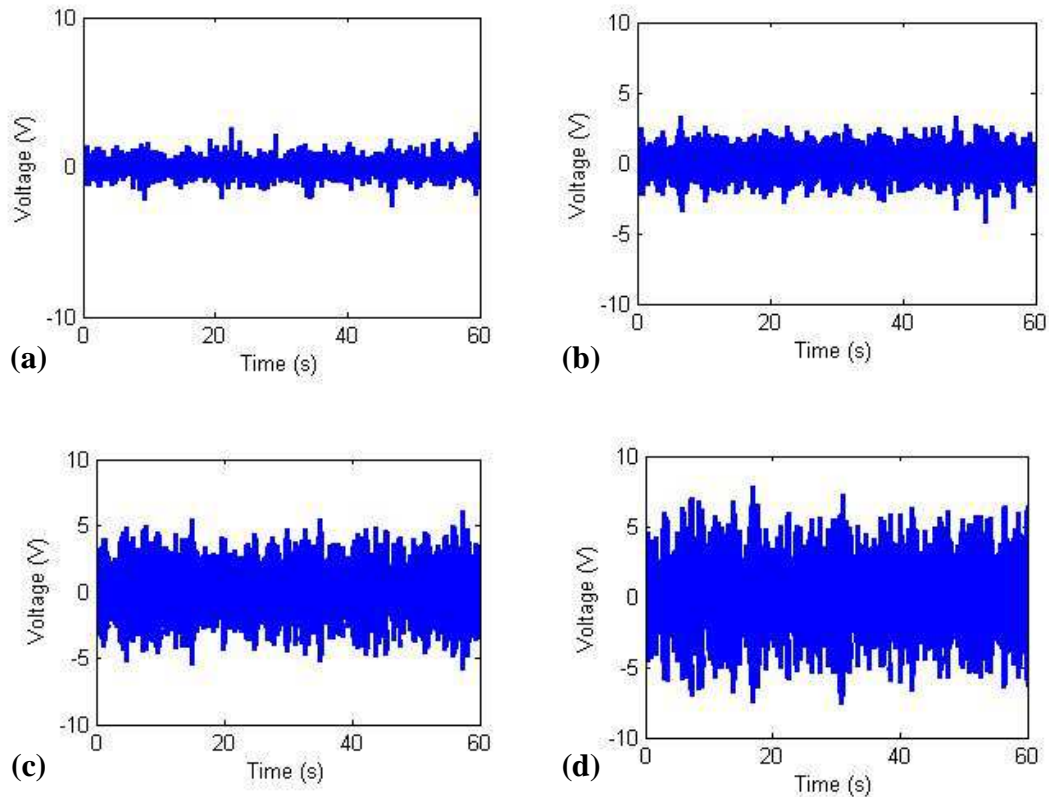


Figure 4.22 Maximum Voltage Generation for Different Diameter of the Cylinder
 (a) 20 mm Diameter (b) 30 mm Diameter (c) 40 mm Diameter (d) 50 mm Diameter

The fundamental resonance frequency of the vortex energy harvester is also calculated under the real operating condition. For this purposes, the PSD of the voltage output of the vortex energy harvester is taken by MATLAB [83] by using the time history data obtained from the wind tunnel test. The PSD of the voltage output of the vortex energy harvester is given in Figure 4.23 and it can be seen from this figure that the fundamental resonance frequency is around 58.00 Hz. This result is very close to the one obtained from the modal shaker test (i.e. 56.64 Hz) and therefore leads to an experimentally verified study.

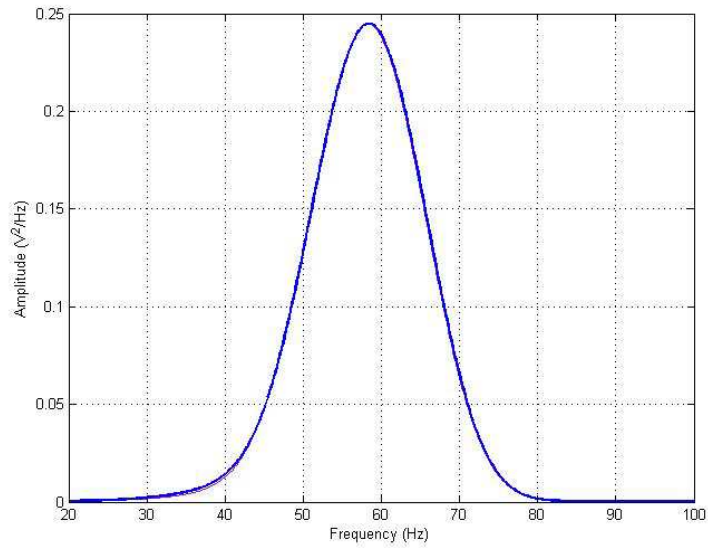


Figure 4. 23 Frequency Response of the Voltage Data for 50 mm Diameter Cylinder in the Determination of the Fundamental Resonance Frequency of the Vortex Energy Harvester

After these tests, it can be seen from the Figure 4. 20 that the voltage output of the vortex harvester increases due to the increase in the flow speed as there is an increase in the turbulence content of the flow as well. Moreover, the voltage output can be maximized for each diameter of the cylinder if the cylinder is positioned roughly in the red circular region as indicated in Figure 4. 21. This study is showed that if the flow is turbulent and it generates vortices, the vortex energy harvester performance can be increased around the fundamental resonance frequency region. Moreover, the correct position of the cylinder should be determined through the wind tunnel test in order to increase the harvested energy. Following these numerical and experimental studies, the vortex energy harvester can be used more efficiently by selecting the diameter and position of the cylinder.

It is practically not very feasible to use this type of voltage output to operate a particular low power level system or to charge a battery. In order to make this voltage useable for the aforementioned purposes, a rectifier circuit should also be

used. Therefore, a rectifier circuit [80] converting AC voltage to DC one with its 2 nF capacitance used during the wind tunnel tests. For a cylinder of diameter 50 mm and at P1/Slot 5 position, DC voltage generation of the vortex energy harvester is given as an example in Figure 4. 24. By using this DC voltage generation of the vortex energy harvester and the capacitance value of rectifier circuit, the average power generation can be obtained by using Equation 4.1 where C is the capacitance of the rectifier circuit, V is the voltage and Δt is the time difference. Average power is also presented in Figure 4. 25.

$$P_{avg} = \frac{1/2 CV^2}{\Delta t} \tag{4.1}$$

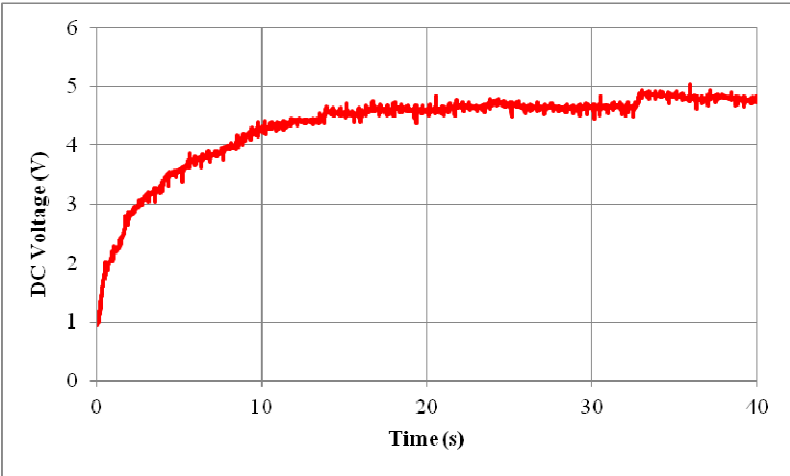


Figure 4. 24 DC Voltage Generation of the Vortex Energy Harvester

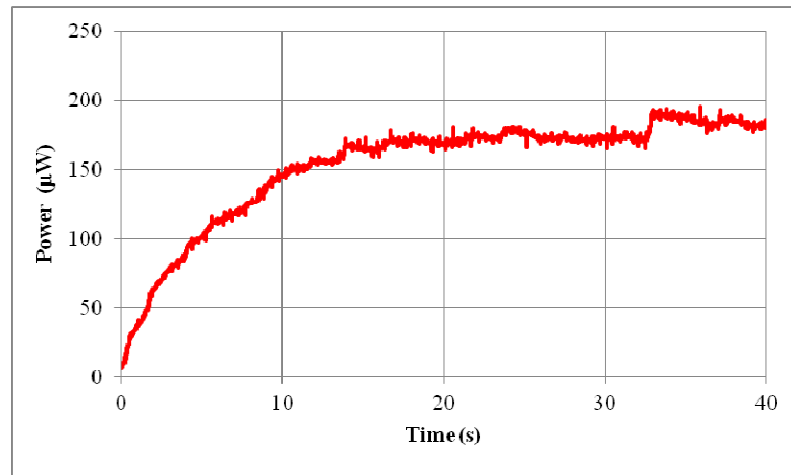


Figure 4. 25 Power Generation of the Vortex Energy Harvester

4.4. Conclusion

In this chapter, the energy harvesting performance of the bimorph piezoelectric beam is investigated under the vortex flow excitation. For this aim, a commercial bimorph piezoelectric beam, Mide Vulture V25W, is selected and a vortex energy harvester is constructed so as to investigate the effect of the diameter and the position of a bluff body which is considered as a cylinder in this particular case.

First of all, the fundamental resonance frequency of the bimorph piezoelectric beam is tuned roughly to 57.00 Hz and then it is also obtained and validated via experimental modal analysis. Following this, the energy generation capability of the vortex energy harvester is examined under real conditions in a wind tunnel through various tests. In this study, the main objective is to arrange a flow speed and decide the diameter of a bluff body in such a way that the fundamental resonance frequency of the vortex energy harvester is excited.

As it can be observed from the test and analysis results that when the flow speed increases, a higher voltage generation levels can be achieved in comparison to low speed applications through the designed vortex energy harvester. Additionally,

the PSD of the time series of vortex energy harvester is taken to obtain the fundamental resonance frequency of the vortex energy harvester and the results indicated that the resonance frequency obtained under operational condition is very close to that of experimentally obtained one. This study also show that the harvested energy depends on both size and the position of the cylinder located in front of the vortex energy harvester. These obtained results are in close agreement with the study [87], which is about the investigation of the effect of different sizes of cylinder diameter on vortex induced vibration for energy generation. In this particular study [87], it is shown that when the cylinder diameter is increased the energy generation of vortex induced vibration also increased within the range of Reynolds number ($300 < Re < 300000$). Having seen the importance of the position and the size of the cylinder in the energy harvesting performance, a conceptual design is then proposed for the tuned vortex energy harvester having the capability of adapting itself to different flow velocities in order to increase the desired harvested energy. A control system including a servo actuator should also be developed and installed to accurately actuate the proposed mechanism.

Finally, this type of harvester can be integrated to any structure which is expected to work against the air flow. Before integration of the vortex energy harvester, the flow characteristics should also be investigated and well understood beforehand. By using the information and the knowledge gathered through both the numerical and the experimental work, the fundamental resonance frequency of the vortex energy harvester can be tuned via positioning the bluff body in order to maximize the amount of harvested energy.

CHAPTER 5

DESIGN OF A PIEZOELECTRIC VORTEX HARVESTER BY USING PLATE AS A BLUFF BODY

5.1. Introduction

In Chapter 4, performance of the piezoelectric bimorph harvester is analyzed under the vortex induced vibration due to the flow passing around cylinder. In this chapter, plate is used as a bluff body instead of a cylinder. The effect of the size, rotation angle with respect to the upcoming flow direction and the position of the plate are also investigated via wind tunnel tests.

5.2 Design of the Bimorph Piezoelectric Beam used as a Piezoelectric Vortex Energy Harvester

The vortex energy harvester comprising piezoelectric material is designed to work under the flow induced vibration. In order to increase the voltage output, a solid plate is used as a bluff body in front of the harvester in order to generate vortices around the piezoelectric vortex energy harvester which can be seen in Figure 5. 1.

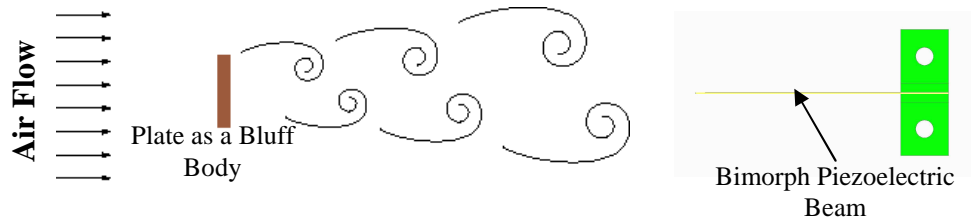


Figure 5. 1 Schematic Representation of the Working Principles of the Piezoelectric Vortex Energy Harvester

The fundamental resonance frequency of the piezoelectric vortex energy harvester can be excited via vortex induced flow. It is stated [88] that Strouhal Number is represented by a function of the ratio of the projected length and plate length. Therefore, Equation 2.1 is modified by considering the plate geometry in order to calculate the flow speed to generate same vortex frequency with respect to frequency of the piezoelectric vortex energy harvester:

$$St = \frac{f_s L_{eff}}{U} \quad (5.1)$$

where; St is Strouhal Number, L_{eff} is the effective length of the plate, f_s is the vortex shedding frequency and U is the flow speed. L_{eff} can be defined as in Figure 5. 2 and it can be calculated as $L_{eff} = L \sin(\alpha)$.

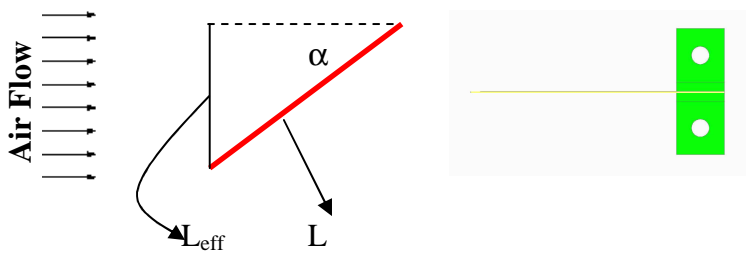


Figure 5. 2 Schematic Representation of the Working Principles of the Piezoelectric Vortex Energy Harvester

In this study, commercially available bimorph piezoelectric energy harvester, Mide Voltage V25W [86], is used to construct the vortex energy harvester. A plate is

also used as a bluff body in order to generate vortices. The 3-D model of the piezoelectric flow harvester can be seen in Figure 5. 3. The vortices do not generally develop downstream the plate; therefore, in order to generate a maximum excitation in the piezoelectric vortex energy harvester, the position of the plate with respect to the vortex energy harvester should be determined correctly. Therefore, there are slots in the base plate to adjust the position of the plate only in X coordinates in order to find the correct position for the maximum excitation of the vortex energy harvester around its fundamental resonance frequency. Moreover, effect of rotation of the plate is analyzed in this study. In order to rotate the plate precisely, step motor [89] is used. This step motor is driven by simple motor driver card and a computer interface.

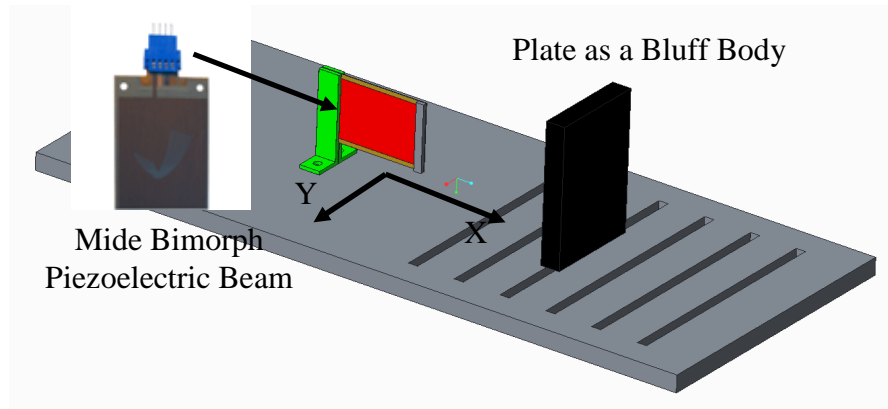


Figure 5. 3 3D Solid Model of Piezoelectric Vortex Energy Harvester

In order to understand the effect of the size, the position and the amount of rotation of the plate in the performance of the vortex energy harvester, the model (Figure 5. 3) is manufactured and shown in Figure 5. 4. In this model, three different width (i.e. effective length) of the plate (i.e. 40, 50 and 60 mm) are used during the wind tunnel test to investigate the effect of the size of the bluff body and geometry details of these plates are shown in Figure 5.5. Flow speeds can be re-calculated by using these plates and the fundamental resonance frequency of the vortex energy

harvester through Equation 5.1 for the generation of vortices. The corresponding obtained flow speeds for three plates are presented in Table 5. 1 to Table 5.3.

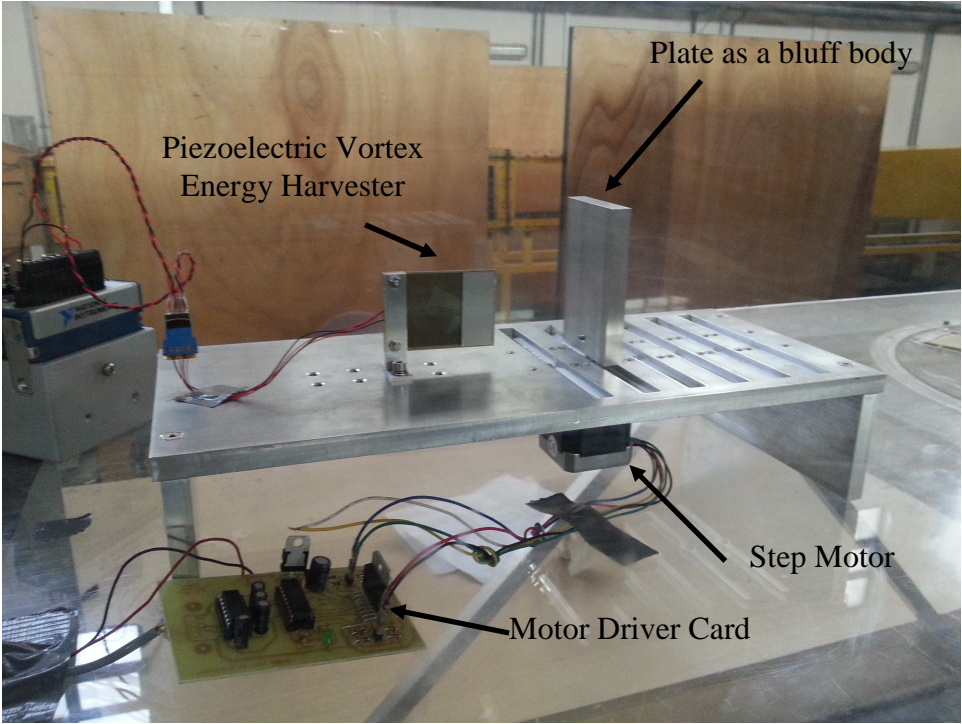


Figure 5. 4 Manufactured Piezoelectric Vortex Energy Harvester and Bluff Body

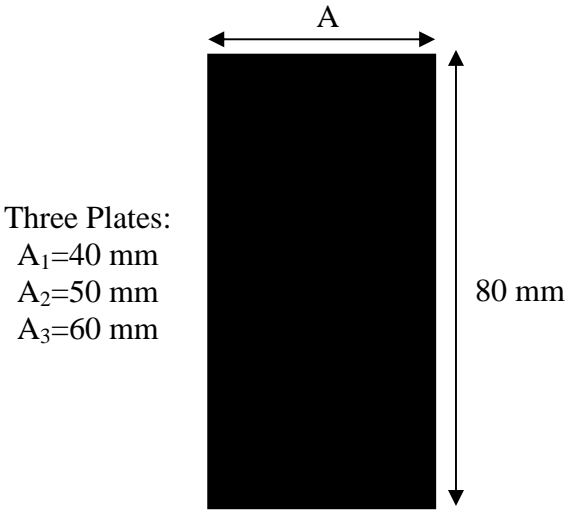


Figure 5. 5 Plate Geometries

Table 5. 1 Rotation Angle and Effective Length of Plate vs. Different Flow Speed for A=40 mm Plate at a Resonance Frequency of 56.64 Hz

Rotation Angle of Plate (degree)	Effective Length of Plate (m)	Flow Speed (m/s)
0	0.040	11.33
30	0.035	7.28
60	0.020	5.66
80	0.007	1.97

Table 5. 2 Rotation Angle and Effective Length of Plate vs. Different Flow Speed for A=50 mm Plate at a Resonance Frequency of 56.64 Hz

Rotation Angle of Plate (degree)	Effective Length of Plate (m)	Flow Speed (m/s)
0	0.050	14.16
30	0.043	12.26
60	0.025	7.08
80	0.009	2.46

Table 5. 3 Rotation Angle and Effective Length of Plate vs. Different Flow Speed for A=60 mm Plate at a Resonance Frequency of 56.64 Hz

Rotation Angle of Plate (degree)	Effective Length of Plate (m)	Flow Speed (m/s)
0	0.060	16.99
30	0.052	14.72
60	0.030	8.50
80	0.010	2.95

In the calculations, the Strouhal Number (St) can be taken as 0.2 as an assumption for Reynolds Number (Re) $< 10^5$ for subcritical flow [81]. After finding the flow speeds, maximum Re is re-calculated as around 65000 for the maximum

flow speed and the Strouhal Number assumption is validated for the subcritical flow before the planned wind tunnel tests.

5.3. Wind Tunnel Test of the Piezoelectric Vortex Energy Harvester

In order to investigate the energy harvesting performance of the vortex energy harvester in real life conditions, wind tunnel test is conducted. Schematic view of the wind tunnel used in the test is given in Figure 2. 22. During the wind tunnel test, the piezoelectric vortex energy harvester is positioned in the test section of the wind tunnel (Figure 5. 6).

The main of aim of the study is to analyze the effect of the effective length and the position of the plate on the energy harvesting performance. In order to find the best position for each plate, 6 slots (seen in Figure 5. 7) are used in order to arrange the position in X direction.

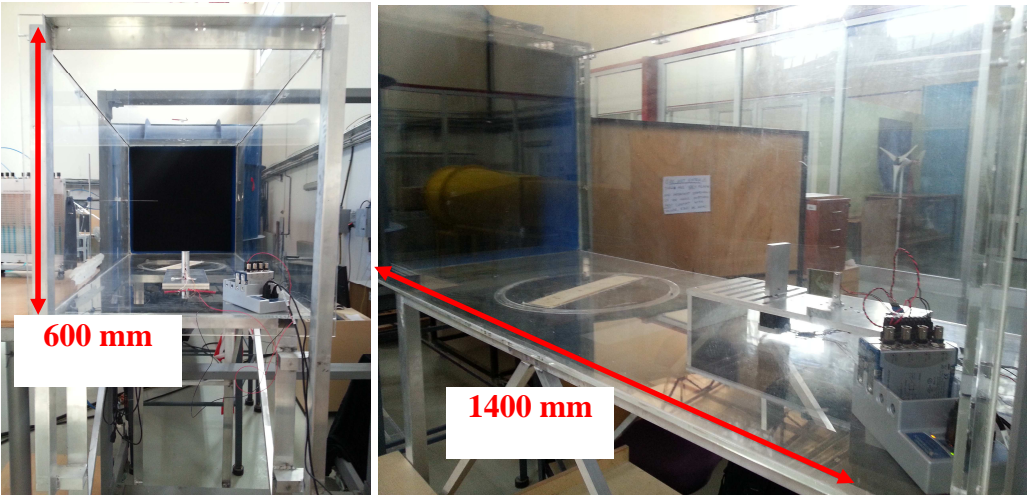


Figure 5. 6 Wind Tunnel Test Setup for the Vortex Energy Harvester

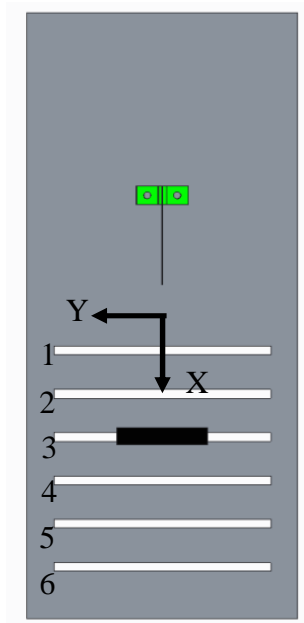


Figure 5. 7 X and Y Coordinates and the Slot Numbers

During the wind tunnel test, the voltage generation of the vortex energy harvester is collected by NI Compact DAQ and read by NI Signal Express Software. In various test cases, X is fixed and angle of plate is changed by using step motor in 15 degree angle increments. There are, in total, 3 different plates are used and 7 different angles (0, 15, 30, 45, 60, 75 90 degree) are selected for the wind tunnel test. Therefore, in order to compare the results of the each test case, the power spectral density (PSD) of the time record of the voltage output is obtained through MATLAB [65] and the maximum PSD values for the 40 mm plate are presented from Table 5. 4 to Table 5. 8. It should be stated that maximum PSD value is obtained at the resonance frequency of piezoelectric energy harvester for each case and one example graph is given for 40 mm plate, Figure 5. 8. Moreover, surface plot is prepared for each wind tunnel speed with respect to slot number and angle of 40 mm plate.

Table 5. 4 Maximum PSD Values ($V^2/\sqrt{\text{Hz}}$) for 40 mm Plate and Slot 1

Slot 1		Wind Tunnel Speed (m/s)			
		1.97	5.66	9.81	11.33
Angle (°)	0	0.00018	0.00019	0.00532	0.01297
	15	0.00019	0.00018	0.00478	0.01424
	30	0.00018	0.00017	0.00582	0.01338
	45	0.00020	0.00018	0.00401	0.01013
	60	0.00018	0.00018	0.00445	0.00809
	75	0.00028	0.00027	0.00463	0.00874
	90	0.00017	0.00037	0.00437	0.00787

Table 5. 5 Maximum PSD Values ($V^2/\sqrt{\text{Hz}}$) for 40 mm Plate and Slot 2

Slot 2		Wind Tunnel Speed (m/s)			
		1.97	5.66	9.81	11.33
Angle (°)	0	0.00004	0.00016	0.00520	0.02200
	15	0.00003	0.00019	0.00572	0.02240
	30	0.00004	0.00019	0.00826	0.02429
	45	0.00003	0.00024	0.00702	0.02494
	60	0.00005	0.00024	0.00581	0.02062
	75	0.00004	0.00031	0.00529	0.02044
	90	0.00004	0.00028	0.00535	0.01873

Table 5. 6 Maximum PSD Values ($V^2/\sqrt{\text{Hz}}$) for 40 mm Plate and Slot 3

Slot 3		Wind Tunnel Speed (m/s)			
		1.97	5.66	9.81	11.33
Angle (°)	0	0.00003	0.00009	0.00276	0.00788
	15	0.00003	0.00010	0.00310	0.00837
	30	0.00003	0.00012	0.00404	0.01053
	45	0.00003	0.00013	0.00384	0.01113
	60	0.00003	0.00013	0.00369	0.00892
	75	0.00003	0.00028	0.00513	0.00861
	90	0.00003	0.00026	0.00409	0.00678

Table 5. 7 Maximum PSD Values ($V^2/\sqrt{\text{Hz}}$) for 40 mm Plate and Slot 4

Slot 4		Wind Tunnel Speed (m/s)			
		1.97	5.66	9.81	11.33
Angle (°)	0	0.00006	0.00007	0.00164	0.00565
	15	0.00004	0.00007	0.00185	0.00746
	30	0.00006	0.00008	0.00223	0.00838
	45	0.00004	0.00008	0.00302	0.00803
	60	0.00005	0.00012	0.00325	0.00696
	75	0.00004	0.00024	0.00516	0.01033
	90	0.00005	0.00016	0.00348	0.00732

Table 5. 8 Maximum PSD Values ($V^2/\sqrt{\text{Hz}}$) for 40 mm Plate and Slot 5

Slot 1		Wind Tunnel Speed (m/s)			
		1.97	5.66	9.81	11.33
Angle (°)	0	0.00004	0.00005	0.00076	0.00185
	15	0.00004	0.00006	0.00070	0.00187
	30	0.00004	0.00006	0.00099	0.00267
	45	0.00005	0.00006	0.00084	0.00273
	60	0.00004	0.00010	0.00188	0.00459
	75	0.00004	0.00017	0.00377	0.00927
	90	0.00004	0.00020	0.00377	0.00693

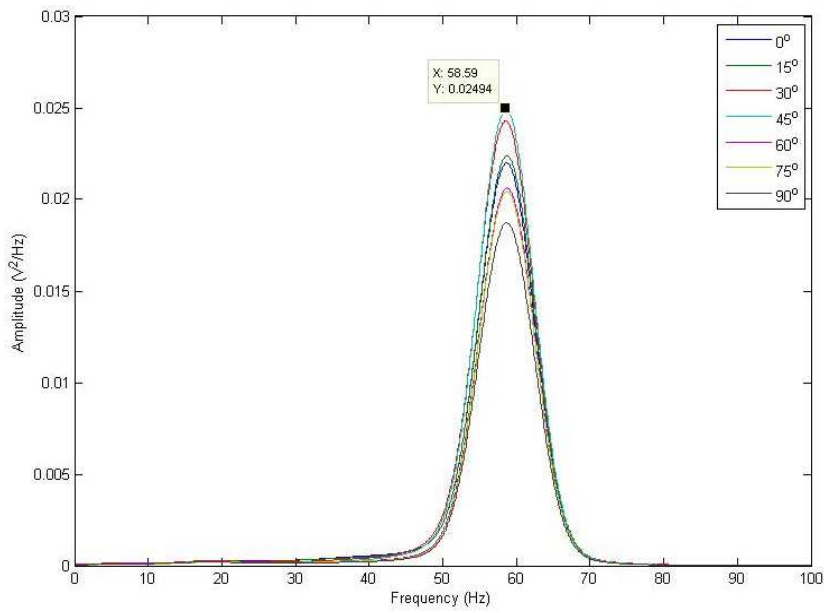


Figure 5. 8 PSD for 40 mm Plate, Maximum Wind Tunnel Speed and Slot 2

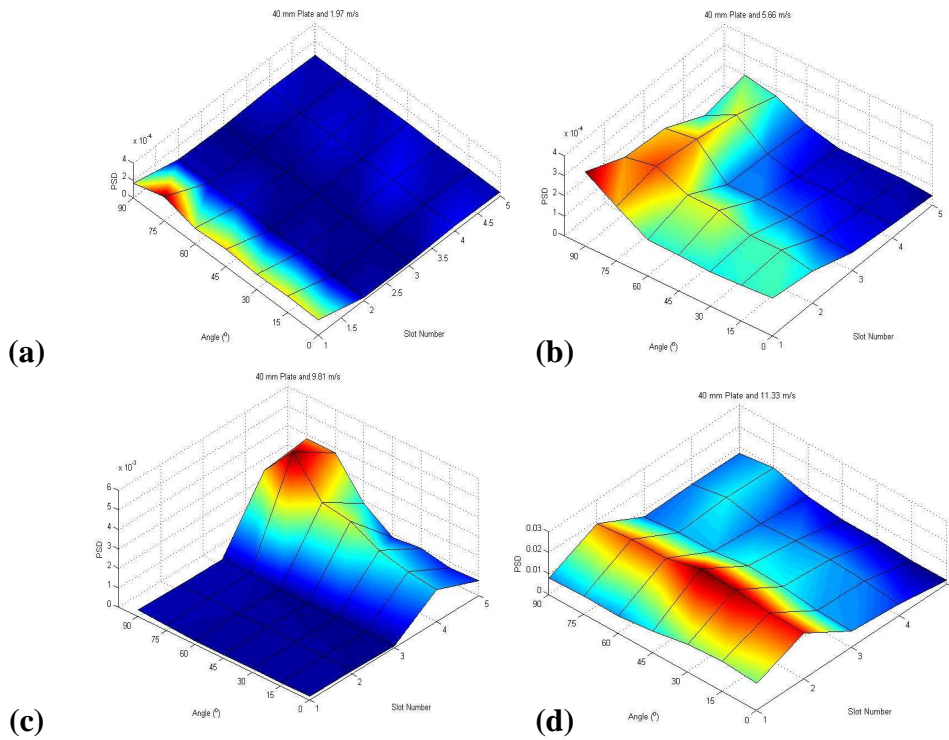


Figure 5. 9 Surface Plots for 40 mm Plate, (a) Wind Tunnel Speed=1.97 m/s, (b) Wind Tunnel Speed=5.66 m/s, (c) Wind Tunnel Speed=9.81 m/s and Wind Tunnel Speed=11.33 m/s

The maximum PSD values for the 50 mm plate are presented from Table 5. 9 to Table 5. 13. It should be stated that maximum PSD value is obtained at the resonance frequency of piezoelectric energy harvester for each case and one example graph is given for 60 mm plate, Figure 5. 10. Moreover, surface plot is prepared for each wind tunnel speed with respect to slot number and angle of 50 mm plate.

Table 5. 9 Maximum PSD Values (V^2/\sqrt{Hz}) for 50 mm Plate and Slot 1

Slot 1		Wind Tunnel Speed (m/s)			
		2.46	7.08	12.26	14.16
Angle (°)	0	0.00037	0.01007	0.02979	0.01297
	15	0.00033	0.01156	0.02519	0.01424
	30	0.00039	0.00987	0.01974	0.01338
	45	0.00040	0.00832	0.01631	0.01013
	60	0.00038	0.00791	0.01676	0.00809
	75	0.00071	0.01141	0.01866	0.00874
	90	0.00098	0.01011	0.01448	0.00787

Table 5. 10 Maximum PSD Values (V^2/\sqrt{Hz}) for 50 mm Plate and Slot 2

Slot 2		Wind Tunnel Speed (m/s)			
		2.46	7.08	12.26	14.16
Angle (°)	0	0.00004	0.00025	0.01343	0.02732
	15	0.00004	0.00043	0.01229	0.02144
	30	0.00005	0.00063	0.01143	0.01830
	45	0.00004	0.00065	0.01059	0.02047
	60	0.00004	0.00054	0.01618	0.01939
	75	0.00005	0.00064	0.01634	0.02419
	90	0.00005	0.00063	0.01699	0.02557

Table 5. 11 Maximum PSD Values ($V^2/\sqrt{\text{Hz}}$) for 50 mm Plate and Slot 3

Slot 3		Wind Tunnel Speed (m/s)			
		2.46	7.08	12.26	14.16
Angle (°)	0	0.00003	0.00025	0.00374	0.01322
	15	0.00003	0.00015	0.00515	0.01766
	30	0.00003	0.00020	0.00645	0.02015
	45	0.00003	0.00023	0.00689	0.02248
	60	0.00003	0.00030	0.00980	0.02567
	75	0.00003	0.00064	0.01075	0.02331
	90	0.00003	0.00073	0.00880	0.01805

Table 5. 12 Maximum PSD Values ($V^2/\sqrt{\text{Hz}}$) for 50 mm Plate and Slot 4

Slot 4		Wind Tunnel Speed (m/s)			
		2.46	7.08	12.26	14.16
Angle (°)	0	0.00005	0.00015	0.00317	0.01155
	15	0.00005	0.00015	0.00427	0.01387
	30	0.00005	0.00019	0.00582	0.02196
	45	0.00005	0.00018	0.00715	0.02093
	60	0.00006	0.00026	0.00937	0.02557
	75	0.00005	0.00067	0.01191	0.02462
	90	0.00006	0.00071	0.01150	0.01777

Table 5. 13 Maximum PSD Values ($V^2/\sqrt{\text{Hz}}$) for 50 mm Plate and Slot 5

Slot 1		Wind Tunnel Speed (m/s)			
		2.46	7.08	12.26	14.16
Angle (°)	0	0.00003	0.00009	0.00198	0.00443
	15	0.00004	0.00007	0.00164	0.00432
	30	0.00003	0.00009	0.00187	0.00406
	45	0.00003	0.00009	0.00219	0.00504
	60	0.00004	0.00022	0.00571	0.01015
	75	0.00004	0.00064	0.01154	0.01512
	90	0.00003	0.00056	0.00783	0.01593

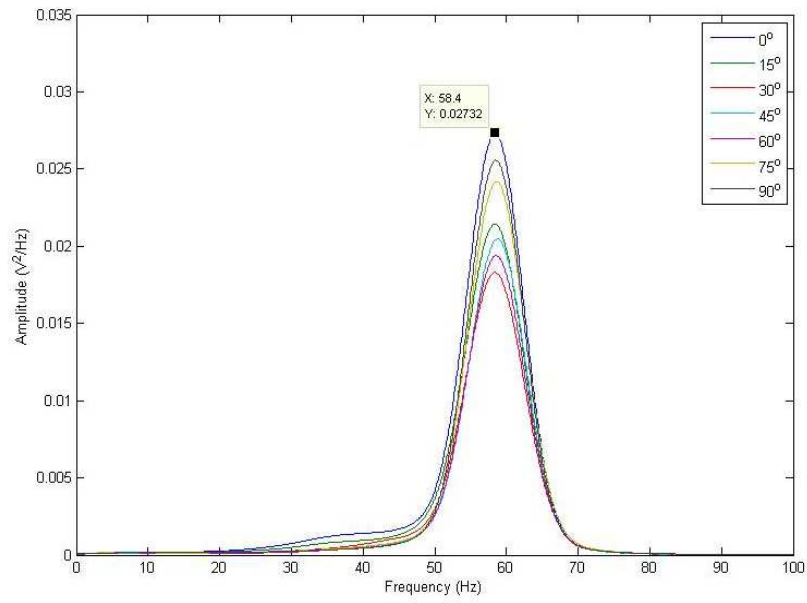


Figure 5. 10 PSD for 50 mm Plate, Maximum Wind Tunnel Speed and Slot 2

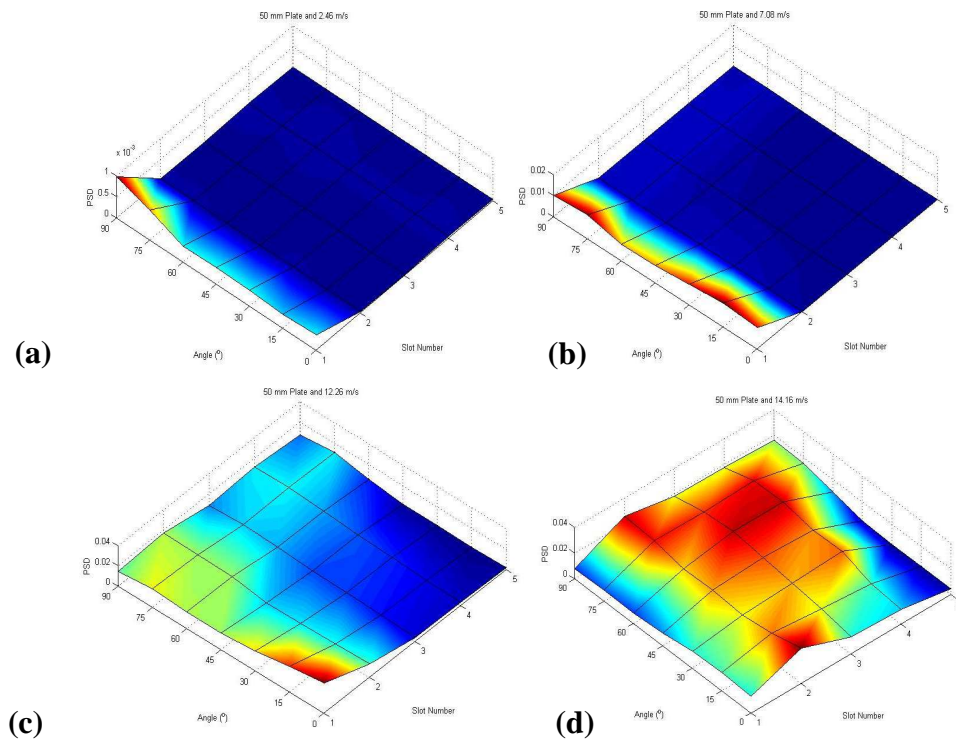


Figure 5. 11 Surface Plots for 50 mm Plate, (a) Wind Tunnel Speed=2.46 m/s, (b) Wind Tunnel Speed=7.08 m/s, (c) Wind Tunnel Speed=12.26 m/s and Wind Tunnel Speed=14.16 m/s

The maximum PSD values for the 60 mm plate are presented from Table 5. 14 to Table 5. 18. It should be stated that maximum PSD value is obtained at the resonance frequency of piezoelectric energy harvester for each case and one sample graph is given for 60 mm plate in Figure 5. 12. Moreover, surface plot is prepared for each wind tunnel speed with respect to slot number and the position angle for the 60 mm plate.

Table 5. 14 Maximum PSD Values (V^2/\sqrt{Hz}) for 60 mm Plate and Slot 1

Slot 1		Wind Tunnel Speed (m/s)			
		2.95	8.50	14.72	16.99
Angle (°)	0	0.00055	0.00073	0.01489	0.03353
	15	0.00056	0.00082	0.01615	0.02736
	30	0.00060	0.00105	0.01645	0.02303
	45	0.00046	0.00083	0.01149	0.02126
	60	0.00052	0.00124	0.01452	0.01922
	75	0.00063	0.00182	0.01961	0.02227
	90	0.00075	0.00259	0.01839	0.02257

Table 5. 15 Maximum PSD Values (V^2/\sqrt{Hz}) for 60 mm Plate and Slot 2

Slot 2		Wind Tunnel Speed (m/s)			
		2.95	8.50	14.72	16.99
Angle (°)	0	0.00002	0.00080	0.01197	0.02402
	15	0.00003	0.00114	0.01426	0.02684
	30	0.00003	0.00108	0.01114	0.02191
	45	0.00003	0.00111	0.01521	0.02009
	60	0.00003	0.00129	0.01900	0.02637
	75	0.00003	0.00171	0.03111	0.04075
	90	0.00003	0.00148	0.02348	0.02548

Table 5. 16 Maximum PSD Values ($V^2/\sqrt{\text{Hz}}$) for 60 mm Plate and Slot 3

Slot 3		Wind Tunnel Speed (m/s)			
		2.95	8.50	14.72	16.99
Angle (°)	0	0.00003	0.00025	0.00791	0.02850
	15	0.00003	0.00028	0.00918	0.02673
	30	0.00003	0.00031	0.01201	0.03069
	45	0.00003	0.00034	0.01247	0.03092
	60	0.00003	0.00066	0.02360	0.04156
	75	0.00003	0.00124	0.02032	0.05309
	90	0.00003	0.00193	0.02217	0.03048

Table 5. 17 Maximum PSD Values ($V^2/\sqrt{\text{Hz}}$) for 60 mm Plate and Slot 4

Slot 4		Wind Tunnel Speed (m/s)			
		2.95	8.50	14.72	16.99
Angle (°)	0	0.00003	0.00017	0.00400	0.01488
	15	0.00003	0.00018	0.00487	0.01270
	30	0.00003	0.00021	0.00666	0.01533
	45	0.00003	0.00025	0.00808	0.01613
	60	0.00003	0.00047	0.01774	0.03477
	75	0.00004	0.00126	0.02615	0.03422
	90	0.00003	0.00194	0.02217	0.02918

Table 5. 18 Maximum PSD Values ($V^2/\sqrt{\text{Hz}}$) for 60 mm Plate and Slot 5

Slot 1		Wind Tunnel Speed (m/s)			
		2.95	8.50	14.72	16.99
Angle (°)	0	0.00003	0.00011	0.00196	0.00467
	15	0.00003	0.00012	0.00262	0.00408
	30	0.00003	0.00016	0.00395	0.00688
	45	0.00003	0.00018	0.00371	0.00660
	60	0.00003	0.00066	0.01181	0.02118
	75	0.00003	0.00207	0.02942	0.03926
	90	0.00003	0.00137	0.01105	0.01655

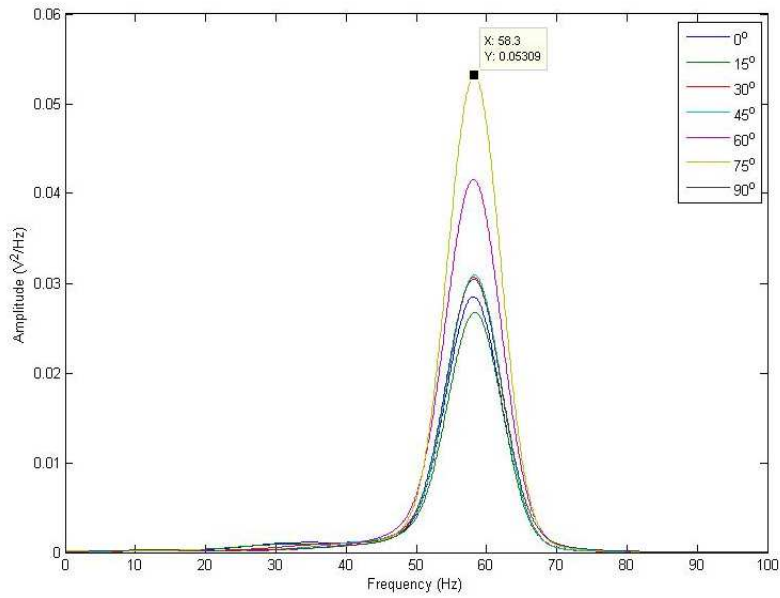


Figure 5.12 PSD for 60 mm Plate, Maximum Wind Tunnel Speed and Slot 3

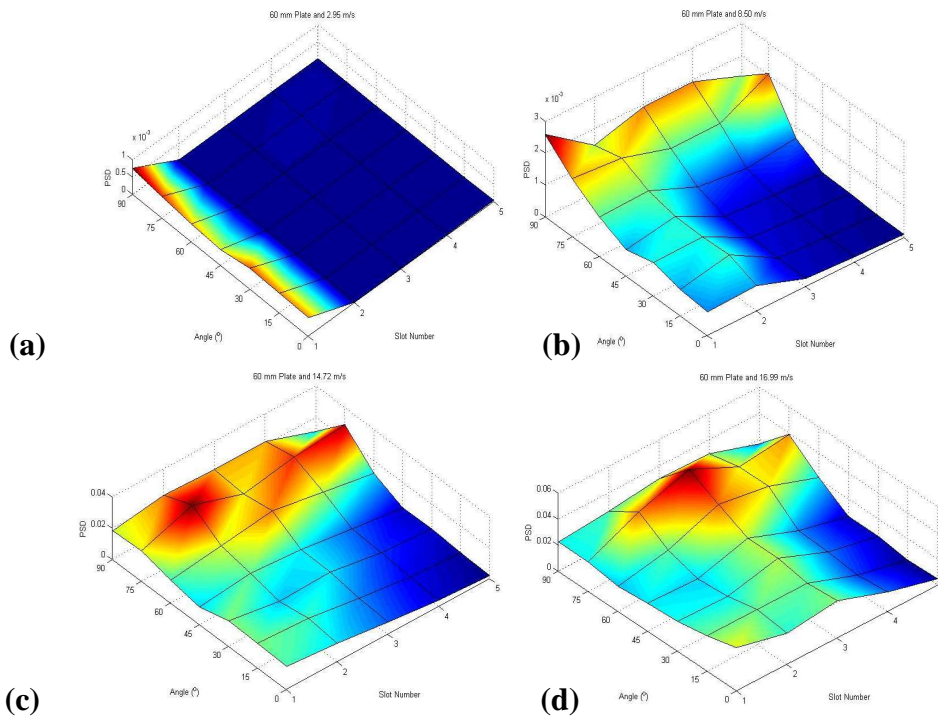


Figure 5.13 Surface Plots for 60 mm Plate, (a) Wind Tunnel Speed=2.95 m/s, (b) Wind Tunnel Speed=8.50 m/s, (c) Wind Tunnel Speed=14.72 m/s and Wind Tunnel Speed=16.99 m/s

After these tests, it can be seen from the results that the voltage output of the vortex harvester increases due to the increase in the flow speed as there is an increase in the turbulence content of the flow as well. Moreover, the voltage output can be maximized for each size of the plate if the plate is positioned roughly in the red circular region as indicated in Figure 5. 14.

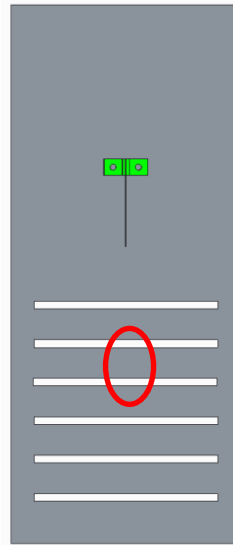


Figure 5. 14 General Locations for the Plate for Maximum PSD Output

This study shows that if the flow is turbulent and it generates vortices, the vortex energy harvester performance can be increased around the fundamental resonance frequency region. However, there is no consistent correlation between angle of plate and harvested voltage; this might be due to flow characteristics for the given wind tunnel speeds. This case can also be seen in the study [85], which is on the investigation of effect of cylinder and plate sizes for vortex generation performance. In this particular study [85], the effect of the angle of plate for vortex generation is also investigated and the results are provided in Figure 5. 15 [85]. As it can be seen from Figure 5. 15 that the vortex frequencies are not varying with the angle of incidence of the plate. However, no direct correlation is observed between angle of incidence of the plate and the intensities of the vortex [85].

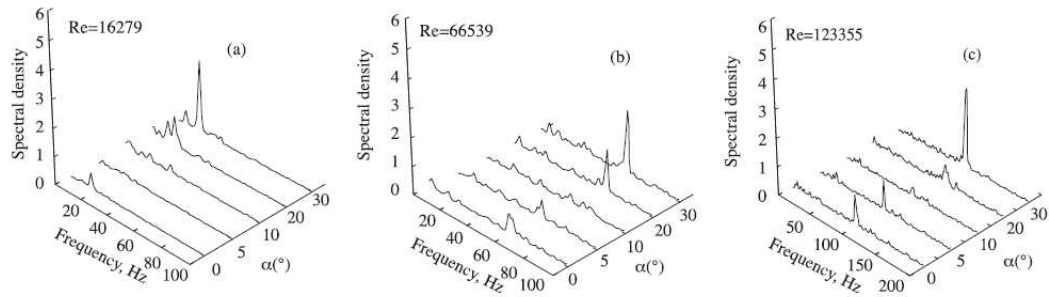


Figure 5. 15 PSD of Different Velocities ((a) Re=16279, (b) Re=66539, (c) Re=123355) versus angle of incidence square the Plate [85]

Moreover, the correct position and angle of the plate should be determined through the wind tunnel test in order to increase the harvested energy. Following these numerical and experimental studies, the vortex energy harvester can be used more efficiently by selecting the size, position and angle of the plate. Finally, the maximum voltage generation obtained for three different plates are presented in Figure 5. 16 in order to better visualize the test results.

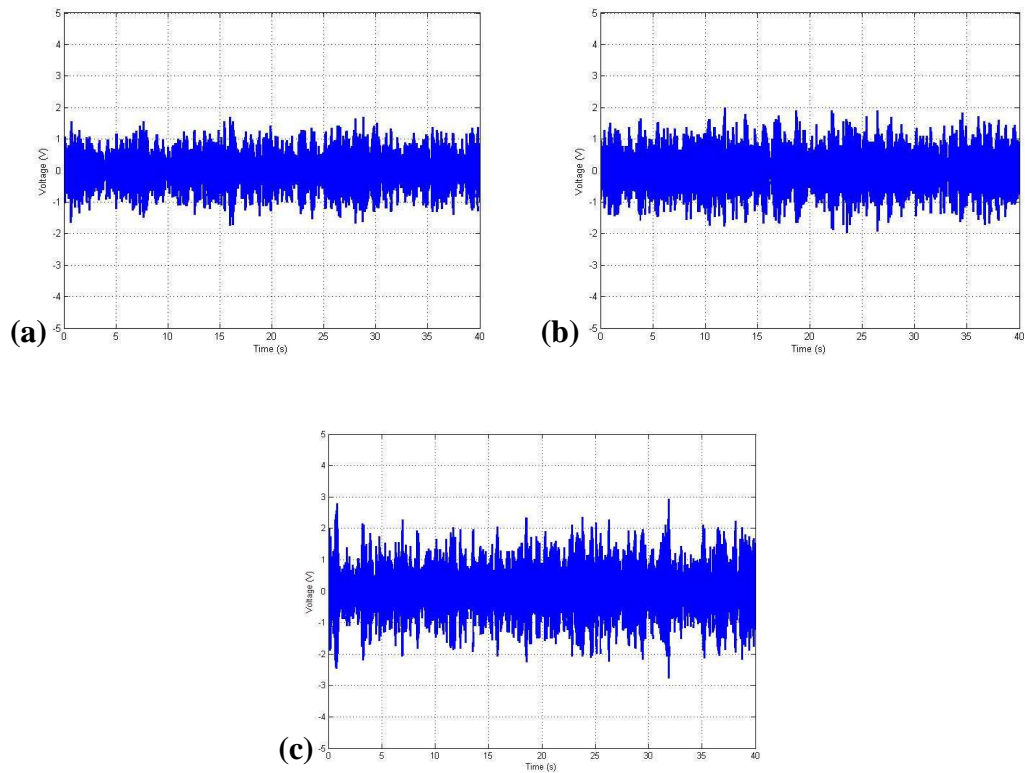


Figure 5. 16 Maximum Voltage Generation for Plates (a) 40 mm Plate (b) 50 mm Plate (c) 60 mm Plate

The fundamental resonance frequency of the vortex energy harvester is also calculated under the real operating condition. For this purposes, the PSD of the voltage output of the vortex energy harvester can be taken by MATLAB by using the time history data obtained from the wind tunnel test. The PSD of the voltage output of the vortex energy harvester is given in Figure 5. 17 and it can be seen from this figure that the fundamental resonance frequency is around 58.30 Hz. This result is very close to the one obtained from the modal shaker test (i.e. 56.64 Hz) and therefore leads to an experimentally verified study.

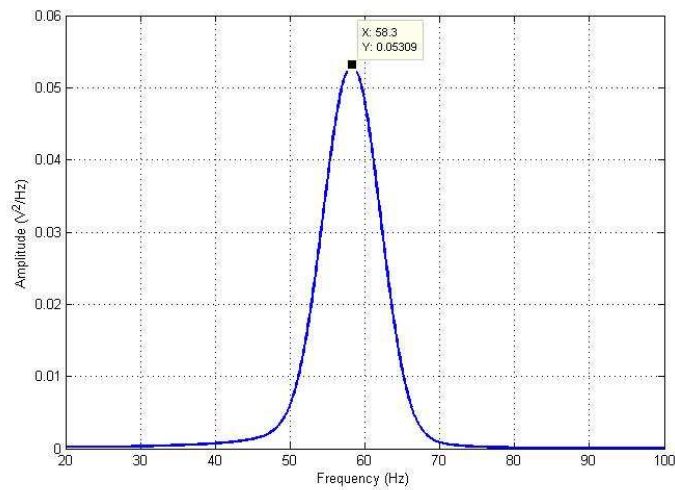


Figure 5. 17 Frequency Response of the Voltage Data for 60 mm Plate in the Determination of the Fundamental Resonance Frequency of the Vortex Energy Harvester

It is practically not very feasible to use this type of voltage output to operate a particular low power level system or to charge a battery. In order to make this voltage useable for the aforementioned purposes, a rectifier circuit should also be used. Therefore, a rectifier circuit converting AC voltage to DC one with its 2 nF capacitance used during the wind tunnel tests. For a 60 mm plate and at maximum wind tunnel speed, DC voltage generation of the vortex energy harvester is given as an example in Figure 5. 18. By using this DC voltage generation of the vortex energy harvester and the capacitance value of rectifier circuit, the average power generation can be obtained by using Equation 4.1. The average power is also presented in Figure 5. 19.

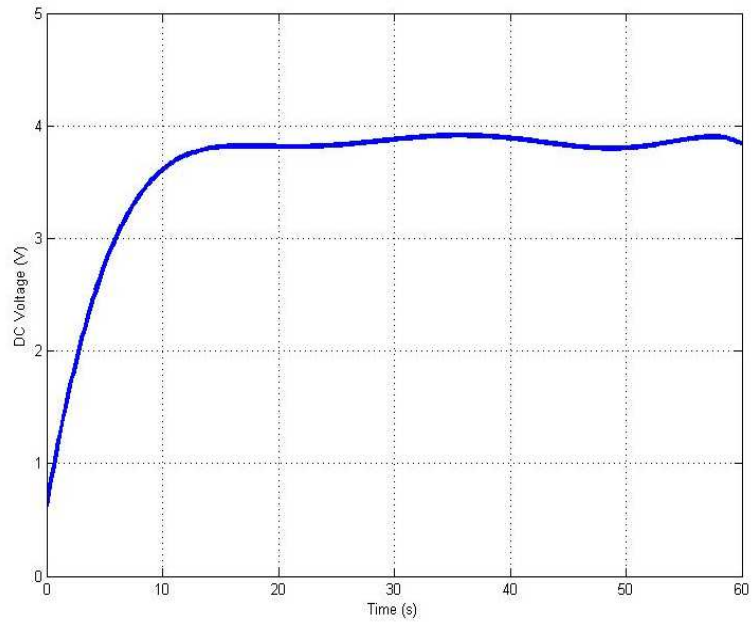


Figure 5. 18 DC Voltage Generation of the Vortex Energy Harvester

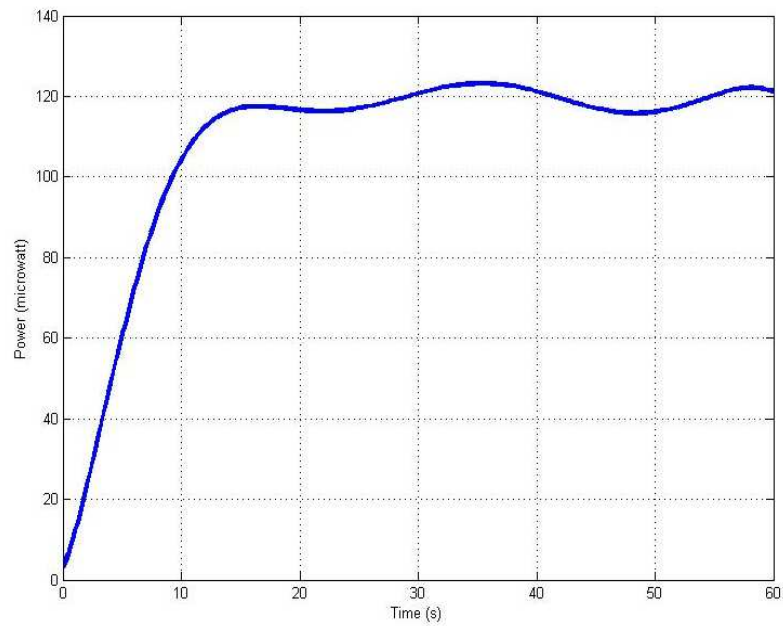


Figure 5. 19 Power Generation of the Vortex Energy Harvester

5.4. Conclusion

In this chapter, the energy harvesting performance of the bimorph piezoelectric beam is investigated under the vortex flow excitation by using plate as a bluff body. For this aim, same vortex energy harvester in Chapter 4 is used to investigate the effect of the size, the position and angle of a bluff body which is considered as a plate in this particular case. The energy generation capability of the vortex energy harvester is examined under real conditions in a wind tunnel through various tests. In this study, the main objective is to arrange a flow speed and choose the size and angle of a bluff body in such a way that the fundamental resonance frequency of the vortex energy harvester is excited.

As it can be observed from the test and analysis results that when the flow speed increases, a higher voltage generation levels can be achieved in comparison to low speed applications through the designed vortex energy harvester. Additionally, the PSD of the time series of vortex energy harvester is taken to obtain the fundamental resonance frequency of the vortex energy harvester and the results indicated that the resonance frequency obtained under operational condition is very close to that of experimentally obtained one. This study also show that the harvested energy depends on both size and the position of the plate located in front of the vortex energy harvester. However, there is no consistent correlation between angle of plate and harvested voltage; this might be due to flow characteristics for the given wind tunnel speeds. This can be further explained as follow.

Flow around flat plate, which is perpendicular to the flow, is more complex than streamlined bodies, such as cylinder [90]. Flow patterns of rectangular plats are given in Figure 5. 20 [90]. In front of the plate, forward bound vortex and strong vortex shedding from corners can be seen during the flow. Also complex wake is created behind the flat plate. Furthermore, there is no stability in the flow and this is shown in Figure 5. 21 [91]. Due to this complexity, there is no theoretical explanation for this case; therefore further wind tunnel tests should be performed in order for better understanding of the flow characteristic.

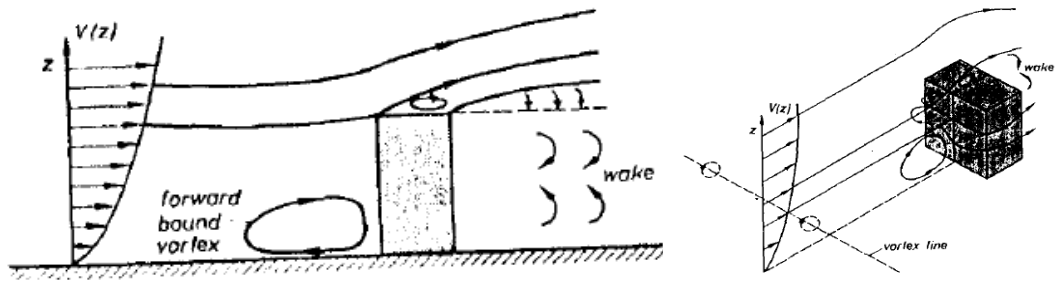


Figure 5.20 Flow Patterns of Flat Plate [90]

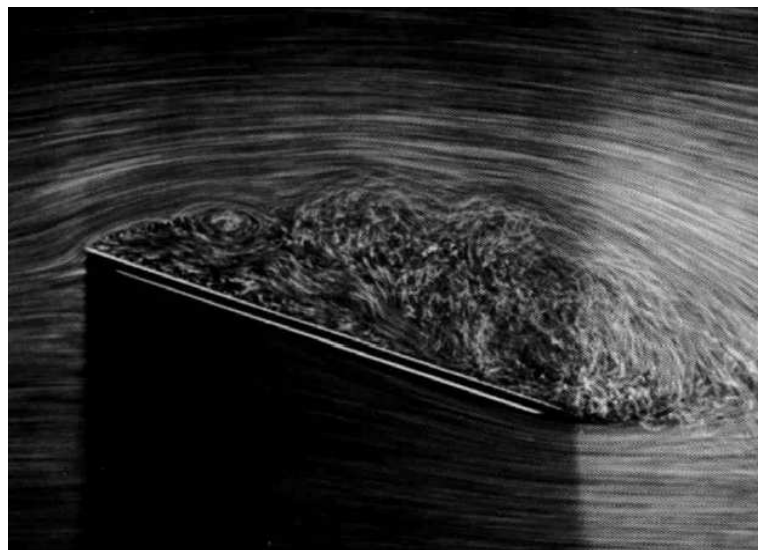


Figure 5.21 Flow Around a Plate, $Re=10000$ and 20° Incidence [91]

Finally, this type of harvester can be integrated to any structure which is expected to work against the air flow. Before integration of the vortex energy harvester, the flow characteristics should also be investigated and well understood beforehand by proper techniques, such as Particle image velocimetry [92]. By using the information and the knowledge gathered through both the numerical and the experimental work, the fundamental resonance frequency of the vortex energy harvester can be tuned via positioning the bluff body in order to maximize the amount of harvested energy.

CHAPTER 6

DEVELOPMENT OF AN ADAPTIVE PIEZOELECTRIC VORTEX ENERGY HARVESTER

6.1. Introduction

As it can be seen from the results of the vortex energy harvester discussed in Chapter 4 and Chapter 5 that the harvested energy changes as the flow velocity varies. Different size of bluff body should also be used for different flow velocity regimes to create vortex in the flow. In the plate case, flow is more complex and unpredictable. It is also more unstable when it is compared with the case of cylinder. This can be better seen from the results available in the literature. By considering all these results, which are playing important roles in the desired harvested energy, an automatic vortex harvester system is proposed for the cylinder. In this system, the diameter and the position of the cylinder can be changed for different flow velocities. The morphing cylinder mechanism can be found in the literature [93]. In this particular study, different mechanisms (Figure 6. 1 to Figure 6. 3) are investigated to change the diameter of the cylinder.

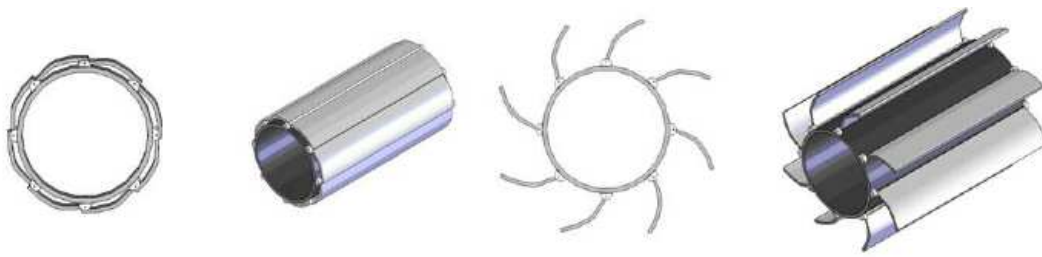


Figure 6. 1 Lens Type Mechanism [93]

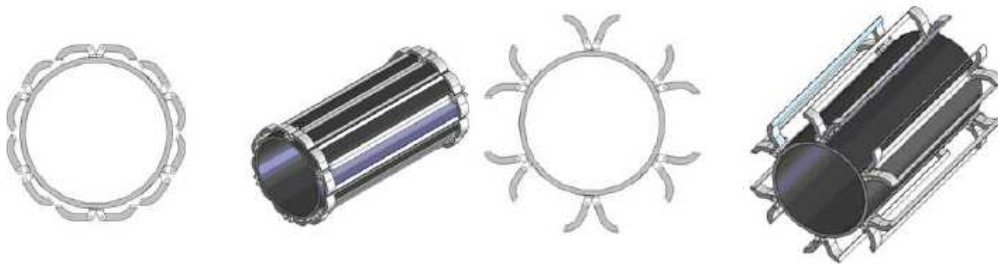


Figure 6. 2 Flower Type Mechanism [93]

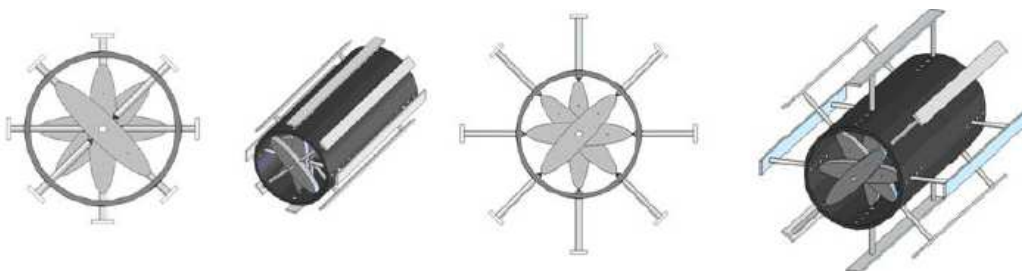


Figure 6. 3 Cam Type Mechanism [93]

By using a flexible skin with this morphing mechanism, the diameter of the cylinder can be increased or decreased. Moreover, the position of the cylinder can also be arranged by using power screw and servomotors on X and Y axes. Furthermore, a control system and various sensors can be used to operate the system automatically. The most important problem in this design is that the consumed energy to operate the system automatically could be much higher than the harvested energy due to the nature of piezoelectric energy harvester. If the energy generation of

the piezoelectric material increases and the consumed energy of the automatic system decreases in the future with the development in the material and the required peripheral equipment, this design can be realized and integrated to an air vehicle structure.

In order to design an efficient vortex energy harvester by using piezoelectric material, the design process should be defined neatly. First of all, air vehicle that will be hosting the energy harvester should be known in advance and the flight profile [94] (Figure 6. 4) of it should also be analyzed and considered at the beginning of the design. The air vehicles generally spend most of their flight time in cruise where the speed and the altitude are generally constant during this particular segment.

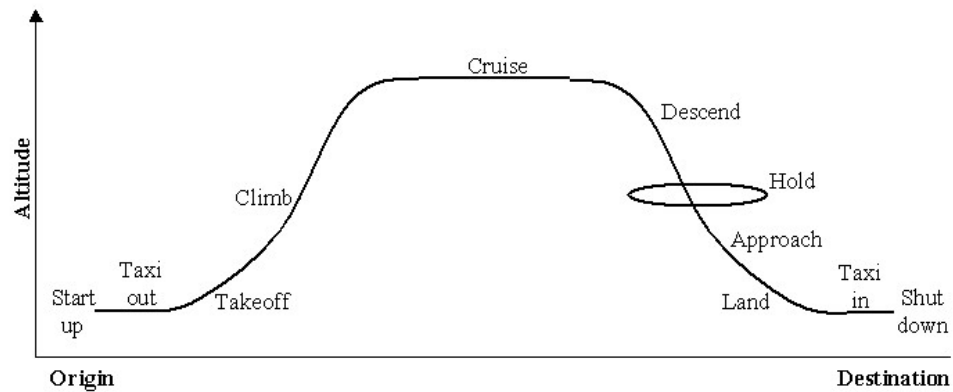


Figure 6. 4 A Sample Flight Profile of an Air Vehicle [94]

During the design process of the adaptive flow harvester, both analytical and finite element methods should be used and experimental modal analysis should also be conducted accompanied with the wind tunnel tests in order to validate the proposed design. Finally, this harvester should be integrated to air vehicle to see the performance of the harvester in real life operating conditions.

6.2. Design of the Diameter Change Mechanism

In order to tune the frequency content of the vortices, the diameter of the cylinder should be changed by considering different flow velocities. For this aim, a diameter change mechanism is proposed.

In this mechanism, the diameter of the cylinder is changed via scissor mechanism. Scissor mechanism can be defined that the supports can be folded in a criss-cross 'X' pattern known as a pantograph by using linkages (Figure 6. 5 [95]). In the scissor mechanism, the system can be operated through a single linear actuator by changing L and H in an increased or decreased fashion. By combining this mechanism and the morphing cylinder mechanism [93] (Figure 6. 3), the diameter of the cylinder can be changed/tuned.

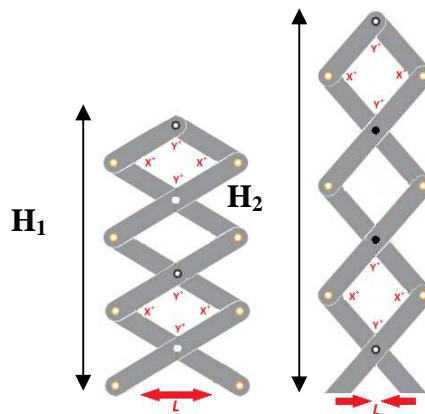


Figure 6. 5 Scissor Mechanism [95]

Proposed mechanism for the diameter change can be seen in Figure 6. 6 and Figure 6. 7. It is stated that [96] flow separates from cylinder skin and generates vortex around 100° . By using this information, a mechanism having five scissors is used to optimize the number of sub mechanism and this mechanism can be operated by using only one linear actuator. This mechanism comprises one supporting cylinder and one flexible skin.

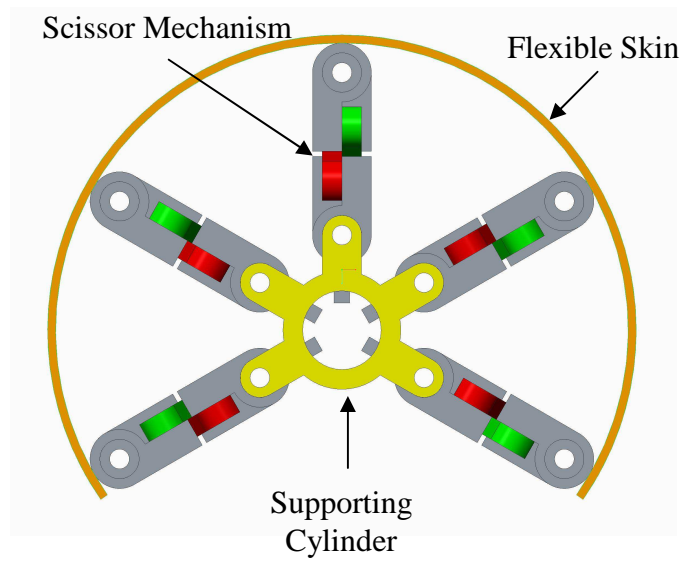


Figure 6. 6 Morphing Cylinder Mechanism (Top View)

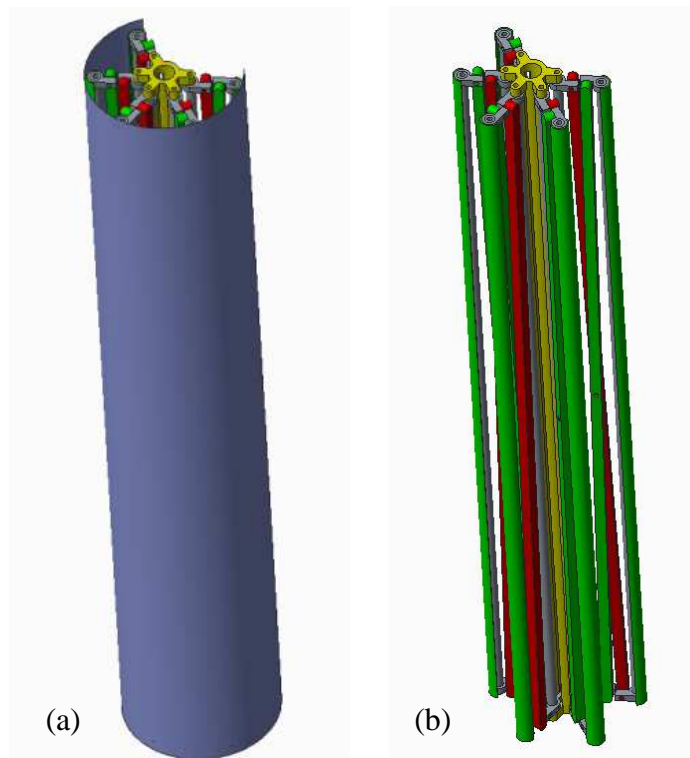


Figure 6. 7 Morphing Cylinder Mechanism: Isometric View (a) with skin (b) without skin

6.2.1. Kinematic Analysis of the Diameter Change Mechanism

Kinematic analysis of this mechanism is performed in ANSYS Workbench Rigid Body modeling module. First of all, the mechanism is modeled in 3-D modeling software; Creo Parametric [97]. In this analysis, a displacement of 20 mm is given to scissor mechanism and the diameter is changed from 15 mm to 110 mm (Figure 6. 8). The view of the morphing cylinder mechanism in an extended configuration can be seen in Figure 6. 9.

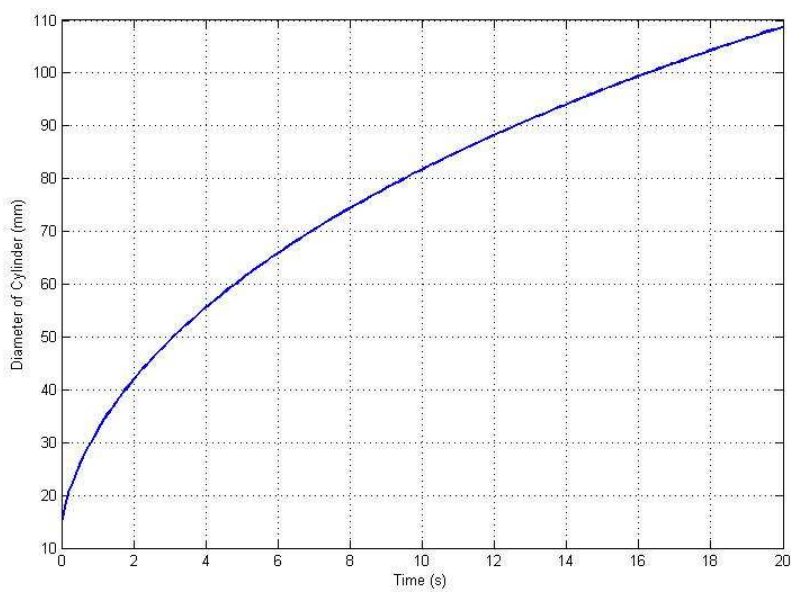


Figure 6. 8 Diameter Change of the Morphing Cylinder Mechanism

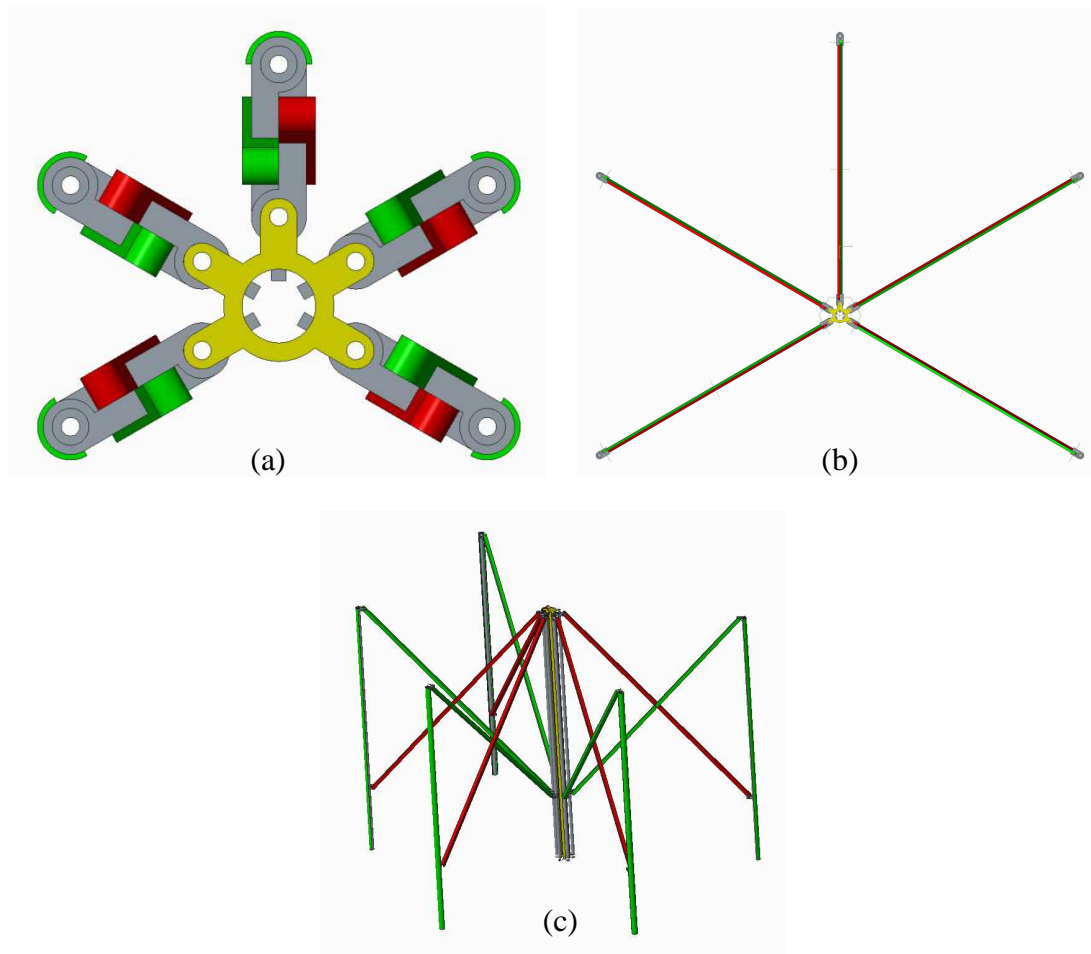


Figure 6. 9 Extended View of the Morphing Cylinder Mechanism

(a) Retracted Position (b) Extended Position Top View and (c) Extended Position Isometric View

6.2.2. Finite Element Analysis of the Diameter Change Mechanism

The diameter change mechanism works against to the flow and therefore it should have enough strength. All part of the mechanism, except the flexible skin which is neoprene, is proposed to be made of aluminium. Neoprene is not included in the finite element analysis of diameter change mechanism due to high element distortion and convergence problem and therefore extension characteristic of the neoprene is analysed separately.

6.2.2.1. Strength Analysis of the Neoprene

During the extension of the diameter change mechanism, neoprene should stretch properly. In order to find the required force, a finite element analysis is performed. During this analysis, rectangular shape for neoprene geometry is taken in order to simplify the analysis. The thickness of this neoprene is taken as 0.1 mm (Figure 6. 10).

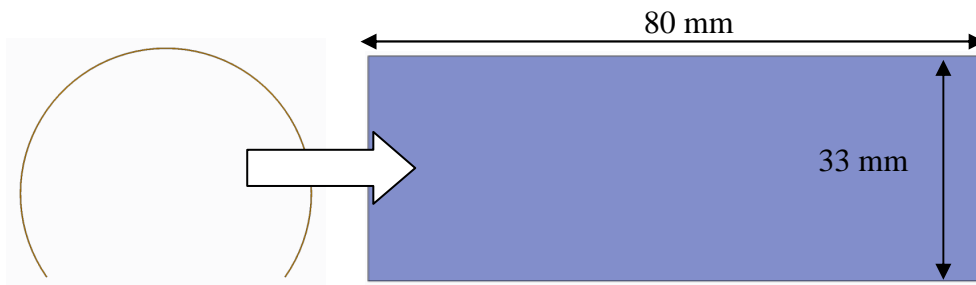


Figure 6. 10 Neoprene Geometry

Finite element analysis is done in ANSYS by using Shell element and mesh consists of 19048 nodes and 2640 elements in total (Figure 6. 11a). Frictionless boundary conditions are given to the short edges and 1 N force is applied to the long edges (Figure 6.11b).

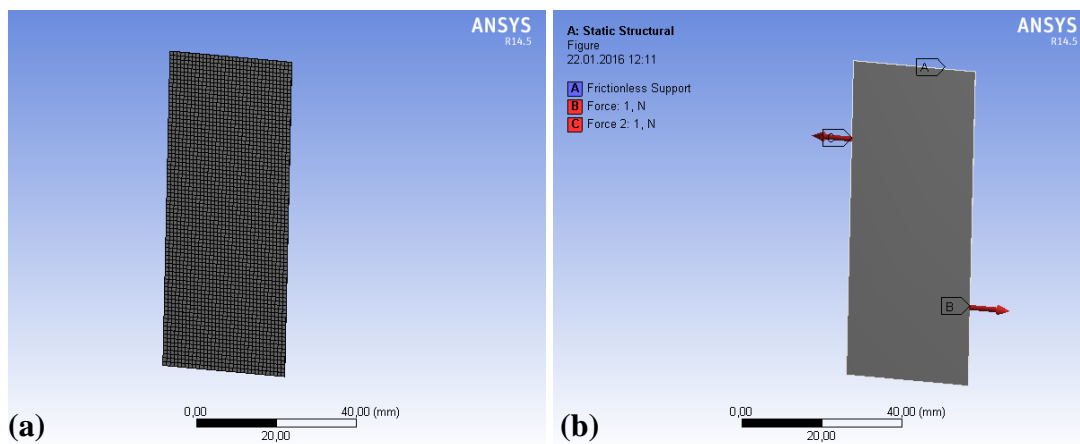


Figure 6. 11 (a) Mesh and (b) Boundary Conditions on Neoprene Geometry

Nonlinear analysis is performed in ANSYS and results are obtained. For 1 N force, short edge of neoprene is deformed up to 500 mm and stress is 0.6 MPa, Figure 6. 12.

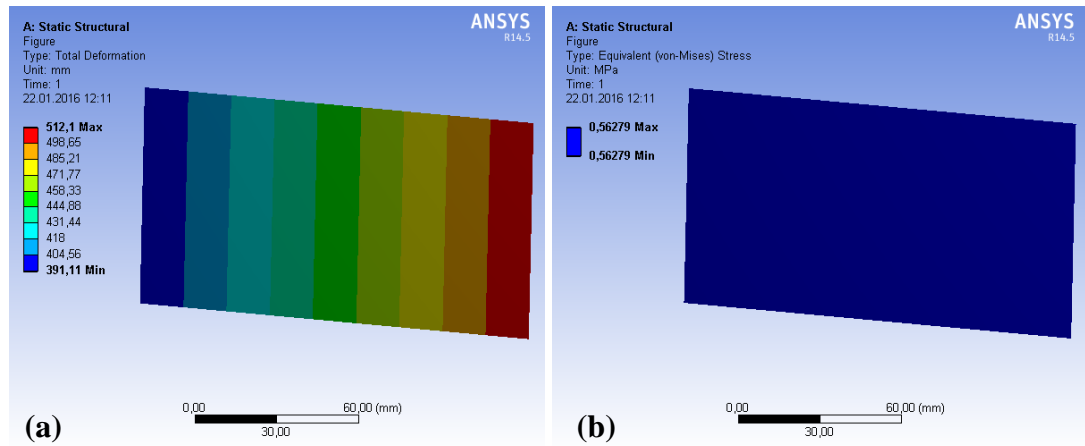


Figure 6. 12 (a) Deformation and (b) Stress in Neoprene Geometry

After this analysis, 1 N force is directly applied to the diameter change mechanism in order to simulate the effect of neoprene on this mechanism.

6.2.2.2. Strength Analysis of the Diameter Change Mechanism

Strength analysis of the diameter change mechanism is performed in ANSYS Workbench 14.5. First of all, the CAD model of the mechanism is directly imported to the finite element analysis software. Mesh of the diameter change mechanism has 109520 nodes and 25700 elements (SOLID 186) in total and shown in Figure 6. 13. Revolute and slider joints are defined for this mechanism (Figure 6. 14). Fixed boundary condition is applied at the end of mechanism and forces due to flow, friction and neoprene are given in Figure 6. 15a. A 1 mm/s joint velocity is also given to the mechanism in order to simulate the system (Figure 6. 15b).

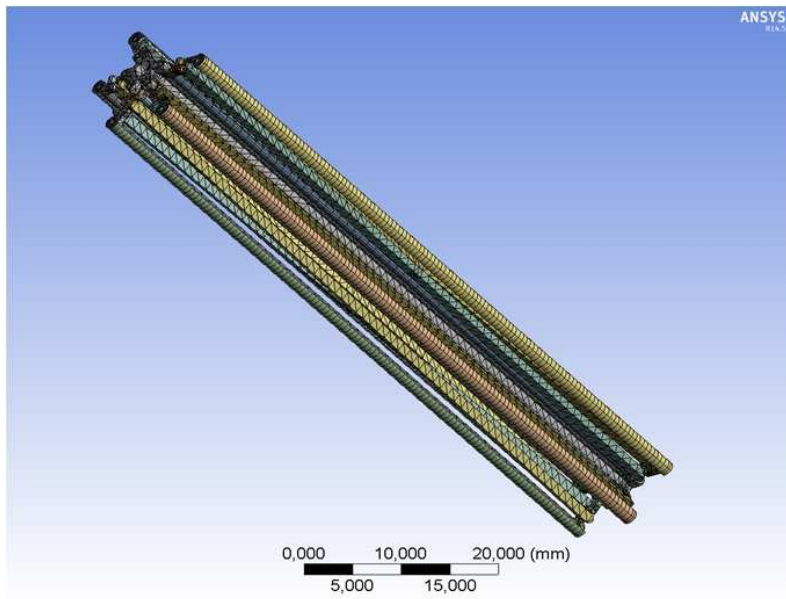


Figure 6. 13 Mesh of Mechanism

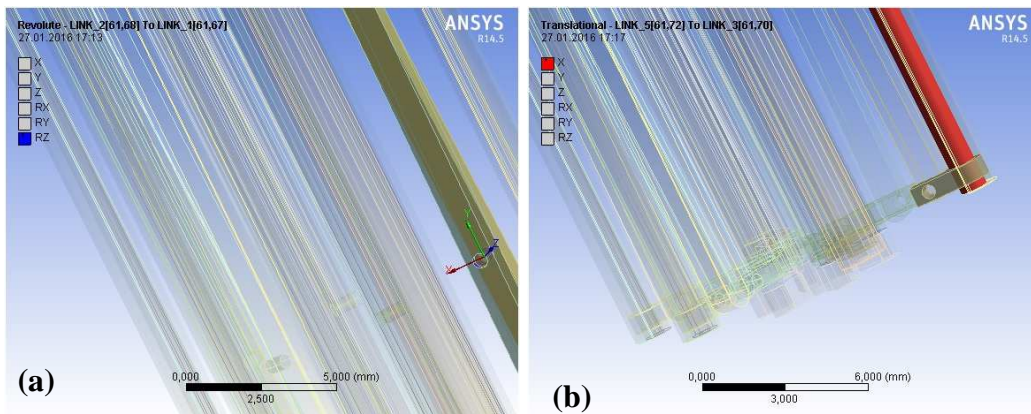


Figure 6. 14 Revolute (a) and Slider (b) Joint Mechanism

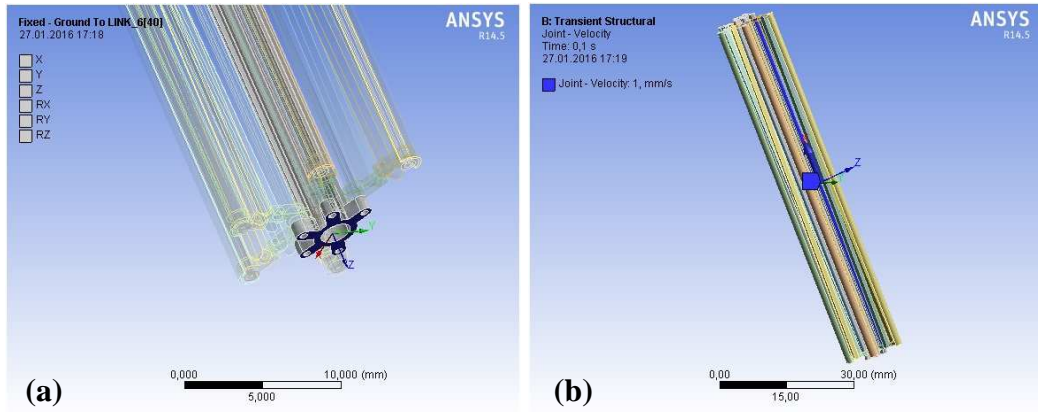


Figure 6.15 (a) Fixed Support and (b) Joint Velocity of Mechanism

Following that a transient analysis is performed. In this analysis, flexible skin is not included due to nonlinear behaviour of the natural rubber. However, the total force calculated in the neoprene analysis is directly applied to the mechanism.

Pressure load due to flow is calculated by the following equation:

$$P = \frac{1}{2} \rho_{\text{air}} V^2 \quad (6.1)$$

where; P is the pressure (Pa), ρ_{air} is the density of air (kg/m^3) and V is the flow speed (m/s^2). Drag force due to flow can also be found by the following equation:

$$F_D = \frac{1}{2} \rho_{\text{air}} V^2 C_D A \quad (6.2)$$

where; F_D is the drag force (N), ρ_{air} is the density of air (kg/m^3) and V is the flow speed (m/s^2), C_D is the drag coefficient and A is the reference area.

From this, a drag pressure, P_D , can be calculated by dividing drag force to the reference area as follow:

$$P_D = \frac{F_D}{A} = \frac{1}{2} \rho_{\text{air}} V^2 C_D \quad (6.3)$$

In Chapter 4, the maximum flow speed is taken as 14.25 m/s^2 and by using this particular speed, the total pressure is calculated as 540 Pa. This pressure is then

applied as shown in Figure 6.16. Moreover, frictional force and moment in the joints are calculated as;

$$F_{\text{friction}} = \mu F_{\text{duetopressure}} \quad (6.4)$$

where, F_{friction} is the frictional force in the slider joint, μ is the friction coefficient and $F_{\text{duetopressure}}$ is the force due to flow pressure.

$$M_{\text{friction}} = r_{\text{revolutejoint}} (\mu F_{\text{duetopressure}}) \quad (6.5)$$

where, M_{friction} is the frictional moment in the revolute joint, $r_{\text{revolutejoint}}$ is the radius of the revolute joint (250 micrometer), μ is the friction coefficient and $F_{\text{duetopressure}}$ is the force due to flow pressure. All components in the mechanism are aluminum and friction coefficient in the two aluminum components is 0.3 if both surfaces are lubricated as greasy surfaces [98]. Finally, all the calculated pressure, the frictional forces, the force due to neoprene and joint velocity are applied in this transient analysis. After that, the total displacement (Figure 6. 17 and Figure 6. 18) and the stresses (Figure 6. 19 and Figure 6. 20) occurred in this mechanism is found as the mechanism is extending.

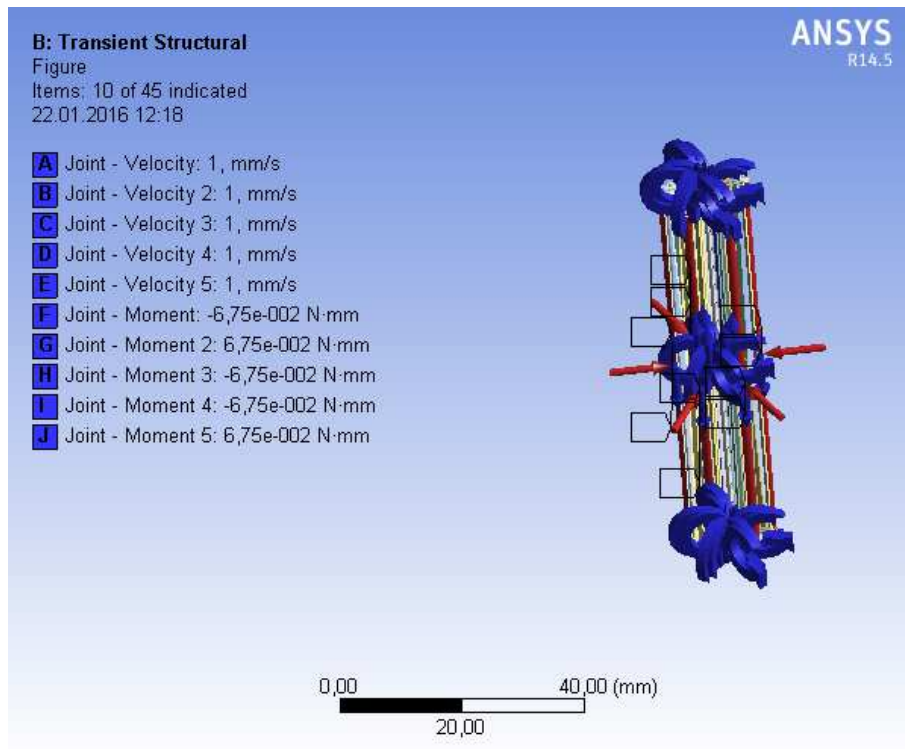


Figure 6. 16 Pressure Application Location

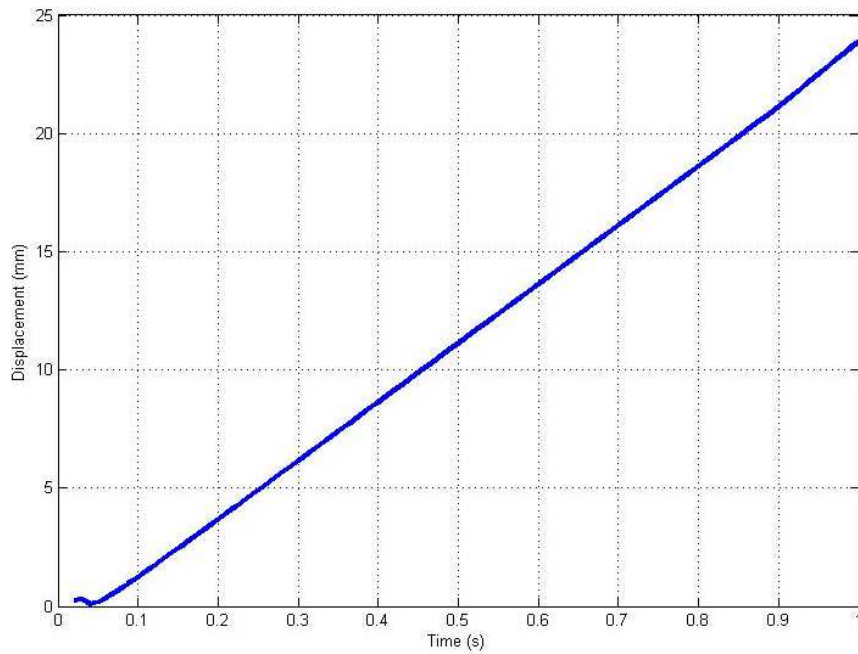


Figure 6. 17 Total Displacement of Mechanism under the Loading

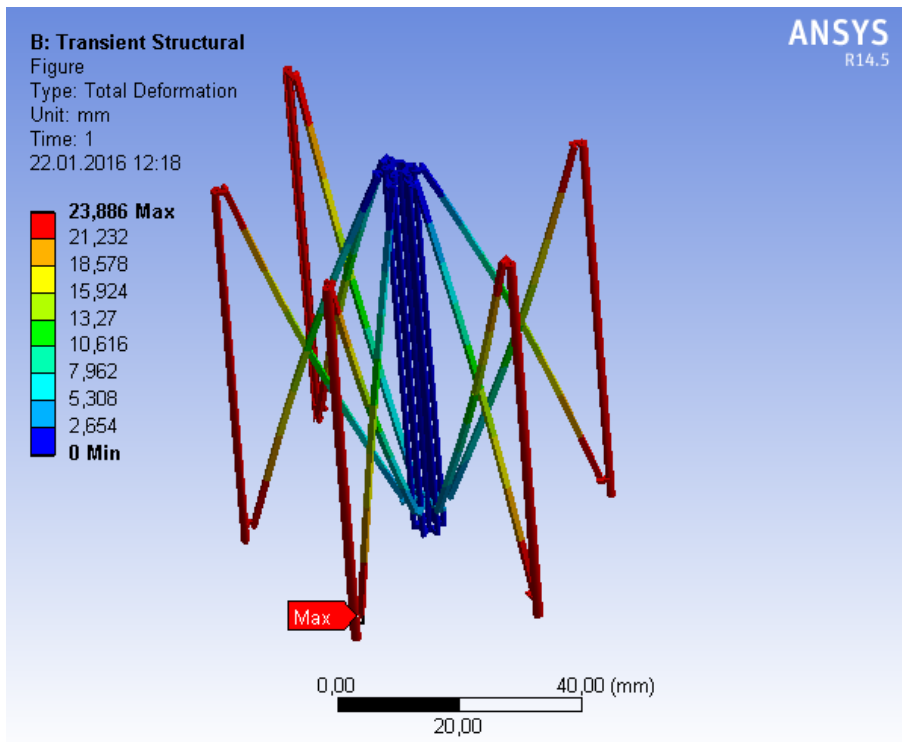


Figure 6. 18 Total Displacement of Mechanism after 1s

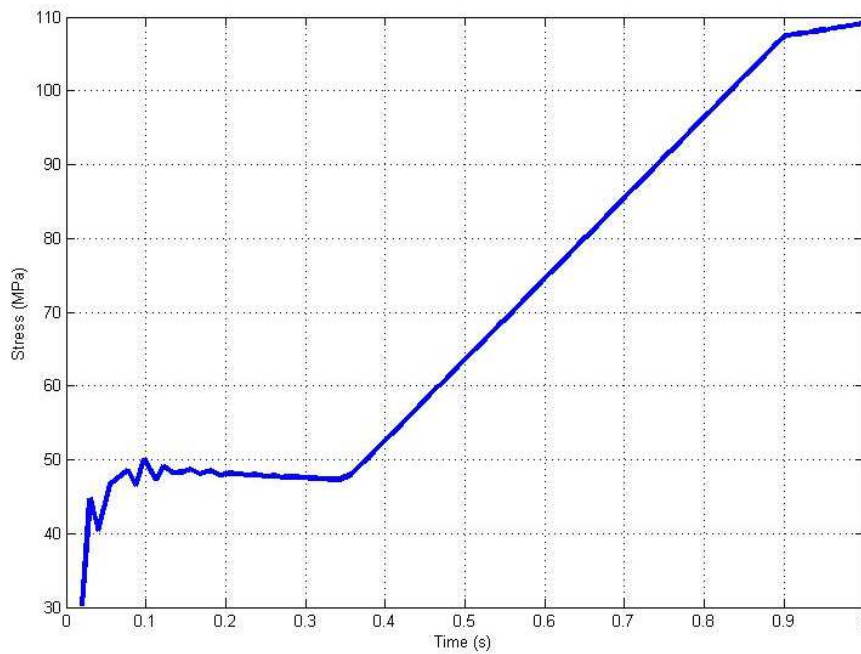


Figure 6. 19 Stress vs Time during the Extension of the Scissor Mechanism

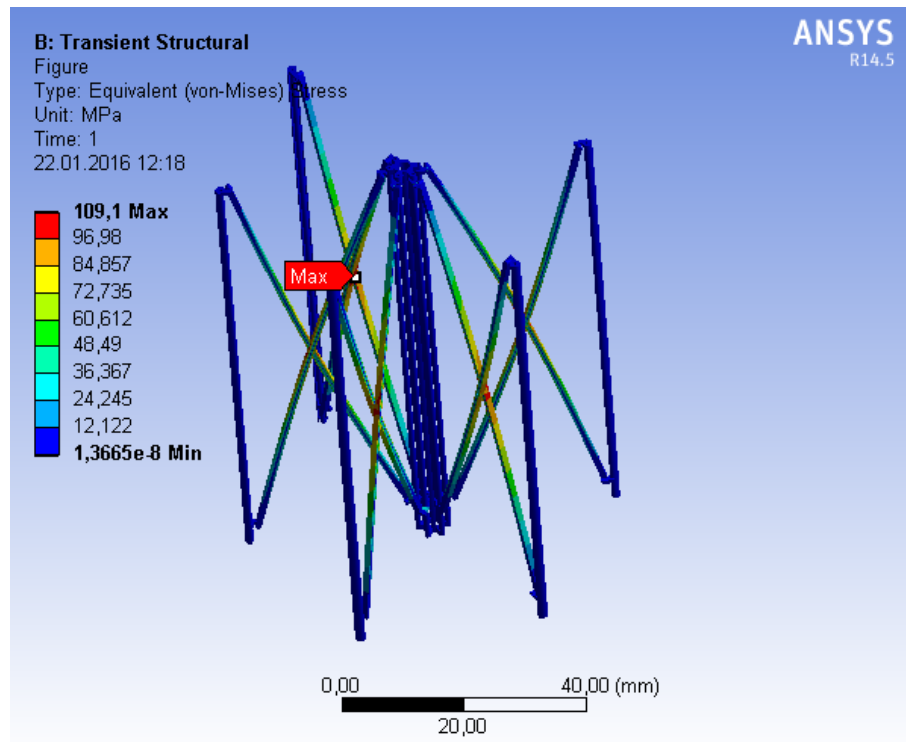


Figure 6. 20 Stress After the Extension of Scissor Mechanism

As it is seen from these analyses results, the stress in this mechanism is much lower 110 MPa than the yield strength of aluminum (i.e. 280 MPa); therefore it can be concluded that the scissor mechanism can safely be used under aforementioned flow condition. Moreover, the reaction force can also be calculated for the slotted joint (Figure 6. 21) where the actuator can possibly be mounted. As seen from the reaction force result, 2.4 N force is enough to open this mechanism under applied load. For the five arm scissor mechanism, required total force is directly calculated as 12 N. By using this information, an actuator for this mechanism can be selected.

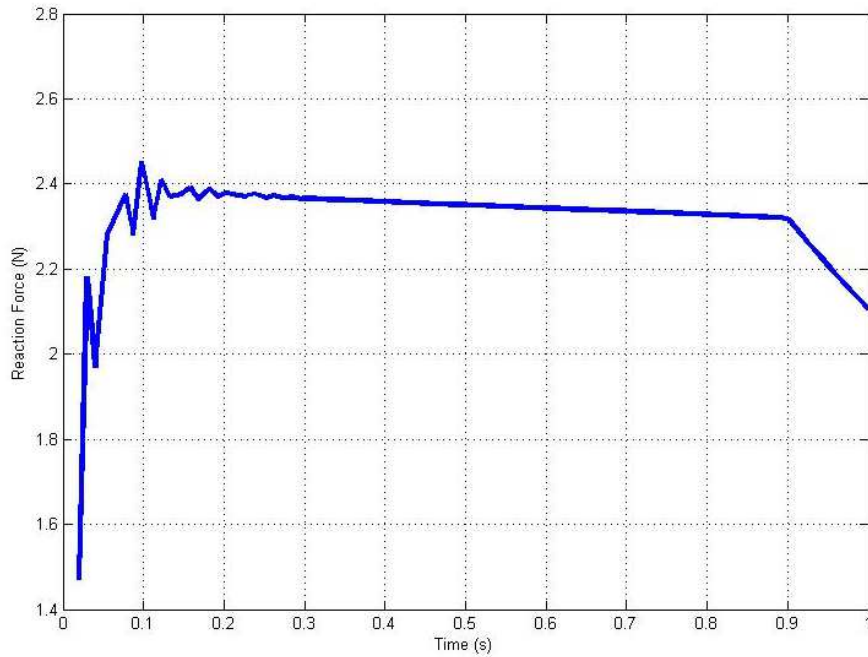


Figure 6. 21 Reaction Force at the Slotted Joint (Possible Actuator Mount Location)

During this analysis, the effect of flexible skin is added as a force. It is known [99] that maximum strain level of neoprene is 600%; therefore if the diameter of the mechanism is increased by 6 times of the initial diameter, no possible failure will be expected in the flexible skin.

6.3. Automation of the Adaptive Piezoelectric Vortex Energy Harvester

In order to automate the proposed adaptive piezoelectric vortex energy harvester, a special linear actuator, a pitot tube and a simple microprocessor should be used. Through a linear actuator, a diameter change mechanism can be operated and the diameter of the adaptive piezoelectric vortex energy harvester can be tuned. For the calculation of the flow speed, the flow pressure is needed and it can be obtained via pitot tube. All the automation process can be performed by a microprocessor.

The conceptual design for adaptive piezoelectric vortex energy harvester can be seen in Figure 6. 22. In this design, a miniature linear actuator, which is a product of Figelli [100], is selected (Figure 6. 23). Properties of this actuator are given in Table 6. 1.

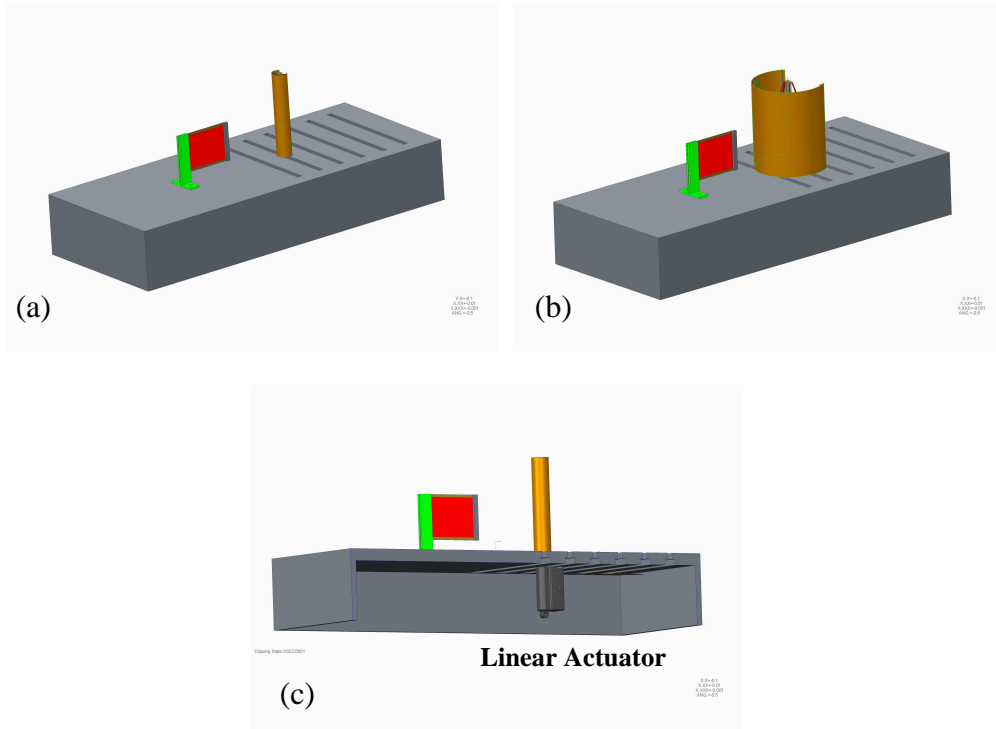


Figure 6. 22 Adaptive Piezoelectric Vortex Energy Harvester

(a) Retracted (b) Extended and (c) View of Actuator



Figure 6. 23 Linear Actuator, Frigelli [100]

Table 6. 1 Specifications of the Linear Actuator [100]

PQ12 Specifications			
Gearing Option	30:1	63:1	100:1
Peak Power Point	15N@15mm/s	30N@8mm/s	40N@6mm/s
Peak Efficiency Point	8N@20mm/s	12N@12mm/s	20N@8mm/s
Max Speed	28 mm/s	15 mm/s	10 mm/s
Max Force (Lifted)	18 N	45 N	50 N
Max Side Force	5 N	10 N	10 N
Back Drive Force	9 N	25 N	35 N
Stroke	20 mm		
Input Voltage	6 or 12V DC		
Stall Current	550mA @ 6V		
Mass	15 g		

The maximum stroke value for this actuator is 20 mm and it is powerful enough to increase the diameter of the cylinder from 10 mm to 50 mm. The maximum reaction force, where the actuator can possibly be mounted, is found from the finite element analysis as 2.4 N for only one scissor mechanism. As it is known that having five identical arms in a scissor mechanisms are used in adaptive piezoelectric vortex energy harvester, therefore the required actuation force is found as 12 N and it can easily be driven by this selected linear actuator.

6.4. Conclusion

Previously in Chapter 4, it was shown that the harvested energy depends on both size and the position of the cylinder, which is located in front of the vortex energy harvester. Having realized the importance of the position and the size of the cylinder in the energy harvesting performance, a conceptual design is then proposed for the adaptive piezoelectric vortex energy harvester having the capability of adapting itself to different flow velocities in order to increase the desired harvested energy.

During the development of the mechanism for the adaptive piezoelectric vortex energy harvester, kinematic and strength analyses are performed to understand the behavior of the system. In this analysis, friction in joints and nonlinear effect of the natural rubber are omitted. The mechanism is proposed as to be driven by a selected linear actuator. A special control system should also be developed in order to operate the adaptive piezoelectric vortex energy harvester effectively. A microprocessor, a pitot tube and special cables should be chosen to develop a control system for the adaptive piezoelectric vortex energy harvester.

CHAPTER 7

CONCLUSION

7.1 General Conclusions

In this thesis, piezoelectric energy harvesting from vortex air load is examined in details. First of all, the direct application of the different piezoelectric materials is analyzed by using the vertical fin-like structure as a host one. During this study, the finite element modelling and analysis tool is used to obtain the dynamic characteristics of the structures. Then, the energy harvesting performance of piezoelectric materials is investigated through both ground vibration and wind tunnel tests. It is observed that the application of the small and thin piezoelectric patch to the host structure does not generally change the dynamic characteristic of the host structure and the energy can be harvested by vortex air load due to the excitation of the fundamental resonance frequency of smart structure.

After this study, a bimorph piezoelectric beam is designed and integrated to the vertical fin-like structure. During the integration process, it is aimed that the bimorph piezoelectric beam is placed on the vertical fin-like structure without changing the dynamic characteristics of it by using a finite element analysis results. Therefore, the bimorph piezoelectric beam is placed to the minimum displacement locations of the mode shape of the vertical fin-like structure around the first two resonance frequencies. This study is then verified by a modal analysis. The energy harvesting performance of the bimorph piezoelectric beam is also investigated by

both ground vibration and wind tunnel tests. During the wind tunnel test, a bluff body is used to create a vortex air load and the frequency content is tuned to be close to the first resonance frequency of the bimorph piezoelectric beam in order to increase the harvested energy.

Following these studies, a piezoelectric vortex energy harvester is designed. In the design process, the main purpose is to find the required size and the position of the bluff body so as to increase the harvested energy. In these studies, a cylinder and a plate are used as bluff bodies separately. Therefore, a special test setup is prepared to investigate the effect of the diameter and position of these bluff bodies. The performance of the individual vortex energy harvester is then investigated through the wind tunnel test.

As it is a known fact that an aerial vehicle generally operates at different cruise speeds therefore in order to use vortex harvester efficiently, the size and the location of the bluff body should be arranged regarding the cruise speed. It is also seen from results of Chapter 4 and 5; the vortex flow is more stable and predictable in the case of cylinder. For this reason, the diameter change mechanism is also proposed. In this proposal, diameter of the bluff body can be increased automatically by using a special mechanism and a control system.

In this thesis, a special piezoelectric vortex energy harvester, which works under different flow speeds, is developed and the background for its design is explained in detail by also providing analytical and experimental studies.

7.2 Recommendations for Future Work

Different applications of the piezoelectric vortex energy harvesters are investigated in this thesis and a special design is proposed for the piezoelectric vortex energy harvester to increase the harvested energy and the proposed designed is then verified by various computer analyses.

As a future work;

- Flow characteristics of vortex energy harvester should be determined during the wind tunnel test and flow pattern should be found by PIV methods.
- After finding flow patterns for both cylinder and plate, position and size should be decided with respect to these patterns in order to increase the efficiency of the designed vortex energy harvester.
- The nonlinear effect of neoprene with mechanism might be analysed in finite element software in order to see the effect on the operation of the mechanism.
- The proposed design might be manufactured and validated through wind tunnel tests. This design comprises very small linkages and therefore they might be manufactured by micro machining technology.
- If there are improvements in the development and manufacturing of piezoelectric materials, the effect of these materials might be analysed and used in order to increase the efficiency of the energy harvester.
- A proper host structure might be selected to integrate the piezoelectric vortex energy harvester. During the integration process, the effect of the piezoelectric vortex energy harvester on host structure should be carefully examined in order not to change both the structural dynamic and the aerodynamic characteristics of it.
- Finally, the performance of the piezoelectric vortex energy harvester might be investigated in real life operational conditions.

REFERENCES

- [1] <http://www.cleansky.eu>, Clean Sky, (page visit, 20.07.2015)
- [2] <http://www.solarimpulse.com>, Solar Impulse, (page visit, 20.07.2015)
- [3] <http://www.greencarcongress.com/2009/07/samulet-20090728.html>, Green Car Congress, 28.08.2009 (page visit, 20.07.2015)
- [4] First Draft of Standard on Vibration Energy Harvesting, 4th Annual Energy Harvesting Workshop, 28-29 January 2009
- [5] F. Cottone, “Introduction to Vibration Energy Harvesting”, NiPS Energy Harvesting Summer School, August 1-5, 2011.
- [6] M. Raju and M. Granzier, “Energy Harvesting”, Texas Instrument White Paper, 2010.
- [7] A. Ertürk, “Piezoelectric Energy Harvesting”, John Wiley and Sons, 2011.
- [8] PI Ceramic, “Energy Harvesting Uses the Piezo Effect, Duraact Piezo Transducer plus Matching Electronics”, White Paper, 2011.
- [9] <https://www.americanpiezo.com/knowledge-center/piezo-theory/piezoelectricity.html> (page visit: 26.02.2014)
- [10] http://www.efunda.com/materials/piezo/piezo_math/transforms.cfm, (page visit, 20.07.2015)
- [11] C. B. Williams, C. Sherwood, M. A. Harradine, P. H. Mellor, T. S. Birch, and R. B. Yates, “Development of an electromagnetic micro-generator”, IEEE Proc. Circuits Devices Syst., 148 [6] 337 – 342 (2001).

- [12] A. Ertürk and D.J. Inman, A distributed parameter electromechanical model for cantilevered piezoelectric energy harvesters, *ASME Journal of Vibration and Acoustics*, 130, 041002.
- [13] A. Ertürk and D. Inman, “An experimentally validated bimorph cantilever model for piezoelectric energy harvesting from base excitations”, *Smart Materials and Structures*, 18, (2009), 1-18.
- [14] ANSYS Help Manuel.
- [15] C. M. Kim, C. Kim, J. Lee, J. Paik, J. Cho, M. Chun, Y. Jeong, and Y. Lee, “Design and Evaluation of a Piezoelectric Energy Harvester Produced with a Finite Element Method”, *Transactions on Electrical and Electronic Materials*, Vol. 11, No. 5, (2010), 206-211.
- [16] A. Ertürk and D. Inman, “An experimentally validated bimorph cantilever model for piezoelectric energy harvesting from base excitations”, *Smart Materials and Structures*, 18, (2009), 1-18.
- [17] M. Umeda, K. Nakamura and S. Ueha, “Energy Storage Characteristics of a Piezo-Generator using Impact Induced Vibration”, *Jpn. J. Appl. Phys.*, Vol. 36, 1997, p. 3146-3151.
- [18] F. Cottone, “Introduction to Vibration Energy Harvesting”, NiPS Energy Harvesting Summer School, August 1-5, 2011.
- [19] M. Raju and M. Granzier, “Energy Harvesting”, Texas Instrument White Paper, 2010.
- [20] U. Wagner, A. Veichtlabauer and E. Muller, “Requirements for battery-free embedded systems”, Extended Abstract.
- [21] R. Freeland, “Vibration Energy Harvesting”, Perpetuum, February 2011.
- [22] Cedrat Technologies, “Vibration Energy Harvesting VEH-APA 400M-MD”, Cedrat Group, July 2010.

- [23] O. Sosnicki, N. Lhermet, F. Claeysen, “Vibration Energy Harvesting in Aircraft Using Piezoelectric Actuator” ACTUATOR 2006, 10th International Conference on New Actuators, 14 – 16 June 2006, p. 968-971.
- [24] S. R. Anton, A. Erturk, N. Ha and D. Inman, “Self-Charging Structures Using Piezoceramics and Thin-Film Batteries, Proceedings of the ASME 2009 Conference on Smart Materials, Adaptive Structures and Intelligent Systems SMASIS2009, September 21-23, 2009
- [25] A. Erturk, S. R. Anton and D. J. Inman, “Piezoelectric energy harvesting from multifunctional wing spars for UAVs – Part 1: coupled modeling and preliminary analysis”, Active and Passive Smart Structures and Integrated Systems 2009, edited by Mehdi Ahmadian, Mehrdad N. Ghasemi-Nejhad, Proc. of SPIE Vol. 7288, 72880C
- [26] A. Erturk, S. R. Anton and D. J. Inman, “Piezoelectric energy harvesting from multifunctional wing spars for UAVs – Part 2: experiments and storage applications”, Active and Passive Smart Structures and Integrated Systems 2009, edited by Mehdi Ahmadian, Mehrdad N. Ghasemi-Nejhad, Proc. of SPIE Vol. 7288, 72880D
- [27] <http://www.designation-systems.net/dusrm/app4/wasp.html>, Designation System, (page visit, 20.07.2015)
- [28] A. Erturk, W. G. R. Vieira C. De Marqui, Jr. and D. J. Inman, “On the energy harvesting potential of piezoaeroelastic systems”, Applied Physics Letters 96, 184103-1 - 184103-3, 2010.
- [29] S. R. Anton, “Multifunctional Piezoelectric Energy Harvesting Concepts”, Phd Thesis, April 25, 2011 Blacksburg, Virginia
- [30] The News Letter of the Piezo Institute, “Piezo News”, Issue 2 – Summer 2008
- [31] S. R. Anton, D. J. Inman, “Vibration energy harvesting for unmanned aerial vehicles”, Active and Passive Smart Structures and Integrated Systems 2008, Proc. of SPIE Vol. 6928, p. 692824-1 - 692824-12

- [32] A. Erturk, J. M. Renno and D. J. Inman, "Piezoelectric Energy Harvesting from an L-Shaped Beam-Mass Structure, Active and Passive Smart Structures and Integrated Systems, 2008, 69280I-1 - 69280I-15.
- [33] S.W. Arms, C.P. Townsend, D.L. Churchill, J.H. Galbreath, B. Corneau, R.P. Ketcham, N. Phan, "Energy Harvesting, Wireless, Structural Health Monitoring and Reporting System", 2nd Asia Pacific Workshop on SHM, Melbourne, 2-4 December 2008.
- [34] S. P. Beeby, M. J. Tudor and N. M. White, "Energy harvesting vibration sources for microsystems applications", *Meas. Sci. Technol.* 17 (2006) p. R175–R195
- [35] S. Priya and D. J. Inman, "Energy Harvesting Technologies", Springer, 2009.
- [36] S. Pobering and N. Schwesinger, "A novel hydropower harvesting device", Munich University of Technology, Proceedings of the 2004 International Conference on MEMS, NANO and Smart Systems (ICMENS'04), 2004
- [37] E. Minazara, D. Vasic and F. Costa, "Piezoelectric Generator Harvesting Bike Vibrations Energy to Supply Portable Devices"
- [38] S. E. Prasad, "Power Harvesting", Lectures on Smart Structures in Middle East Technical University, March 2012.
- [39] A. Messineo, A. Alaimo, M. Denaro, D. Ticali, "Piezoelectric Bender Transducers for Energy Harvesting Applications", *Energy Procedia* 14 (2012) p. 39 – 44
- [40] L. Miller and P Wright, "Micro scale energy harvesting from ambient vibrations", California Energy Commission - Public Interest Energy Research Program.
- [41] X. Chen, T. Yang, W. Wang, X. Yao, "Vibration energy harvesting with a clamped piezoelectric circular diaphragm", *Ceramics International* 38S (2012) S271–S274

- [42] A. F. Arrieta, P. Hagedorn, A. Erturk and D. J. Inman , "A piezoelectric bistable plate for nonlinear broadband energy harvesting", *Applied Physics Letters*, 97 (2010), 104102-1-104102-3.
- [43] A. Erturk, J. Hoffmann, and D. J. Inman, "A piezomagnetoelastic structure for broadband vibration energy harvesting", *Applied Physics Letters*, 94 (2009), 254102-1-254102-3.
- [44] C. Eichhorn, F. Goldschmidtboeing, Y. Porro and P. Woias, "A Piezoelectric Harvester With An Integrated Frequency Tuning Mechanism", *PowerMEMS 2009*, Washington DC, USA, December 1-4, 2009.
- [45] C. Eichhorn, F. Goldschmidtboeing and P. Woias, "A Frequency Tunable Piezoelectric Energy Converter Based On A Cantilever Beam", *Proceedings of PowerMEMS 2008+ microEMS2008*, Sendai, Japan, November 9-12, (2008).
- [46] Swee-Leong, Kok, M. F. A. Rahman, D. F. Weng, Yap, Yih Hwa, Ho, "Bandwidth Widening Strategies for Piezoelectric Based Energy Harvesting from Ambient Vibration Sources", *International Conference on Computer Applications and Industrial Electronics (ICCAIE 2011)*, p. 469-473, 2011.
- [47] L. Tang, Y. Yang, H. Wu. Modeling and Experiment of a Multiple-DOF Piezoelectric Energy Harvester, *Active and Passive Smart Structures and Integrated Systems 2012*, Proc. of SPIE Vol. 8341 83411E-1 - 83411E-1, 2012.
- [48] www.smart-material.com, Smart Material, (page visit, 20.07.2015)
- [49] www.mide.com, Mide, (page visit, 20.07.2015)
- [50] www.faceinternational.com, Face International, (page visit, 20.07.2015)
- [51] J. R. Farmer, "A comparison of power harvesting techniques and related energy storage issues", *Master of Science in Mechanical Engineering of Virginia Polytechnic Institute and State University*, May 15, 2007.
- [52] D. Zhu (2011), "Chapter 2: Vibration Energy Harvesting: Machinery Vibration, Human Movement and Flow Induced Vibration", www.intechopen.com.

- [53] A. Abdelkefi (2016), “Aeroelastic energy harvesting: A review”, *International Journal of Engineering Science* 100, 112–135.
- [54] M. Bryant and E. Garcia (2011), “Modeling and Testing of a Novel Aeroelastic Flutter Energy Harvester”, *Journal of Vibration and Acoustics* Copyright 133, 011010 (11pp).
- [55] J. S. Bae and D. Inman (2013), “Aeroelastic characteristics of linear and nonlinear piezo-aeroelastic energy harvester”, *Journal of Intelligent Material Systems and Structures* 0(0), 1–16.
- [56] C. D. Marqui Jr. and A. Erturk (2012), “Electroaeroelastic analysis of airfoil-based wind energy harvesting using piezoelectric transduction and electromagnetic induction”, *Journal of Intelligent Material Systems and Structures* 24(7), 846–854.
- [57] C. D. Marqui Jr., W. G. R. Vieira, A. Erturk and D. J. Inman (2011), “Modeling and Analysis of Piezoelectric Energy Harvesting From Aeroelastic Vibrations Using the Doublet-Lattice Method”, *Journal of Vibration and Acoustics* 133, 011003-1 (9pp).
- [58] V. C. Sousa, M. D. M. Anicezio, C. D. Marqui Jr. and A. Erturk (2011), “Enhanced aeroelastic energy harvesting by exploiting combined nonlinearities: theory and experiment”, *Smart Mater. Struct.* 20, 094007 (8pp).
- [59] Zhu, D., Beeby, S., Tudor, J., White, N. & Harris, N. (2010)., “A novel miniature wind generator for wireless sensing applications”, *Proceedings IEEE Sensors 2010*, ISBN 978-1-4244-8170-5, Waikoloa, Hawaii, USA, November 1-4, 2010
- [60] X. Gao, “Vibration and Flow Energy Harvesting using Piezoelectric”, Thesis of Doctor of Philosophy, Drexel University, March 2011
- [61] L. Miller, A. Chen, D. Madan, L. Weinstein, P. So, T. Devloo, E. Reilly, Dr. Y. Zhu, P. Wright, J. Evans, “Energy Harvesting From Vibrations, Air Flow, & Temperature Change”

- [62] K. H. Kim, D. Choi, Y. H. Seo, “Piezoelectric Energy Harvester Using Flow-Induced Vibration”, Proceedings of PowerMEMS 2008+ microEMS2008, Sendai, Japan, November 9-12, (2008).
- [63] A. Mehmood, A. Abdelkefi, M. R. Hajj, A. H. Nayfeh, I. Akhtar and A. O. Nuhait (2013), “Piezoelectric energy harvesting from vortex-induced vibrations of circular cylinder”, *Journal of Sound and Vibration* 332, 4656–4667.
- [64] H. Liu, S. Zhang, R. Kathiresan, T. Kobayashi, and C. Lee (2012), “Development of piezoelectric microcantilever flow sensor with wind-driven energy harvesting capability”, *Appl. Phys. Lett.* 100, 223905; doi: 10.1063/1.4723846
- [65] J. D. Hobeck and D. J. Inman (2012), “Artificial piezoelectric grass for energy harvesting from turbulence-induced vibration”, *Smart Mater. Struct.* 21, 105024 (10pp).
- [66] K. Koyvanich, P. Smithmaitrie and N. Muensit (2015), “Perspective microscale piezoelectric harvester for converting flow energy in water way”, *Adv. Mater. Lett.*, 6(6), 538-543.
- [67] H. L. Dai, A. Abdelkefi and L. Wang (2014), “Theoretical modeling and nonlinear analysis of piezoelectric energy harvesting from vortex-induced vibrations” *Journal of Intelligent Material Systems and Structures*, 1–14, doi: 10.1177/1045389X14538329.
- [68] H. L. Dai, A. Abdelkefi and L. Wang (2014), “Piezoelectric energy harvesting from concurrent vortex-induced vibrations and base excitations”, *Nonlinear Dyn* 77, 967–981.
- [69] M. Ali, M. Arafa, and M. Elaraby (2013), “Harvesting Energy from Galloping Oscillations”, Proceedings of the World Congress on Engineering 2013 Vol III, WCE 2013, July 3 - 5, 2013, London, U.K.
- [70] H. D. Akaydin, N. Elvin and Y. Andreopoulos (2013), “Chapter 10, Flow Induced Vibrations for Piezoelectric Energy Harvesting”, Niell Elvin and Alper

Erturk (eds), *Advances in Energy Harvesting Methods*, pp 241-267, Springer Science and Business Media, Newyork, USA.

[71] X. Shan, R. Song, B. Liu and T. Xien (2015), “Novel energy harvesting: A macro fiber composite piezoelectric energy harvester in the water vortex”, *Ceramics International* 41, 763–767.

[72] R. Song, X. Shan, F. Lv, J. Li and T. Xie (2015), “A Novel Piezoelectric Energy Harvester Using the Macro Fiber Composite Cantilever with a Bicylinder in Water”, *Appl. Sci.* 5, 1942-1954.

[73] Sensor Technology Limited, “BM500 – Lead Zirconate Titanate Brochure”

[74] Smart Material Corp., “Macro Fiber Composite – MFC”

[75] www.matweb.com, (page visit 20/07/2015).

[76] www.bksv.com/Products/transducers/vibration/accelerometers/accelerometers/4517.aspx (page visit, 20/07/2015)

[77] www.bksv.com/products/pulse-analyzer.aspx, (page visit 20/07/2015).

[78] www.bksv.com/Products/transducers/vibration/impact-hammers/8206.aspx (page visit 20/07/2015).

[79] NI Data Acquisition System Help Manuel

[80] Energy Harvester Development Kit, Smart Material, www.smart-material.com, (page visit 20/07/2015)

[81] Techet, A.H. (2010) *Vortex Induced Vibration- Lecture Notes*. s.l., Massachusetts Institute of Technology

[82] E. Kahraman (2011), “Investigation of the Dynamic Properties of Plate-Like Structures”, MSc. Thesis, METU, Turkey.

[83] MATLAB Help Manuel.

[84] NI Signal Express Software Help Manuel.

- [85] M. Sarioğlu and T. Yavuz (2000), “Vortex Shedding From Circular and Rectangular Cylinders Placed Horizontally in a Turbulent Flow”, Turk J. Engin. Environ. Sci. 24: 217-28.
- [86] Mide Energy Harvester, “Vulture Data Sheet”.
- [87] M. A. Zhari and S. S. Dol (2015), “Effect of Different Size of Cylinder Diameter on Vortex-Induced Vibration of Energy Generation”, Journal Applied Sciences, 15 (5), 783-791.
- [88] R. R. Matty (1979), “Vortex Shedding from Square Plates Near a Ground Plane: An Experimental Study”, MSc. Thesis, Texas Tech University, USA.
- [89] <https://www.pololu.com/product/1200>, , (page visit 01.10.2015).
- [90] H. Schlichting, “Boundary Layer Theory”, McGraw Hill Book Company, 1979.
- [91] Milton Van Dyke, “An Album of Fluid Motion”, The Parabolic Press, 1982.
- [92] https://en.wikipedia.org/wiki/Particle_image_velocimetry, (page visit 01.02.2016)
- [93] T. F. Miller, F. Gandhi and R. J. Rufino, “Morphing Hull Implementation for Unmanned Underwater Vehicles”, 50th AIAA/ASME/ASCE/AHS/ASC Structures, Structural Dynamics, and Materials Conference, 2009.
- [94] <http://flightdeck.ie.orst.edu/ElectronicChecklist/HTML/mission.html>, (page visit 01.05.2015).
- [95] http://en.wikipedia.org/wiki/Scissors_mechanism, (page visit 20.07.2015).
- [96] S. P. Singh and S. Mittal, “Flow Past a Cylinder: Shear Layer Instability and Drag Crisis”.
- [97] Creo Parametric 2.0 Help Manuel.
- [98] http://www.engineeringtoolbox.com/friction-coefficients-d_778.html, (page visit 01.05.2015).

[99] Materials Data Book, 2003 Edition, Cambridge University Engineering Department.

[100] Miniature Linear Motion Series PQ12, Datasheet, Frigelli.

CURRICULUM VITAE

PERSONAL INFORMATION

Surname, Name: AHMET LEVENT AVŞAR
Date and Place of Birth: 11.12.1982 and Diyarbakır
Phone: +90 533 577 03 53
e-mail: aleventavsar@gmail.com

EDUCATION

1. Mechanical Engineering, M.S., GPA: 3.5/4.0, Middle East Technical University, (2005-2008)
2. Mechanical Engineering, B.S., GPA: 3.36/4.0, Middle East Technical University, (2000-2005)

WORK EXPERIENCE

1. Chief Electroacoustic Design Engineer, Meteksan Defense, 2012-date
2. Researcher, METU Scientific Research Project, (Hava Araçları Üzerinden Piezoelektrik Malzemeler Yardımıyla Titreşim Kaynaklı Enerji Hasatı), 2011-2013
3. Mechanical Test and Analysis Senior Expert Engineer, ASELSAN Electronic Industries Inc., 2005-2012,
4. Summer Practice, ASELSAN Electronic Industries Inc., 2004
5. Summer Practice, Türk Traktör ve Ziraat Makineleri A.Ş., 2003

RESEARCH INTERESTS

Structural Dynamics, Structural Design, Finite Element Analyses, Piezoelectric Materials, Transducer and Hydrophone Design

FOREIGN LANGUAGES

Advanced English

INTERNATIONAL JOURNAL

1. A. Bereketli, M. B. Gldođan, T. Kolak, T. Gd and A. L. AVŐAR, “Experimental Results for Direction of Arrival Estimation with a Single Acoustic Vector Sensor in Shallow Water”, Journal of Sensors, vol. 2015, article ID 401353, 10 pages, 2015. doi: 10.1155/2015/401353

INTERNATIONAL CONFERENCE

1. A. L. Avsar and M. Sahin, “Energy Harvesting Studies on Fin-Like Structure via Piezoelectric Material”, AIAC 2013, 2013.
2. A. L. AvŐar, İ. Tatar and C. Duran, Dynamical Modeling and Verification of Underwater Acoustic System, IMAC XXXI, 2013.
3. Y. Eldođan, A. L. AvŐar and E. Ciđerođlu, “Vibration Fatigue Analysis of a Cantilever Beam Exposed to Random Loading”, UMTIK 2012, 2012.
4. A. L. AvŐar, H. A. Salman, A. E. S. Őzhan and A. M. olakođlu, “Development and Verification of High Durability Infrared Transparent Coating for Airborne Usage”, SPIE Optics and Photonics, 2010.
5. A. L. AvŐar and H. Ő. Őzgiven, “Dynamic Modeling of Optical Systems in Order to Study Vibration Effect on Performance”, SPIE Optics and Photonics, 2010.

NATIONAL CONFERENCE

1. A. L. Avsar ve M. Sahin, “Hava Yapısı Üzerinden Çift Taraflı Piezoelektrik Kiriş Aracılığı İle Enerji Hasatı Çalışmaları”, SAVTEK 2014. 2014.
2. A. L. Avsar ve M. Sahin, “Hava Yapıları Üzerinden Farklı Tip Piezoelektrik Malzemeler Kullanılarak Enerji Hasatı Çalışmaları”, UHAT 2013, 2013.
3. İ. Tatar, A. L. Avşar. C. Orhun ve C. Duran, “Transdüser Uygulamaları İçin Piezoelektrik Malzeme Özelliklerinin Belirlenmesi”, 5. DSS, 2012 (Presentation).
4. A. L. Avşar, M. Şansal ve C. Duran, “Düşük Frekanslı Sualtı Akustik Transdüser Tasarımı ve Karakterizasyonu”, 5. DSS, 2012 (Presentation).
5. A. L. Avşar ve M. Şahin, “Hava Aracı Üzerinden Titreşim Kaynaklı Enerji Hasatı Çalışmaları”, UHUK 2012, 2012
6. A. L. Avşar ve M. Şahin, “Piezoelektrik Malzemeler Yardımıyla Enerji Hasatı”, Savtek 2012, 2012
7. A. L. Avşar ve A. M. Çolakoğlu, “Platform Entegrasyon Çalışmalarında İzolatör Kullanımı”, SAVTEK 2010, 2010
8. A. C. Gözükara, A. L. Avşar, A. M. Çolakoğlu, “Harici Yük Sertifikasyonuna Yönelik Güvenli Ayrılma Analizleri”, ASES 2010, 2010
9. A. L. Avşar ve H. Ö. Özgüven, “Basit Optik Sistemin Dinamik Modelinin Analitik Olarak Oluşturulması ve Doğrulanması”, UMTS 09, 2009
10. A. L. Avşar ve A. M. Çolakoğlu, “Platform Entegrasyonu Çalışmalarında Titreşim Uygulamaları”, SAVTEK 2008, 2008